VYSOKÉ UČENÍ TECHNICKÉ V BRNĚ
BRNO UNIVERSITY OF TECHNOLOGY

FAKULTA CHEMICKÁ
ÚSTAV FYZIKÁLNÍ A SPOTŘEBNÍ CHEMIE

FACULTY OF CHEMISTRY
INSTITUTE OF PHYSICAL AND APPLIED CHEMISTRY

SELF-CLEANING PROPERTIES OF THIN PRINTED LAYERS OF TITANIUM DIOXIDE

DIZERTAČNÍ PRÁCE
DOCTORAL THESIS

AUTOR PRÁCE
AUTHOR

Ing. MARCELA ČERNÁ

BRNO 2012

VYSOKÉ UČENÍ TECHNICKÉ V BRNĚ
BRNO UNIVERSITY OF TECHNOLOGY

FAKULTA CHEMICKÁ
ÚSTAV

FACULTY OF CHEMISTRY
INSTITUTE OF

SELF-CLEANING PROPERTIES OF THIN PRINTED LAYERS OF TITNIUM DIOXIDE

SAMOČISTÍCÍ VLASTNOSTI TENKÝCH TIŠTĚNÝCH VRSTEV OXIDU TITANIČITÉHO

DIZERTAČNÍ PRÁCE
DOCTORAL THESIS

AUTOR PRÁCE
AUTHOR
Ing. MARCELA ČERNÁ

VEDOUCÍ PRÁCE
SUPERVISOR
Doc. Ing. MICHAL VESELÝ, CSc.

BRNO 2012

Brno University of Technology
Faculty of Chemistry
Purkyňova 464/118, 61200 Brno 12

Doctoral thesis Assignment

Number of doctoral thesis:	**FCH-DIZ0061/2011**	Academic year:	**2011/2012**
Institute:	Institute of Physical and Applied Chemistry		
Student:	**Ing. Marcela Černá**		
Study programme:	Physical Chemistry (P1404)		
Study field:	Physical Chemistry (1404V001)		
Head of thesis:	**doc. Ing. Michal Veselý, CSc.**		
Supervisors:			

Title of doctoral thesis:

Self-cleaning properties of thin printed layers of titanium dioxide

Doctoral thesis assignment:

Preparation of thin titanium dioxide layers by printing of nanocrystalline particles and by CVD method. Study of physico-chemical properties and photocatalytic activity of prepared layers.

Deadline for doctoral thesis delivery: 30.6.2012

Doctoral thesis is necessary to deliver to a secreatry of institute in three copies and in an electronic way to a head of doctoral thesis. This assignment is enclosure of doctoral thesis.

Ing. Marcela Černá Student	doc. Ing. Michal Veselý, CSc. Head of thesis	prof. Ing. Miloslav Pekař, CSc. Head of institute

In Brno, 1.9.2011

prof. Ing. Jaromír Havlica, DrSc.
Dean

ABSTRACT

Titanium dioxide was immobilized on soda-lime glass substrates and glassy carbon substrates by two techniques: material printing and chemical vapour deposition. Two methods of sol preparation were used; sol-gel and hydrothermal synthesis. Morphology of all prepared titania layers were studied by scanning electron microscopy and atomic force microscopy analysis. Crystallite phase of prepared TiO_2 was determined using XRD analysis. Photoinduced superhydrophilicity was examined using the sessile drop method.

Photocatalytic activity was investigated as a degradation rate of 2,6-dichloroindophenol or formic acid. We studied the influence of sol-loading and amount of PEG on final activity in case of sol-gel process. PEG was added as an anticracking agent. The influence of time and temperature of hydrothermal synthesis or amount of layers on final efficiency was examined for hydrothermally synthesized samples. The influence of different intensities of irradiation was investigated for the layers deposited by CVD process. The activity of titania thin films prepared by material printing and CVD process was compared and the best sample was evaluated.

KEY WORDS

titanium dioxide, hydrothermal process, photocatalysis, self-cleaning surfaces, nanoparticles, material printing

ABSTRAKT

Tenké vrstvy oxidu titaničitého byly imobilizovány na sodnovápenatá skla a skelný uhlík použitím jak techniky materiálového tisku tak metodou chemického napařování. Pro přípravu titaničitých solů byly použity metody sol-gelu a nebo hydrotermální syntézy. Struktura připravených vrstev byla zkoumána rastrovací elektronovou mikroskopií a mikroskopií atomárních sil. Krystalická struktura připravených TiO_2 byla analyzovány pomocí XRD metody. Fotoindukováná superhidrofility pripravených vzorků byla charakterizována měřením kontaktních úhlů.

Fotokatalytická aktivity připravených vzorků byla testována na fotokatalytické oxidaci 2,6-dichlorindofenolu a kyseliny mravenčí. V případě sol-gel vrstev byl zkoumán vliv množství naneseného TiO_2 a množství PEG, který byl do solu přidán jako praskliny potlačující činidlo. V případě hydrotermálních vrstev byl zkoumán vliv času a teploty syntézy a množství vrstev na výslednou účinnost vzorku. U chemicky napařených vzorků byl zjišťován vliv intenzity záření. Byla porovnána fotokatalitická aktivita vrstev připravených materiálovým tiskem a chemickým napařováním a byl vyhodnocen nejaktivnější vzorek.

KLÍČOVÁ SLOVA

oxid titaničitý, hydrotermální proces, fotokatalýza, samočisticí povrchy, nanočástice, materiálový tisk

ČERNÁ, M. S*amočistící vlastnosti tenkých tištěných vrstev oxidu titaničitého*. Brno: Vysoké učení technické v Brně, Fakulta chemická, 2012. 120 s. Vedoucí dizertační práce doc. Ing. Michal Veselý, CSc.

DECLARATION

I declare that the doctoral thesis has been elaborates by myself and all the quotations from the used literary sources are accurate and complete. The content of the doctoral thesis is the property of the Faculty of Chemistry of Brno University of Technology and all commercial uses are allowed only if approved by the supervisor and the dean of the Faculty of Chemistry, BUT.

……
Student's signature

In this place, I sincerely thank to my supervisor Doc. Ing. Michal Veselý, CSc. for his advices and help during all my doctoral study.

Sincere acknowledgement belongs to Dr. Chantal Guillard and Eric Puzenat for the possibility to work in their laboratory at Université Claude Bernard Lyon 1.

I thank also to Mrs. Claire Tendero, Mr. Pierre Gros, Mrs. Katia Fajerwerg and Mr. David Evrard for their help and advices during the work in their laboratory in CIRIMAT-INPT, ENSIACET in Toulouse.

My words of thanks are also addressed to my colleagues from laboratory of photochemistry; especially to Ing. Petr Dzik Ph.D. for his big help during all work.

Thanks to my friends and my family, to my mum and dad, my sister and especially to my best friend Patrik.

CONTENT

1 INTRODUCTION

Environmental pollution is becoming more and more serious. The green house effect is brought about by increasing in carbon dioxide concentration in the atmosphere. This, as well as the acid rain, is closely related to the use of fossil fuels. In order to solve such environmental and energy resource problems, photocatalysis has been attracting a great deal of attention.[1]

Among the semiconductors, titanium dioxide (TiO_2) is one of the most popular and promising materials as a photocatalyst because it is stable in various solvents under photoirradiation, available commercially and easy to prepare in the laboratory and has a potent ability to induce various types of redox reactions.

Since the start of its commercial production in the early twentieth century, titanium dioxide (TiO_2) has been widely used as a pigment[2], in paints[3], toothpaste[4], and sunscreens[5], etc. In 1972, Fujishima and Honda discovered the photocatalytic splitting of water on TiO_2 electrodes under ultraviolet light.[6] Since this date, enormous efforts have been made to the research of TiO_2 material, which has led to many promising applications in areas ranging from photovoltaic to photocatalysis.[7, 8] These applications can be roughly divided into "energy" and "environmental" categories, many of which depend not only on the properties of the TiO_2 material itself but also on the modifications of the TiO_2 materials host (e.g., with inorganic and organic dyes) and on the interactions of TiO_2 materials with the environment.[9]

As a promising photocatalyst,[10, 11] TiO_2 materials are expected to play an important role in helping to solve many environmental and pollution challenges; water and air purification, prevention of staining, and disinfection. Many approaches to improve the photocatalytic activity of TiO_2 have been tested. These studies proved that TiO_2 activity depends generally on its morphology, crystal composition, crystallinity and surface area.[12, 13]

Ultraviolet radiation has been used for disinfection purposes since the early 20^{th} century. Nowadays, wastewater and drinking water disinfection are important technical applications of direct UV irradiation in the wavelength range between 240 nm and 290 nm. Other significant contributions of UV disinfection include the photo-inactivation of surface bound or airborne microorganisms by using TiO_2 based photocatalytic techniques or solar photocatalytic disinfection of water, which is of importance in tropical developing countries.[14]

Titanium dioxide photocatalysts consists of nanometer scale particles which are either suspended or immobilized into the reactor. So far, mostly suspended systems have been used to investigate the degradation of a variety of components. However, the major drawback of suspended systems in practical applications is the costly separation step necessary after the purification. Therefore, an immobilized system is preferred for an efficient reactor scalable to industrial sizes, especially since the efficiency of the immobilized system can be comparable to that of the suspended system.[15]

2 THE TEORETICAL PART

2.1 Photocatalysis

Photocatalysis, i.e., catalysis under light radiation, is a reaction in the presence of a catalyst which causes the acceleration of the whole process. The main difference between the catalyst and photocatalyst is that a catalyst contains active sites on which substrate is converted into a products whereas no active sites are present on a photocatalyst (Fig. 1). Photocatalysis can be homogenous or heterogeneous. The homogenous photocatalysis is taking place in homogenous phase. The heterogeneous is carrying out at the interfacial boundary between two phases (solid-liquid, solid-gas, liquid-gas).[16]

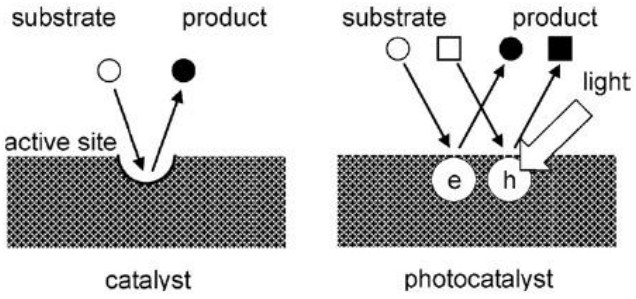

Fig. 1 *Difference in concepts of catalytic and photocatalytic reaction*[17]

2.1.1 Mechanism of heterogeneous photocatalysis

The basic principles of heterogeneous photocatalysis can be summarized as follows. A semiconductor's electronic shell consists of valence band (vb), it is the highest occupied energy band, and of conduction band (cb), it is the lowest empty band. These energy bands are separated by a band gap. It is the region of forbidden energies.

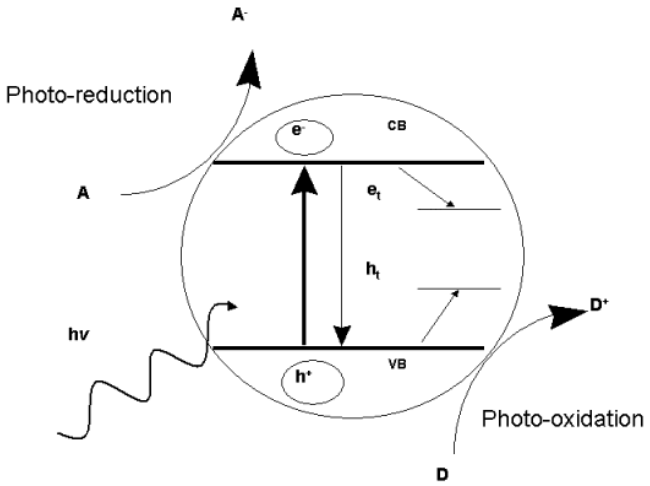

Fig. 2 *Simplified diagram of the heterogeneous photocatalytic process occurring on an illuminated semiconductor particle*[18]

The initial process for heterogeneous photocatalysis of organic and inorganic compounds by semiconductors is the generation of electron–hole pairs in the semiconductors particles.[19]

When a photon, with energy higher or equal to the band gap energy, is absorbed by a semiconductor particle, an electron from vb goes over to the cb with simultaneous generation of hole (h^+) in the vb. The electrons and holes are not localized in the valence and conduction bands. Therefore electrons and positives holes can migrate within a crystal. These electrons and holes can be trapped at the surface where they can react with donor (D) or acceptor (A) species adsorbed or close to the surface of the particle. In this way, anodic or cathodic redox reactions can be initiated (Fig. 2). On the other hand, apart from the trapping of the species, electrons and holes can recombine on the surface or in the bulk of the particle in a few nanoseconds; the energy is dissipated as heat. In a real system recombination occurs and concentration of electrons and holes on the surface is not equal. Obviously, this recombination is detrimental to the efficiency of the semiconductor photocatalyst. Modifications to semiconductors surfaces such as addition of metals, dopants, or combinations with other semiconductors are beneficial for decreasing the electron and hole recombination rate and thereby increasing the quantum yield of the photocatalytic process.

2.1.2 Band gap energy

Band gap correspond to difference in potential of cb bottom and vb top. Optical band gap can be estimated form Kubelka–Munk (K–M) function which is defined as:

$$\frac{\alpha}{s} = \frac{\left(1 - R_d^2\right)}{2R_d}, \tag{1}$$

where R_d is diffused reflectance, α is absorption coefficient and s is scattering coefficient. For samples diluted with a medium of less photoabsorption, K–M function can be a measure of sample concentration. The K–M function is often recognized, through this requires assumptions, to be proportional to the absorption coefficient. Usually optical band gap is evaluated from the following relation, where scattering coefficient is supposed to be constant throughout a wavelength range for measurement.

$$\alpha = \frac{\left(h\nu - E_g\right)^n}{h\nu} \tag{2}$$

In this equation, h is Planck constant, ν is oscillation frequency, E_g is optical band gap and n is constant relating to a mode of transition. The constant n is 1/2, 3/2 or 2 for allowed direct transition, forbidden direct transition and indirect transition (Fig. 3). But the forbidden direct transition has often been neglected.[17]

In indirect transition, the electron cannot shift from the lowest energy state in the conduction band to the highest energy state to valence band without a change in momentum (Fig. 3). In this case the band gap energy is analyzed from the following relation[20] by extrapolation to $\alpha_{KM} = 0$.

$$\left(\alpha_{KM} \cdot h\nu\right)^{\frac{1}{2}} = f(h\nu) \tag{3}$$

In the case of the direct transition, the electron can shift from the lowest-energy state in the conduction band to the highest energy state to valence band without a change in momentum (Fig. 3). Here, the band gap energy is analyzed from other relation[20] by the same extrapolation as in previous case.

$$(\alpha_{KM} \cdot h\nu)^2 = f(h\nu). \tag{4}$$

The ability of a semiconductor to undergo photoinduced electron transfer to adsorbed species on its surface is governed by the band energy positions of the semiconductor and the redox potentials of the absorbate. The relevant potential level of acceptor species is thermodynamically required to be below (more positive than) the conduction band potential of the semiconductor. The potential level of the donor needs to be above (more negative than) the valence band position of the semiconductor in order to donate an electron to the vacant hole. The band edge positions for a few semiconductors are presented in Fig. 4. On the left side we can see the internal energy scale for comparison to vacuum level and on the right we can observe the scale for comparison to normal hydrogen electrode (NHE). The positions are derived from the flat band potentials in a contact solution of aqueous electrolyte at pH = 1. The pH of the electrolyte solution influences the band edge positions of the various semiconductors compared to the redox potentials for the absorbate.[19]

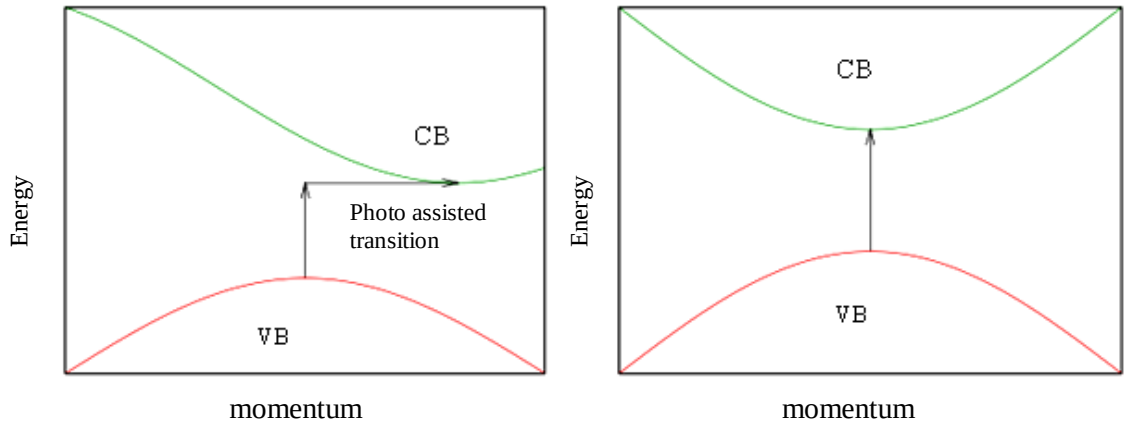

Fig. 3 *Indirect transition (left) and direct transition (right)*

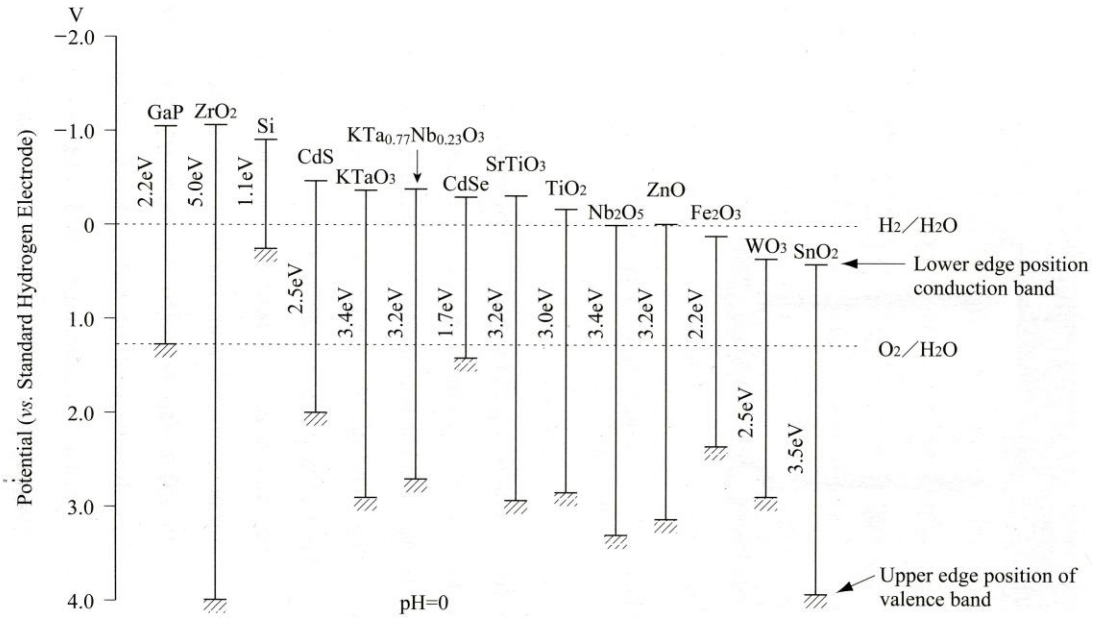

Fig. 4 *Energies for various semiconductors in aqueous electrolytes at pH = 0*[21]

It is necessary to mention that there are a lot of factors which can influence the photocatalytic reaction rate, such as the life time of charge carriers, molecule adsorption and desorption kinetics on the surface, catalytic surface character, particle size and other. The most important factors influencing the reaction rate are semiconductor type and radiation which is used for its activation. The other very important factors are

- The pH of the solution which determines the surface charge on the semiconductor and the speciation of the substrate to be transformed
- The substrate concentration
- The adsorption process
- The temperature, high temperature generally leads to higher rates, because there is a higher frequency of collision between the substrate and the semiconductor. Nevertheless the optimum temperature for photocatalytic reaction was discovered to be between 20 and 80 °C.[22, 23]
- The presence of metal cations and inorganic anions

2.1.3 Applications of photocatalysis

There are many applications of environmental photocatalysis that are already at or near the stage of implementation or commercialization. Some of them are summarized in Table 1. Photocatalysis belongs to the clean technologies; organic water pollutants are transformed into CO_2 and H_2O. TiO_2-coated substrate shows unexpectedly effective self cleaning effect in both ordinary indoor conditions and outdoor conditions. Particularly in the outdoor spaces, inorganic contaminants such as sand may be mainly responsible for stains, so photocatalytic oxidative power may not be considered useful for the self-cleaning process. However, it was found that TiO_2-coated materials show very effective anti-fouling effect even against

inorganic substances. This is probably because such substances adhere on the substrate surface by oil spots, which serve as a binder. Therefore the decomposition of the oil also decreases the amount of inorganic materials bound to the surface.[1]

Table 1 *Selected application of photocatalysis*

Property	Category	Application
Self-cleaning	Materials for residential and office buildings	Exterior tiles, kitchen and bathroom components, interior furnishings, plastics surfaces, aluminium siding, building stone and curtains, paper window blinds[24]
	Indoor and outdoor lamps and related systems	Translucent paper for indoor lamp covers, coatings on fluorescent lamps and highway tunnel lamp cover glass[25]
	Materials for roads	Tunnel wall, soundproofed wall, traffic signs and reflectors[25]
	Others	Tent material, cloth for hospital garments and uniforms and spray coating for cars[26]
Air cleaning	Indoor air cleaners	Room air cleaner, photocatalyst-equipped air conditioners and interior air cleaner for factories[27]
	Outdoor air purification	Concrete for highways, roadways and footpaths, tunnel walls, soundproofed walls and building walls[28]
Water purification	Drink water	River water, ground water, lakes and water storage tanks[29]
	Others	Fish feeding tanks, drainage water and industrial wastewater[30]

Antitumor activity	Cancer therapy[31]	Endoscopic-like instruments
Self-sterilizing	Hospital	Tiles to cover the floor and walls of operating rooms, silicone rubber for medical catheters and hospital garments and uniforms[32]
	Others	Public rest rooms, bathrooms and rat breeding rooms[32]

2.1.4 Kinetics of photocatalytic reactions

Photocatalytic reactions belong to the reactions which run on the interface of solution/photocatalyst. Interactions between charge carries and adsorbent reactant occur during the reaction, which evoke chemical changes of reactant. Thus, photocatalytic reaction involving light absorption by a catalyst includes processes of adsorption and desorption.[33]

Photocatalytic reaction takes place in the following five steps:[34]

- Transport of reagents in liquid (or gaseous) phase to the photocatalyst surface
- Adsorption of reagents onto the photocatalyst surface
- Chemical reaction on the surface of photocatalyst
- Desorption of created products from the surface
- Products transport to the liquid (gaseous) phase

All of these mentioned steps can considerably influence the final process rate. Transport of reagents to the photocatalyst surface is caused by convection and diffusion, which follows the Fick's laws. The overall reaction rate mainly depends on the adsorption of reactants rather than the actual chemical reaction on the photocatalyst surface because the rate of transport is higher than reaction rate in reactor. So it is not the rate limiting step. There are few kinetics models which describe photocatalytic oxidation on irradiated photocatalysts.

2.1.4.1 Langmuir-Hinshelwood kinetic mechanism

Consider that only two reactants take part in the reaction on the surface of photocatalyst. The most common surface reaction mechanism is that where both reactants are adsorbed on the surface and subsequently they collide and create products. This is known as the Langmuir-Hinshelwood mechanism. It was derived from ideas proposed by Hinshelwood based on Lanqmuir's principles for adsorption.[35]

This mechanism is based on the following hypotheses

- Surface is homogeneous
- Adsorption occurs only on the specific places of surface
- Each active center use only one molecule of adsorbed reactant
- Adsorbed molecules do not react with each other
- Only monolayer is formed during the adsorption process

The photocatalytic surface reaction mechanism is based on the reaction between a molecule of semiconductor and an atom of molecule adsorbed to the surface of this semiconductor.[36] Therefore, these reactions run according to 2nd order kinetics:

$$A + B \xrightarrow{k} P \tag{5}$$

The reaction rate in this case is given by the following formula:

$$v = \mathrm{k} \cdot \theta_A \cdot \theta_B \tag{6}$$

The Langmuir isotherm implies:

$$\theta_A = \frac{\mathrm{K_A} \cdot c_A}{1 + \mathrm{K_A} \cdot c_A + \mathrm{K_B} \cdot c_B} \tag{7}$$

$$\theta_B = \frac{\mathrm{K_B} \cdot c_B}{1 + \mathrm{K_A} \cdot c_A + \mathrm{K_B} \cdot c_B}, \tag{8}$$

where K_A and K_B are adsorption constants for reactant A and B, θ_A and θ_B are coverage of the photocatalyst surface by reactants A and B. By applying the expressions (7) and (8) to the expression (6), we get the following equation for the reaction rate:

$$v = \frac{\mathrm{k} \cdot \mathrm{K_A} \cdot \mathrm{K_B} \cdot c_A \cdot c_B}{\left(1 + \mathrm{K_A} \cdot c_A + \mathrm{K_B} \cdot c_B\right)^2} \tag{9}$$

The rate constant k and adsorption constant K_A and K_B are thermally dependent.

Analysis of heterogeneous kinetics of photocatalytic reaction can be simply quantified by the rate equation; by Langmuir-Hinshelwood equation:[37]

$$v = \frac{\mathrm{k} \cdot \mathrm{K} \cdot c}{1 + \mathrm{K} \cdot c} \tag{10}$$

At lower concentration, reaction can be simplified to the reaction of 1st order:

$$v = \mathrm{k} \cdot \mathrm{K} \cdot c \tag{11}$$

2.1.4.2 Eley-Rideal kinetic mechanism

This mechanism describes the situation where are already adsorbed molecules of substance A on the surface and these molecules get into contact with molecules of substance B which come to the surface from gaseous or liquid phase.[37]

$$A_{ads} + B \xrightarrow{k} P \tag{12}$$

The final reaction rate depends on the concentration of species B (non-adsorbed compound) in the solution, or on the partial pressure if the compound B is in gaseous phase and on the coverage degree of the photocatalyst surface by adsorbed substance A:

$$v = \mathrm{k} \cdot \theta_A \cdot c_A \tag{13}$$

The reaction rate can be described by the concentration of the compound A, if its adsorption isotherm is known. When the adsorption of compounds A follows the Langmuir isotherm, the reaction rate can be expressed by the equation:

$$v = \frac{\mathrm{k} \cdot \mathrm{K} \cdot c_A \cdot c_B}{1 + \mathrm{K} \cdot c_A} \tag{14}$$

2.2 Titanium dioxide

In nature, titanium dioxide exists in three crystalline modifications, anatase (tetragonal), rutile (tetragonal) and brookite (orthorhombic). Apart from these three natural forms, there are four other artificial titanium dioxide modifications which can be prepared by hydrothermal synthesis under high pressure. They are TiO_2-B, ramsdellite, hollandite and TiO_2-II.[38, 39] The most common crystallized phase is rutile. Anatase and brookite both convert to rutile upon heating.[40]

2.2.1 Anatase

The anatase phase shows a higher photocatalytic activity that rutile due to its low recombination rate of photo-generated electrons and holes.[19, 41, 42] The band gap energy of this titanium oxide modification is 3.23 eV, corresponding to the wave length of 384 nm. Pure anatase can be synthesized by many ways; using an alkoxide precursor, anatase is formed by the hydrolytic reaction in aqueous solutions of a variety of acids or bases.[43]

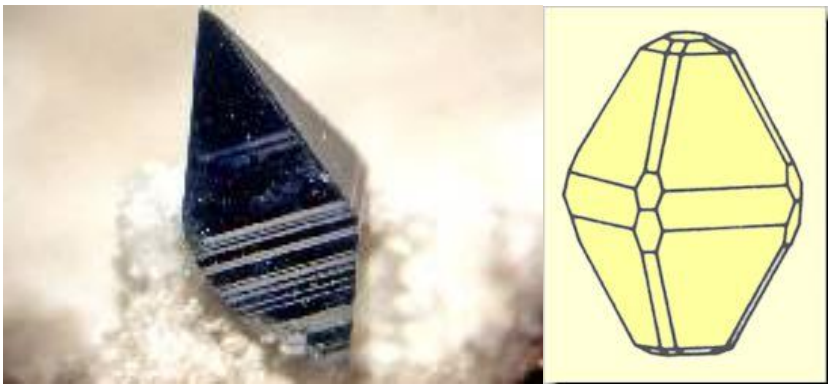

Fig. 5 *TiO_2 in crystalline modification of anatase* [44, 45]

The crystallite phase of a laboratory prepared TiO_2 can be identified by Raman spectroscopy. Typical spectrum for pure anatase from Raman spectroscopy can be observed in (Fig. 6). The characteristic peaks are in positions 143, 197, 395, 517 and 638 cm^{-1}.[46] The crystallinity of synthesized TiO_2 can be evaluated by X-ray diffraction. The XRD spectrum for pure anatase is shown in Fig. 7. The highest intensity have the peak (101), its intensity is always 100 %. 2Θ of this peak is equal to 25.23° and the width of this peak is important for calculation of the crystallite size.

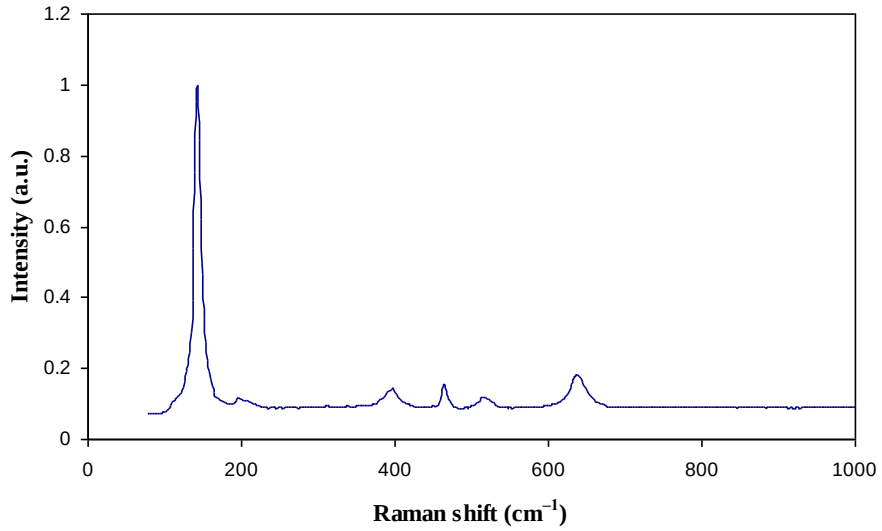

Fig. 6 *Raman spectrum for anatase*[46]

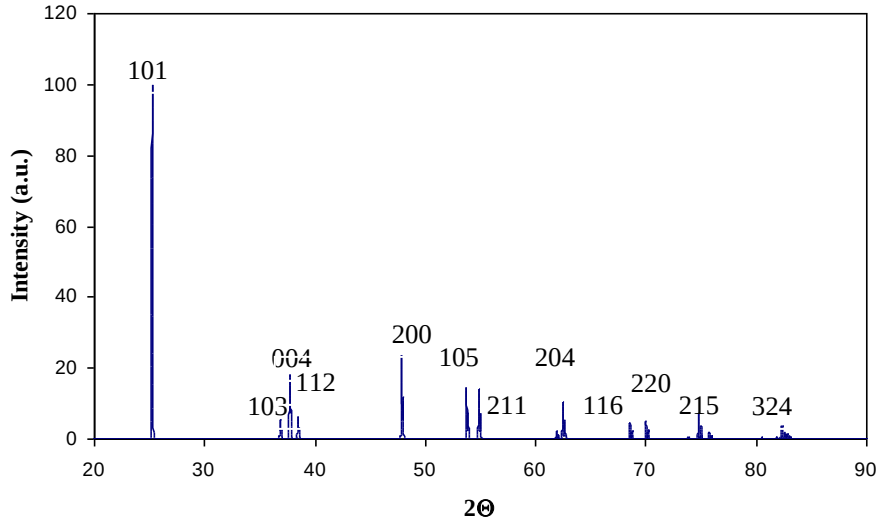

Fig. 7 *XRD spectrum of pure anatase*[47]

2.2.2 Rutile

Rutile is thermodynamically stable form while the other two phases are metastable ones.[48] The band gap energy of this crystalline phase is 3.02 eV, corresponding to the wave length of 411 nm. Pure rutile nanoparticles have been prepared from $TiCl_4$ or $TiCl_3$ in HCl solution or from titanium (IV) isopropoxide in nitric acid at pH = 0.5.[49]

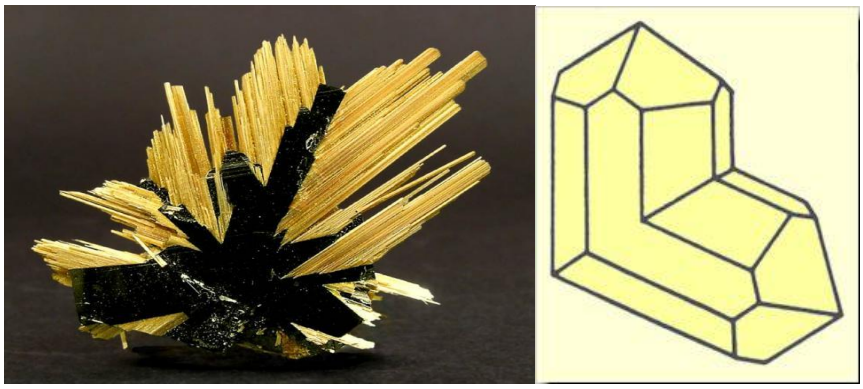

Fig. 8 *TiO_2 in crystalline modification of rutile*[50, 45]

As in previous cases the crystallinity of prepared TiO_2 can be studied by Raman spectroscopy or by X-ray diffraction. The Raman spectrum for rutile is depicted at Fig. 9. The characteristic peaks in Raman spectra have the position 230, 447 and 612 cm^{-1}. In the XRD spectrum, the peak with 100 % intensity is peak (110) and the position of this peak (2Θ) is equal to 27.45°. This peak is used for calculation of the crystallite size.

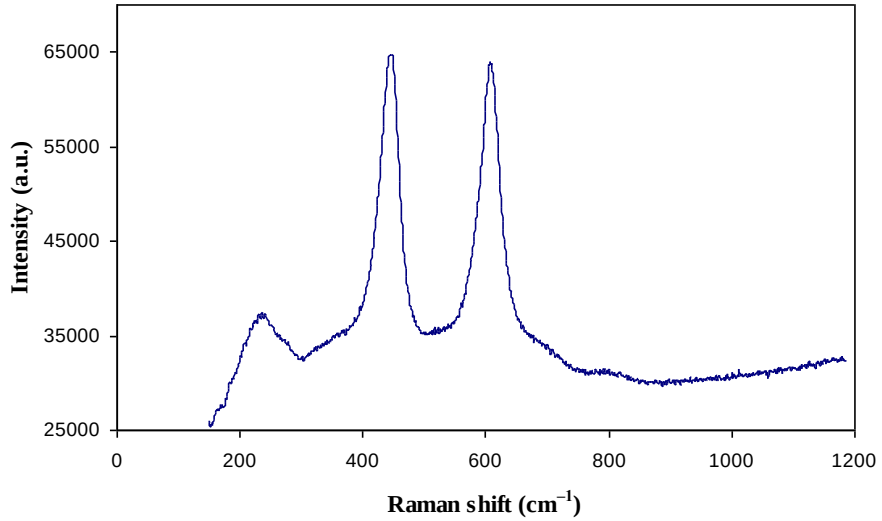

Fig. 9 *Raman spectrum for pure rutile*[47]

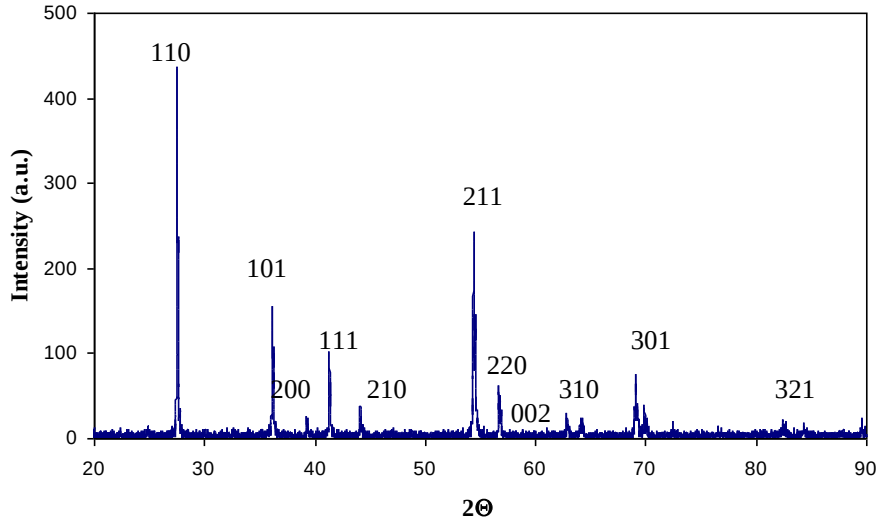

Fig. 10 *XRD spectrum for pure rutile*[47]

2.2.3 Brookite

Brookite phase is stable only at very low temperatures and hence not so useful practically. Moreover, it features a very low band gap energy which could contribute to a higher rate of recombination reaction. The exact value of band gaps is not known but Zallen et al. in their study discovered that the brookite form of TiO_2 is an indirect-gap semiconductor with a band gap of about 1.9 eV.[51] Pure brookite particles have been prepared using amorphous titania as the starting material and hydrothermal treatment with NaOH[52] or by thermolysis of $TiCl_4$ in aqueous HCl solution[53].

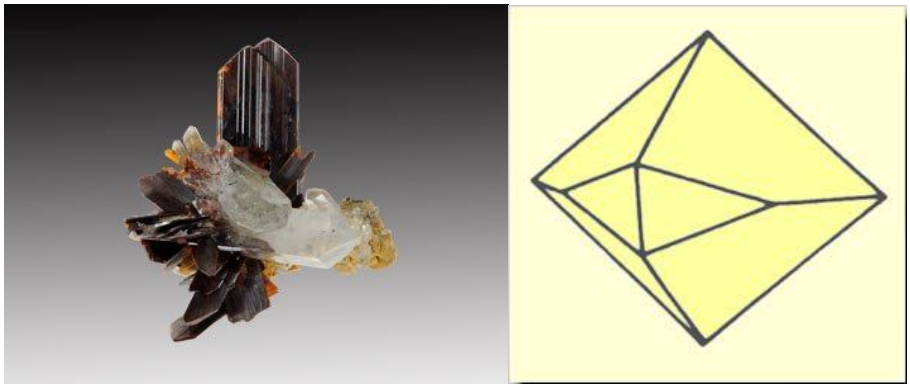

Fig. 11 *TiO_2 in crystalline modification of brookite*[45, 54]

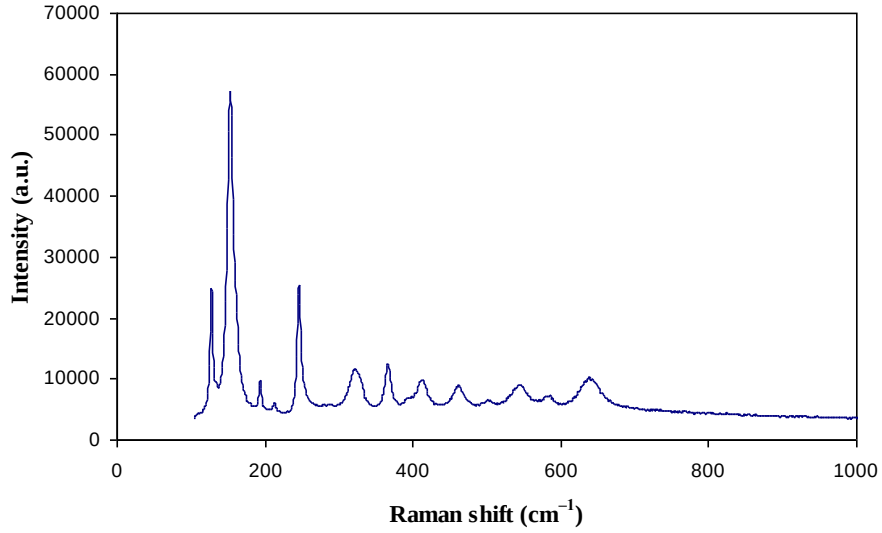

Fig. 12 *Raman spectrum for pure brookite*[47]

A typical Raman spectrum for pure brookite is shown in Fig. 12. The positions of characteristic peaks are following; 127, 150, 250, 320, 365, 406, 458, 538, 640. XRD spectra can be observed in Fig. 13. The peak with intensity 100 % is peak 210, the angle of which equals 25.23. This peak is again the most important for the calculation of the crystallite size.

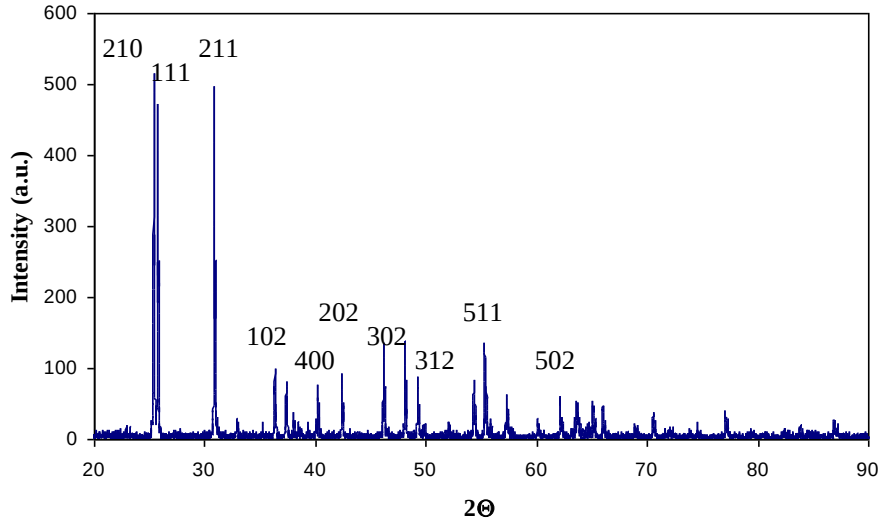

Fig. 13 *XRD spectrum for pure brookite*[47]

Degussa P25 is one of the most common commercial titanium semiconductor types. This type of TiO_2 is produced through a high temperature (greater than 1200 °C) flame hydrolysis of $TiCl_4$ in the presence of hydrogen and oxygen. The TiO_2 is treated with steam to remove HCl which is also produced as a by-product of the reaction. The product is 99.5% pure TiO_2 (anatase : rutile ratio, 70 : 30), which is non-porous, with cubic particles with rounded edges.[55]

It is not surprising that the different samples of titanium dioxide exhibit different photocatalytic activity towards the same organic substrate under same reaction conditions.[56] These differences can be qualitatively attributed to the differences in crystallinity, morphology, specific surface area, particle aggregate size and surface density of OH groups in the TiO_2 samples. On the other hand, it may be surprising that a TiO_2 photocatalyst which is good at destroying one organic substrate can be ineffective at destroying another and that for a different sample of TiO_2 the situation can be reversed.

The main advantages of using TiO_2 as photocatalyst are:

- Relatively high photoactivity
- Biological and chemical inertness
- Photostability (i.e. not liable to photoanodic corrosion for example)
- Exceptional optical and electronic properties
- Non-toxicity and relatively low cost

The disadvantages of TiO_2 semiconductor photocatalysts include:[57, 58]

- The requirement of large amounts of TiO_2 photocatalysts
- Difficulty in re-cycling TiO_2 photocatalysts
- Problematic agglomeration of TiO_2 nanocrystals into large particles for better removing
- In the other size, TiO_2 have the tendency to lose efficiency when they agglomerate into larger particles
- The separation processes required to recover the TiO_2 at the end of the photocatalytic treatment and it is difficult to perform because of the small particles of TiO_2 and the high stability of the TiO_2 hydrocolloid

2.3 Preparation of Titanium dioxide

Generally, two forms of TiO_2 in photocatalysis have been widely used; highly dispersed fine particles or suspended particles in liquid medium and thin films on supporting materials.[59] The main disadvantage of using the powder form of TiO_2 is the suspension instability in time. This instability is monitored by sedimentation due to the aggregation. The other very important disadvantage is the energy consumption for catalyst removal and recovery. Due to these reasons, it is obvious that the use of active immobilized photocatalyst is more popular than using of this catalyst in powder form.

The photocatalyst can be immobilized onto a suitable inert support. In this case there is no need to remove the catalyst. Unfortunately, when the catalyst in immobilized, there is a decrease in the available surface area for the reaction since the catalyst must adhere to the solid support.[60] We have to point out, that in the case of immobilized photocatalyst, layer thickness is very important property of prepared films. When the photocatalyst films are too thick, most of the electrons and holes are generated deep in a semiconductor and never get up to the surface. So they are unable to participate in the reaction. On the other side, when the

layers are too thin, semiconductor can absorb only a very small amount of incident photons. The efficiency of photocatalytic process decreases as well.[61]

2.3.1 Methods of preparation TiO_2 sols

There are many methods of synthesizing TiO_2 nanostructures. Generally these methods can be divided to two main groups; solution routes and gas phase methods. The advantages of solution route are the control over the stochiometry, production of homogenous materials, ability to coat complex shapes and preparation of composite materials. The disadvantages include the use of expensive precursor, long processing times and the presence of carbon as an impurity. In the case of gas phase methods, the synthesis can be of chemical or physical nature.

2.3.1.1 Sol-gel process

Sol-gel processing is one of the most common methods to produce photocatalyst TiO_2 in both forms; coating and powder. This process is categorized as a wet chemical method based on the hydrolysis and polycondensation of precursor.

In a typical sol-gel process, a colloidal suspension, or a sol, is formed by the controlled hydrolysis and polycondensation reaction of precursors, which are usually inorganic metal salts or organometalic compounds. In this process, the liquid sol is transformed into a solid gel phase during the complete polymerisation and loss of solvent. The thin layers on the substrate can be produced by various coating techniques such as spin-coating or dip-coating.

TiO_2 nanomaterials have been synthesized with the sol-gel method by the hydrolysis of titanium precursor.[62, 63, 64] This process normally proceeds via an acid-catalyzed hydrolysis step of titanium(IV) alkoxide followed by condensation.[65, 66] The development of Ti–O–Ti chains is supported by a low content of water, low hydrolysis rates, and excess titanium alkoxide in the reaction mixture. Three-dimensional polymeric skeletons with a close packing result from the development of Ti–O–Ti chains. The formation of $Ti(OH)_4$ is favored with high hydrolysis rates for a medium amount of water. The presence of a large quantity of Ti–OH and insufficient development of three-dimensional polymeric skeletons lead to loosely packet first-order particles. Polymeric Ti–O–Ti chains are developed in the presence of a large excess of water. Closely packed first-order particles are yielded via a three-dimensionally developed gel skeleton.[67, 68]

The strong reactivity of the alkoxide towards water often results in an uncontrolled precipitation and limits the use of the sol-gel technology. These problems can be eliminated with the aid of chelating agents, such as acetyl acetone (AcAc)[69] and acetic acid.[70] These chemical additives react with alkoxides and modify the ligand structure, enabling the hydrolysis and polycondensation reactions to be controlled.

The interest in application of sol-gel method is due to its many advantages, such as:

- Possibility of preparation homogenous films
- Ease of composition control
- Low processing temperature
- Large area coatings
- No special equipment with low cost
- Preparation of films with high photocatalytic activity

2.3.1.2 Hydrothermal synthesis

Hydrothermal synthesis is widely used in industry to manufacture ultra-fine powders and particles. The process is usually realized in a steel pressure vessel called autoclave with or without Teflon or glass liners under controlled temperature and/or pressure with the reaction in aqueous solutions. The temperature can be elevated above the boiling point of water at standard conditions, reaching the pressure of vapour saturation. The temperature and the amount of solution added to the autoclave largely determine the internal pressure produces. It is a method that is widely used for the production of small particles, for the preparation of TiO_2 nanoparticles[71, 72], TiO_2 nanorods[73, 74], nanowires[75, 76], and nanotubes[77, 78]. Hydrothermal treatment enhances the phase transformation of the TiO_2 powders from amorphous to crystallite phase, by re-crystallization and restructuring.

The initial step in hydrothermal synthesis is the precipitation of the precursor solution, usually consisting of titanium alkoxide or halide. Prepared precipitate is mixed into aqueous slurry, possibly with the addition of a surfactant. The precursor slurry is then placed into an autoclave and heated to a given temperature over some period time. The precipitate formed is then collected either by filtration or centrifugation, washed with an appropriate solvent and dried. With this relative simplicity, hydrothermal reaction leads to the synthesis of various TiO_2 nanomaterials simply by varying the experimental parameters.

The hydrothermal method of preparation TiO_2 particles has many advantages. A major advantage of using the hydrothermal process is the ability to produce different crystalline phases without the need of following heat treatment as it provides the capacity to grow good-quality crystals and to control the crystalline composition simultaneously.[79] The other very important feature is that the hydrothermal synthesis favours a decrease in agglomeration between particles, narrow particle size distributions, phase homogeneity, and controlled particle morphology. It also offers uniform composition, purity of the product, monodispersed particles, a control over the shape and size of the particles, and so on. The hydrothermal method has been evaluated as one of the best techniques to prepare TiO_2 particles of desired size and shape with homogeneity in composition and a high degree of crystallinity.

Several authors studied in details the influence of different parameters on final properties of TiO_2. These include the starting materials (commercial, self-prepared, amorphous, crystalline anatase, rutile and brookite), sonication pre-treatment, hydrothermal temperature, treatment time, and post-treatment (washing, calcination). The characteristic and morphology

of titania such as specific surface area, crystal structure and others are dependent on the selected hydrothermal conditions.

Effect of the starting materials

A large amount of various compounds like rutile or anatase TiO_2, Degussa TiO_2 (P25) nanoparticles, layered titanate $Na_2Ti_3O_7$, Ti metal, $TiOSO_4$, $TiOCl_2$, molecular Ti^{IV} alkoxide, dopped anatase TiO_2, or SiO_2–TiO_2 mixture can be used as the precursor for the preparation of TiO_2 by hydrothermal synthesis. Sol of titanium dioxide can also be utilized as the starting reactant in the hydrothermal process. Basically, using of different starting reagents cause formation of final TiO_2 with different particle size.[80]

Effect of sonication pre-treatment

Nawin and his colleagues analyzed the effect of sonication pretreatment on the control of titanate nanotubes length in the hydrothermal reaction.[81] Sonication causes breaking the intermolecular interaction between titanium dioxide particles and concentrated sodium or potassium hydroxide solution and thus speeds up the dispersion of nanoparticles in the hydrothermal process. When the samples are irradiated by ultra sound waves, the milky mixture becomes a smoother. The sonication step has a strong influence on the length distribution and the length of synthesized product. Thus, the average length of titanate nanotubes without sonication treatment is much shorter than with such a step in the hydrothermal process. Sonication aids to migrate the OH^- or Na^+ (K^+) ions across the restrict interparticle gaps of cluster titania precursors that otherwise retard the mechanism of nanotubes formation.[82] Many research projects indicate that when the sonication pretreatment is incorporated into the process, it caused the creation of much longer titania nanoparticles with smaller diameters.[83]

The use of sonication method during the preparation of titania nanotubes helps to avoid or reduce the crystallite growth. In conclusion, smaller homogeneous titania nanotubes are formed with the use of ultrasonic pretreatment. Longer titania nanotubes with smaller diameters and higher surface area are formed effectively using the sonication pretreatment.[82]

Effect of time and temperature of hydrothermal synthesis

The hydrothermal treatment temperature is one of the parameters which influence morphological properties of the TiO_2 particles. This temperature plays an important role in promoting the nucleation and crystal growth of TiO_2 nanoparticles. The degree of crystallinity and also the crystallite size in the final product increases with increasing hydrothermal temperature. The usual range of temperature used for hydrothermal synthesis of TiO_2 is 110°C–250°C, it depends also on the autoclaves used. The rutile phase is more dominant in the resultant product, the presence of a small amount of anatase persisted except when the experimental temperature is approximately 200 °C.

Duration of the hydrothermal treatment is another very important parameter which influences considerably morphology and crystallinity of final TiO_2. Many previous studies proved that with increasing time and temperature of hydrothermal treatment, the average crystallite size and average pore size increased. On the other hand, the BET specific surface

area, pore volumes and porosity continuously decrease.[42] For temperature lower than 100°C, almost all researchers concluded that nanoparticles of TiO_2 are not formed.[84]

Effect of the post-treatment process

The morphology and the dimensions of the nanostructures are generally determined by the hydrothermal treatment, rather than by the washing process. Nevertheless, the acidity of the washing agent has a significant influence on other important properties like on elemental composition, annealing behaviour and specific surface area of nanoparticles.[80]

The calcinations process which takes place during post-treatment very significantly affects the phase structure and microstructure of final titanium dioxide. Heat treatment can advance the phase transformation of titanium dioxide nanotubes to the anatase phase. It is also conductive with elimination of the ions which participate of primary precipitation reaction in the sample.[80]

Effect of pH

The creation of a pure phase (either anatase or rutile) required the proper selection of pH of the media and the crystallization temperature. When the pH of the medium is low (pH equals 1 to 2), only rutile phase was formed. When the pH is kept even lower, i.e., in the negative range, the final TiO_2 contains also a small amount of anatase. As the pH of the medium is increased, the product contained essentially anatase with very little part of rutile. With the addition of KOH or NaOH, the formation of anatase phase is favoured. With a further increase of the pH, i.e., above the twelve, only amorphous TiO_2 is obtained.[85]

2.3.1.3 Solvothermal routes

Solvothermal reactions are very similar to hydrothermal reactions, the only difference being that the reaction medium is a non-aqueous solvent. However, the temperature can be elevated much higher than in the case of hydrothermal method, since a variety of organic solvents with high boiling points can be chosen. As with hydrothermal methods, also solvothermal synthesis is conducted in stainless steel autoclaves. The solvothermal methods normally have better control than hydrothermal methods of the size and shape distributions and the crystallinity of the TiO_2 nanoparticles.

By varying the initial parameters of synthesis such as the reaction temperature and time, solvent, the presence or not of a surfactant, titanium precursors, different shape of TiO_2 can be obtained (e.g.; nanoparticles[86], nanorods[87], or nanowires[88]).

2.3.2 Methods of preparation TiO_2 thin films

Thin film formation is described as a sequential process which includes nucleation, coalescence and subsequent thickness growth. The mode of film creation can be categorized into three basic types, which are illustrated schematically in Fig. 14.

- Layer-by layer mode (Frank–van der Merwe mode) is two-dimensional growth mode, where is deposited step by step first layer, second layer, third layer and so on. In this case, the atomic bonding between the substrate surface and the film is greater than the bond between atoms of film layers.
- Three-dimensional island mode (Volmer–Weber mode) is mode where firstly three dimensional separate islands are created. This happens when the bonding between atoms in clusters is much greater and stronger than that between the atom and the substrate. This growth mode can be observed in metal deposition around the room temperature.[89]
- Layer plus island mode (Stranski–Krastanov mode) is an intermediate combination of the two growth modes mentioned above. The substrate is first covered with one or few monolayers grown in Frank–van der Marwe mode, and then some three-dimensional islands are formed on the surface in Volmer–Weber growth mode. This mode has been observed in metal–metal and metal–semiconductors systems.

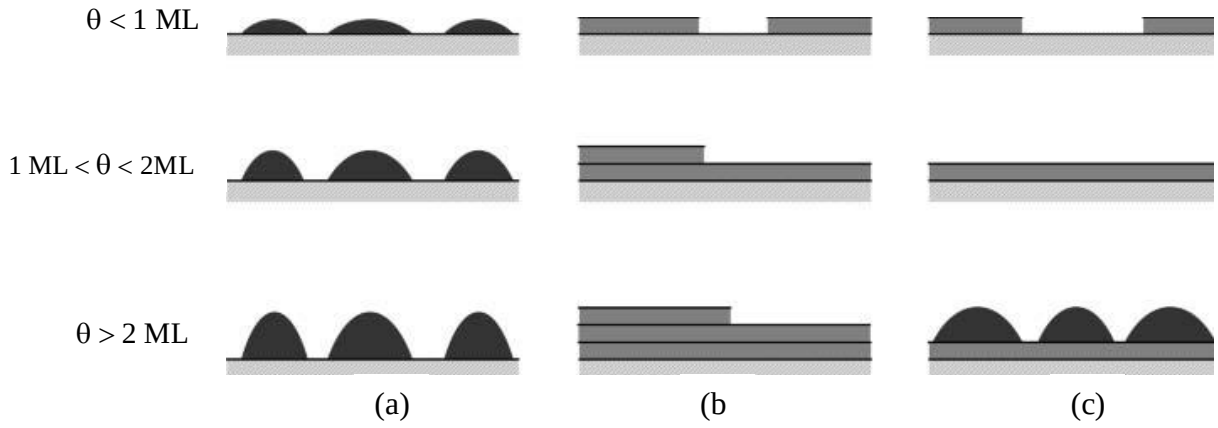

Fig. 14 *Three types of growth mode; θ is coverage; ml is monolayer; (a) Volmer–Weber mode, (b) Frank–van der Merwe mode, (c) Stranski–Krastanov mode*[91]

Glass, especially soda-lime glass, is common substrate used for photocatalytic experiments. One of the problems in the implementation of TiO_2 on these glasses is that the prepared films are inactive. This is because the Na^+ cations from the glass diffuse into the TiO_2 film when this film is calcinated, with an adverse effect on the subsequent photocatalytic activity. When TiO_2 films are prepared on high-purity silica glass, this problem does not arise, so an obvious solution is to deposit a thin intermediate layer of silica prior to depositing the titania film. The silica layer effectively blocks the diffusion of Na^+ cations from the glass into the titania film.[1] Heller and co-workers have solved this problem by acid treating the glass to remove the Na^+ cations prior to the deposition of the TiO_2 layer.[90]

2.3.2.1 Physical/chemical vapour deposition

Vapour deposition refers to any process in which materials in a vapour state condenses to form a solid phase material. These processes are normally used to form coatings to alter the mechanical, electrical, thermal, optical, corrosion resistance, and wear resistance properties of various substrates. They are also used to form free-standing bodies, films, and fibres and to infiltrate fabric to form composite materials.[9] If no chemical reaction occurs, this process is called physical vapour deposition (PVD); otherwise, it is called chemical vapour deposition (CVD).

In CVD process, precursor is delivered into a reaction chamber at a suitable determined temperature. As they pass through a rector this precursor (in gaseous phase) come into contact with a heated substrate. It can react and form a solid layer deposited onto the surface of the substrate. Usually, an inert gas, such as Ar or N_2, is used as a diluting gas. The depositing temperature and pressure are the critical parameters. Whole process can be summarized as follows:

- Mass transport of precursor (in gas phase) to environs of substrate
- Diffusion of gaseous reactant through the boundary layer to the substrate surface or homogenous chemical reactions to form intermediates
- Adsorption of reactant species or intermediates on substrate surface
- Surface migration, heterogeneous reaction, creation of layers on the substrate surface, formation of by-product species
- Desorption of by-products from the substrate
- Diffusion of by-products to the bulk gas
- Transport of by-product gaseous species away from reaction chamber (exhaust)

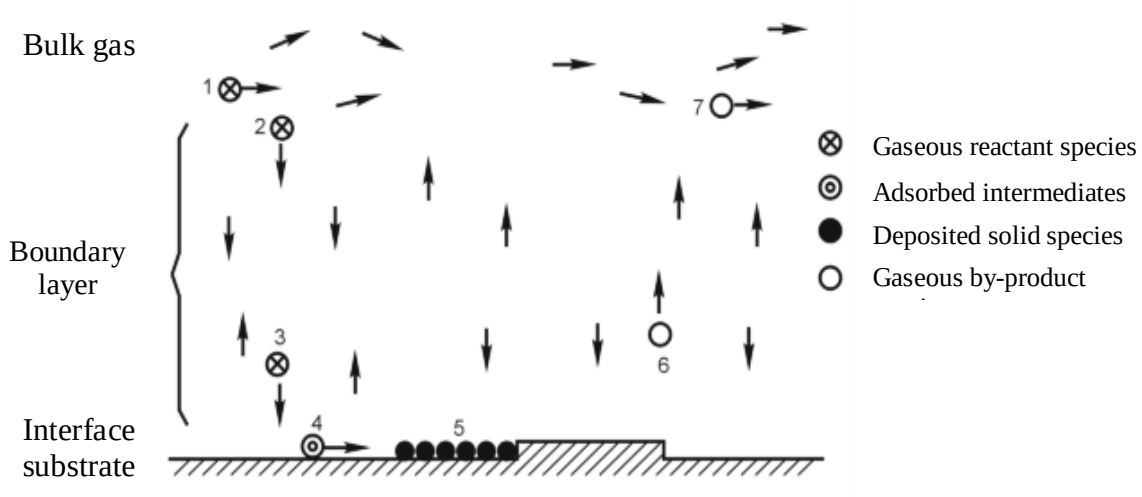

Fig. 15 *Model of CVD process*[91]

CVD method carries a lot of advantages but also many disadvantages. The main advantages are:

- Possibility of formation of uniform thickness layers
- Possibility of using quite wide range of chemical precursors
- This method requires relatively low deposition temperature
- Ability to control the crystal structure, stoichiometry, surface morphology
- It is also possible prepare epitaxial film

To main disadvantages belong:

- Precursors are usually reactants which are extremely toxic, corrosive, explosive and also quite expensive
- By-precursors can be also very explosive, flammable, toxic and it is necessary their trapping and their treatment before being released to the atmosphere

CVD methods are generally classified and categorized into seven main types of fabrication. The parameters used to characterize a CVD process include temperature, pressure, wall/substrate temperature, precursor nature, depositing times, gas flow state and activation manner.[92, 93]

Table 2 *Classification of CVD methods*

Chemical vapour deposition	Temperature	Low-temperature CVD
		High-temperature CVD
		Ultra-high-temperature CVD
	Pressure	Atmospheric pressure CVD
		Low-pressure CVD
		Ultra-high-vacuum
	Wall/substrate	Cold-wall CVD
		Hot-wall CVD
	Precursor nature	Inorganic CVD
		Metal organic CVD
	Depositing time	Continuous CVD
		Discontinuous CVD
		Pulsed CVD

	Gas flow state	Open CVD
		Closed CVD
	Activated manner	Thermal CVD
		Laser-induced CVD
		Plasma-enhanced CVD
		Photo CVD
		Combustion CVD
		Catalyst-assisted CVD

Low-temperature CVD (around 300 °C) is mainly used for creation of layers where the substrate is not stable at higher temperature. High temperature CVD (usually in the range above 1000 °C) is predominantly in this technique. Ultra-high temperature CVD techniques were developed for the single-crystal epitaxial growth of semiconductor materials.

Pressure has a considerable effect on the deposition rate and quality of the finished products, in term of coating thickness uniformity. Mainly for CVD purpose is used low-pressure (low vacuum or medium vacuum).

Only the substrates are heated in a cold-wall CVD, the wall of the reactor is colder. Therefore, the deposition mainly occurs on the heated substrate, and negligible deposition takes place on the walls of the reactors. This type of reactor is usually used for continuous deposition. In the other side, hot-wall CVD reactors represent one of the major categories of CVD reactors. In general, hot-wall reactors have the advantages of being able to process a large number of substrates and having good process parameter control.[91]

In terms of the process time control, CVD can be divided into three categories. Discontinuous CVD is used in most CVD processes, whereas continuous CVD is extensively used for fiber coating and high-volume production of semiconductors devices.[91]

CVD can be performed in a so-called “closed” or “open” system. In “closed” CVD, both reactant and products are recycled for refuse within an enclosure.[94] The “closed reactor” is primarily used for metal purification and protection coating for aero-engine blades. In most cases, CVD happens in an open state.[91]

CVD can also be classified according to activation methods. Thermally activated CVD processes are initiated only with the thermal energy of resistance heating or by infrared radiation. In some cases enhanced CVD methods are employed, which includes plasma enhanced CVD (PECVD) laser-induced CVD (LCVD), photo CVD (PCVD), catalysis-assisted CVD and so on.

Methods of deposition include electrostatic spray[95] or ultrasonic-assisted hydrolysis[96] and pyrolysis reaction such as diffusion flame[97], thermal plasma[98], ultrasonic spray[99] and laser-induced pyrolysis[100]. All of these methods have been found to influence the final product in

terms of size, orientation and crystalline structure[101] however samples obtained from CVD/PVD often required further annealing in order to increase the crystallinity.

Large number of precursors can be used for CVD method. Criteria for suitable chemical precursor are followed:

- Low vaporization and sufficient volatility
- High stability at relatively low temperature
- High safety
- Low cost

Gaseous, liquid and also solid precursors can be used for CVD technique.

- Gaseous precursors can be dangerous therefore it is necessary to dilute them with other inert gases to avoid safety problems. But it is also very important to ensure that there are not any chemical reactions between the gaseous precursors and all components to minimise corrosion effect.
- Liquid precursors must be heated to a proper temperature for vaporization and transported to the reaction chamber by a carrier gas. The usual carrier gas used for the CVD processes is H_2 because of its low density and viscosity for better flow behavior.
- Solid precursors exhibit some problems because they have to be heated to their vaporization temperature, which may be relatively high in some cases.[91]

2.3.2.2 Wet-coating techniques

Spin-coating

Spin-coating is a process used to apply uniform thin films to flat substrates. This method is very simple where an excess amount of precursor solution is placed on the substrate. Consequently the substrate rotated at a high speed to spread the fluid by centrifugal force and create of wet films. The thickness of the final film depends on the angular velocity of substrate rotation, concentration and viscosity of precursor and evaporation rate. Range of thickness which can be created by this method is from 100 nm to 200 μm.[102]

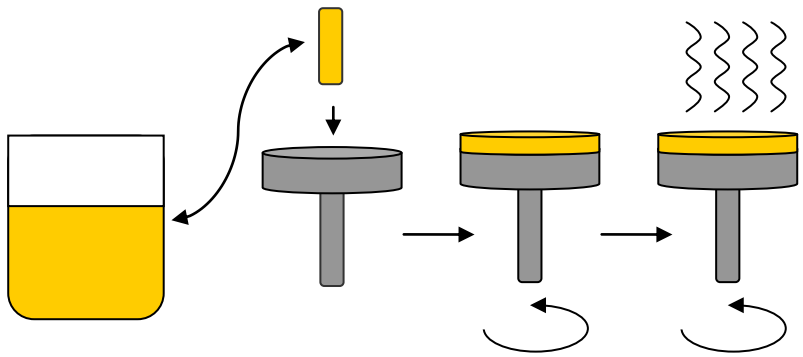

Fig. 16 *Spin-coating*

Dip-coating

During the dip-coating process, a substrate is dipped into a liquid coating solution and then its is withdrawn from the solution at a controlled speed. The thickness of coated films generally increases with higher withdrawing speed. The thickness is determined by the balance of forces at the stagnation point on the liquid surface. A higher withdrawing speed pulls more liquid up onto the surface of the substrate before it has time to flow back down into the solution. The thickness of prepared films depends on viscosity and density used sols and on surface tension.

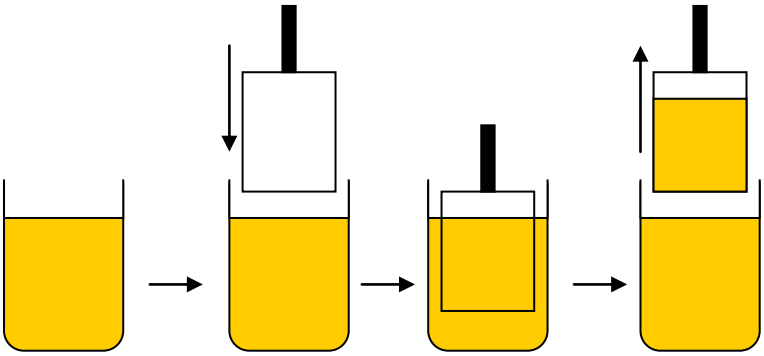

Fig. 17 *Dip-coating*

2.3.2.3 Material printing

Up to this date, material printing has become another very important and very popular method of coating. For this purpose, a conventional inkjet printer can be used. During the coating small droplets of low viscosity ink are ejected from a print head and fall onto printed substrate. The movement of the printed head and the substrate is precisely controlled by computer, also the volume of eject droplets and their loading per unit area can be changed by the computer. The printer and also prepared sol of precursor have to fulfil certain requirements in order to be employed as a thin layer deposition tool. The printer has to be able to handle rigid media so that solid materials can be used as layer support. The precursor must be of a very low viscosity (less than 20 mPa·s) to prevent damage of the printer. If solid particles are present in the precursor, their diameter has to be well below the print head nozzle diameter and their aggregation must be prevented. Despite these limitations, inkjet printing has been successfully used for the deposition of a wide variety of functional liquids so far, such as conducting polymers, metallic nanoparticles dispersion, etc.[103]

One of the inherent advantages of this method is the possibility of direct control the amount of the deposited sol by changing the grey-scale level of the printed image. In the case of inkjet printing, a combination of amplitude modulation screening and frequency modulation screening is used: ink droplets of varying size are placed at different pitch.[104]

The second possibility how to create the thin layer of TiO_2 by material printing is using a specialized device, such as the Dimatix material printer (Fig. 18). This printer allows deposition of liquid materials on A4 substrate, utilizing disposable piezo inkjet cartridge. This printer can create and define patterns over an area of about 200×300 mm and handle substrates up to 20 mm thick with an adjusted Z height.[105]

The temperature of the vacuum platen, which secures the substrate in place, can be adjusted up to 60 °C. Holder of print head can be turned in the range from 0° to 90°. It allows continuous changing of print resolution (from 100 dpi to 5080 dpi). The mechanical movements are extremely precise and they enable very precise work (resolution 5 μm) and reproducibility of printing.[106]

The Dimatix material printer offers a variety of patterns by employing a pattern editor program. Additionally, a waveform editor and a drop-watch camera system allows the manipulation of the electronic pulses to the piezo jetting device for optimization of the drop characteristics as it is ejected from the nozzle. There is a built-in cleaning station with a program editor that includes an automatic capping mechanism. This system thereby enables easy printing of structures and samples for process verification and prototype creation.[105]

Fig. 18 *Commercial inkjet printer Epson R220 and Dimatix material printer 2800*

2.4 Principles of characterization techniques

2.4.1 Ultraviolet-visible spectroscopy

Ultraviolet-visible spectroscopy (UV-VIS) is a method based on the absorption of certain portion of light from ultraviolet or visible range (from 200 to 800 nm) by transmissive samples. This method is used in analytical chemistry for the quantitative determination of different analytes. Determination is usually performed in solutions, but measurement of solid samples is also possible.

The UV-VIS spectrophotometer is employed to measure the amount of light that sample absorbs. It uses two light sources; a deuterium lamp for ultraviolet light and a tungsten lamp

for visible light. The light beam passes through a group of slits and mirrors, after that it slits into two beams. One of the beams is allowed to pass through a reference cuvette with solvent and the other passes through the sample cuvette. The intensity of the light beams is then measured at a detector.

Absorbance, transmission or reflection can be measured by this method. Spectrophotometer equipped with an integration sphere is usually used for transmission and reflection.

The degradation rate of different compounds in consequence of presence of TiO_2 can be studied by absorbance measurement and subsequently the photocatalytic activity of titania samples can be evaluated. The band gap energy of prepared TiO_2 can be investigated by reflectance measurement.

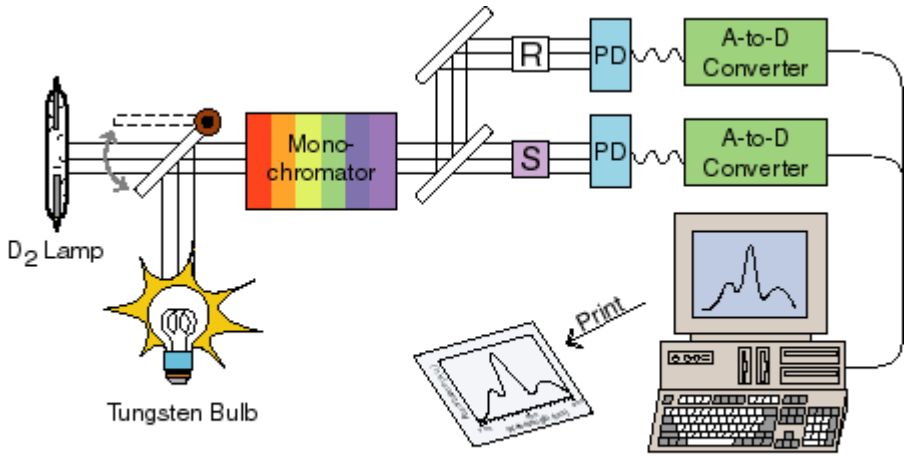

Fig. 19 *UV-VIS spectrophotometer*[107]

2.4.2 Scanning electron microscopy

The scanning electron microscopy (SEM) is a method which uses a focused beam of high-energy electrons to generate a variety of signals on the surface of solid specimens. Accelerated electrons in SEM carry significant amount of kinetic energy. This energy is dissipated as a various signals produced by electron-sample interactions when the incident electrons are decelerated in the solid samples. The types signals produced by SEM include secondary electrons (which produced SEM images), back scattered electrons (BSE), diffracted back scattered electrons (EBSD that are used to determined crystal structures and orientation of minerals), photons (characteristic X-rays which are used for elemental analysis and continuum X-rays), visible light (cathodoluminiscence CL) and heat.[108]

Secondary electrons and back scattered electrons are commonly used for imaging samples. The secondary electrons are the most important for showing morphology and topography on samples. On the other hand, back scattered electrons are the most valuable for illustrating

contrast in composition in multiphase samples. X-ray generation is produced by inelastic collision of the incident electrons with electrons in discrete orbitals of atoms in the sample.

The advantages of this method are:

- It is a non-destructive method
- X-rays generated by electron interactions do not lead to volume loss of sample
- It is possible to analyze the same materials repeatedly

Scanning electron microscopy gives the information about the surface morphology, chemical composition, crystalline structure and orientation of materials making up the sample. The particle size or thickness of TiO_2 layers can be also studied by this method. The thickness in the range 2–1000 nm[109] can be measured by SEM.

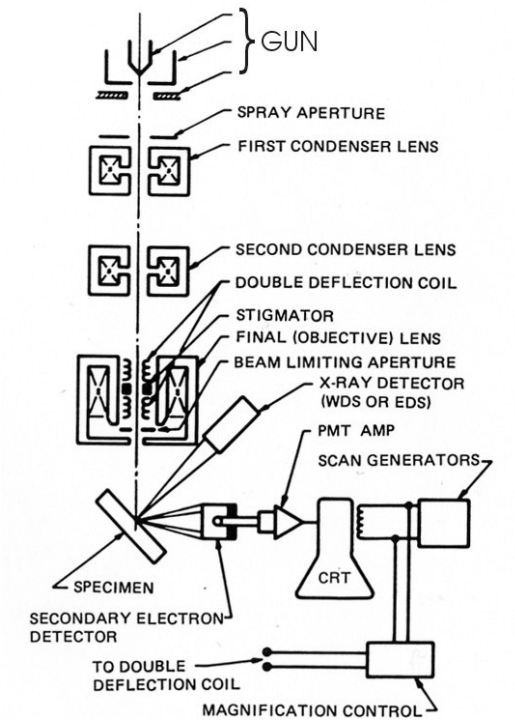

Fig. 20 *Scanning electron microscopy*

2.4.3 Atomic force microscopy

Atomic force microscopy (AFM) belongs to the group of scanning force microscopy techniques, a group of techniques which are based on the measurement of the different forces (as attractive, repulsive, magnetic electrostatic, Van der Waals) between a sharp tip and the sample surface. Imaging is accomplished by measuring the interaction force via deflection of a soft cantilever while raster-scanning the tip across the surface. Signal in AFM is essentially based on interaction repulsive forces which are of extreme short range nature.[110]

The most common operating modes of AFM are contact, noncontact and tapping. In contact mode AFM, there is a repulsive force between the sample and tip (ca. 10^{-9} N);

the piezoelectric response of the cantilever either raises or lowers the tip to maintain a constant force. Noncontact AFM overcomes the frictional and adhesive forces between the tip and sample by hovering the tip a few Angstroms above the surface. In this mode the attractive Van der Waals forces between the tip and surface are monitored. Because these attractive forces are much weaker than those generated in contact mode it leads to lower resolution. During tapping AFM, the cantilever oscillation amplitude remains constant when not in contact with the surface. The tip is then carefully moved downward until it gently taps the surface. As the tip passes over an elevated surface feature, the cantilever has less room to oscillate, and the amplitude of oscillation decreases.[111]

Atomic force microscopy (AFM) is used for studying surface morphology especially for the investigation the roughness of TiO_2 thin layers.

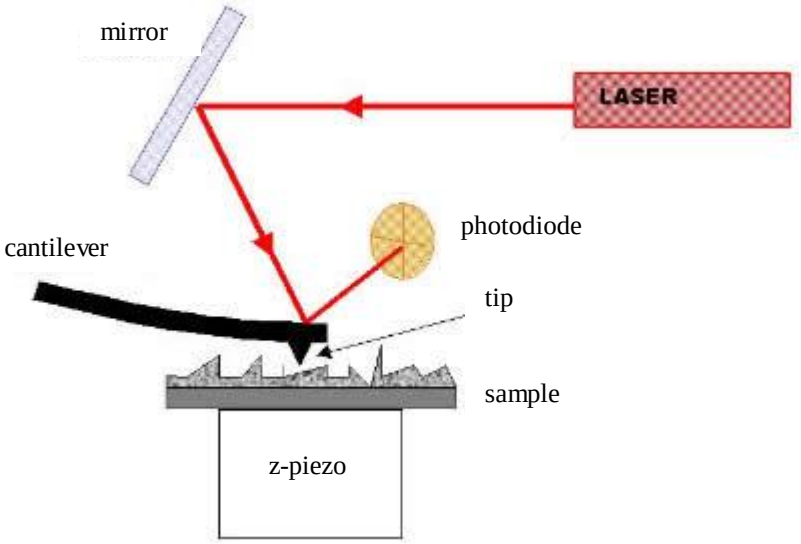

Fig. 21 *Atomic force microscopy*

2.4.4 X-ray diffraction

X-ray diffraction (XRD) is an analytical technique used for phase identification of crystalline material. The analyzed materials are finely ground, homogenized and average bulk composition is determined. This technique is common for the study of crystal structures and atomic spacing.

XRD is based on constructive interference of monochromatic X-rays and a crystalline sample. These X-rays are generated by a cathode ray tube, filtered to produce monochromatic radiation, collimated to concentrate and direct toward the sample. The interaction of the incident rays with the sample produces a constructive interference pattern when conditions satisfy Bragg's Law.

$$n\lambda = 2d \cdot \sin\theta \tag{15}$$

This law relates the wavelength of electromagnetic radiation to the diffraction angle and the lattice spacing in a crystalline sample. These diffracted X-rays are then detected, processed and counted. By scanning the sample through a range of 2θ angles, all possible

diffraction directions of the lattice should be attained due to the random orientation of the powdered material. Conversion of the diffraction peaks to d-spacing allows identification of the mineral because each mineral has a set of unique d-spacing. Typically, this is achieved by comparison of d-spacing with standard reference patterns.[112]

XRD can be used for:

- Identification of unknown crystalline materials (e.g. minerals, inorganic compounds)
- Characterization of crystalline materials
- Determination of unit cell dimensions
- Measurement of sample purity

One of the problems in XRD analyses is that only crystals are detected, while an amorphous part, if present in samples, exhibits no diffractions peaks. Thus, amorphous content must be determined as a rest of crystalline part and therefore precise determination of crystalline contents is necessary.[17]

Sharpness of the peak indicated higher crystallinity of photocatalyst. The width of XRD peak reflects the size of particle. Crystallinity can show us also perfectness of crystals, i.e., higher crystallinity means lesser density of crystalline defects.[17]

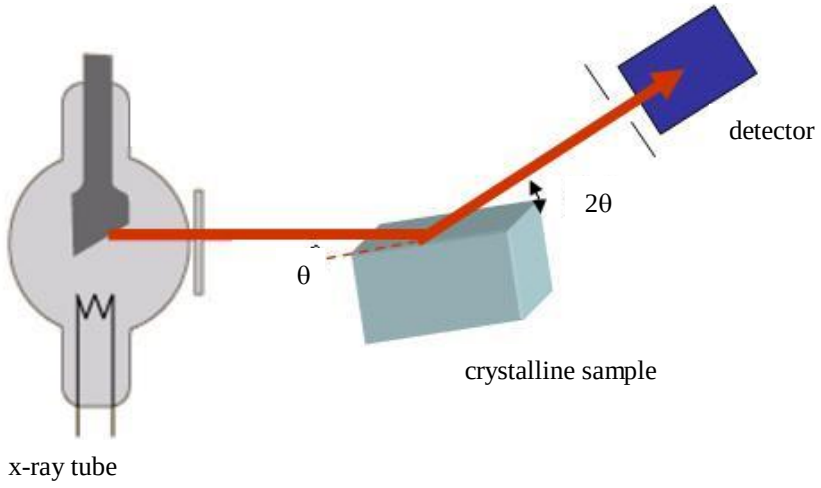

Fig. 22 *X-ray diffraction*[113]

Particle size of a photocatalyst is often evaluated using Scherrer's equation (16) using data of powder X-ray diffraction patterns. Disadvantage of using this equation is that it neglects the effect of crystal lattice distortion. For samples that are expected to have a large degree of distortion, analyses using the Williamson-Hall equation should be carried out.

Scherrer's equation is given bellow (16) where d is size of the particles in the direction vertical to the corresponding lattice plane, B is constant, λ is wavelength of X-ray, β is corrected full width at half maximum (FWHM) of the XRD peak, θ is angle of diffraction.

$$d = \frac{B\lambda}{\beta \cos\theta}, \tag{16}$$

2.4.5 Transmission electron microscopy

A transmission electron microscopy (TEM) is a method where a beam of electrons is transmitted through an ultra thin sample. When these electrons come through the sample they can interact with this sample (e.g., inelastic or elastic scattering, diffraction). If the undiffracted beam is selected to form an image, it is referred to as bright-field imaging; in contrast, selection of strongly diffracting regions of the sample, which would appear brighter than the transmitted beam, is known as dark-field imaging. The electrons could also be absorbed by molecules containing large atoms, or by surface contamination (e.g., dust, grease). The absorption of a high density of electron in a specific region will cause a cumulation of heat, leading to sample destruction and poor image quality.[111]

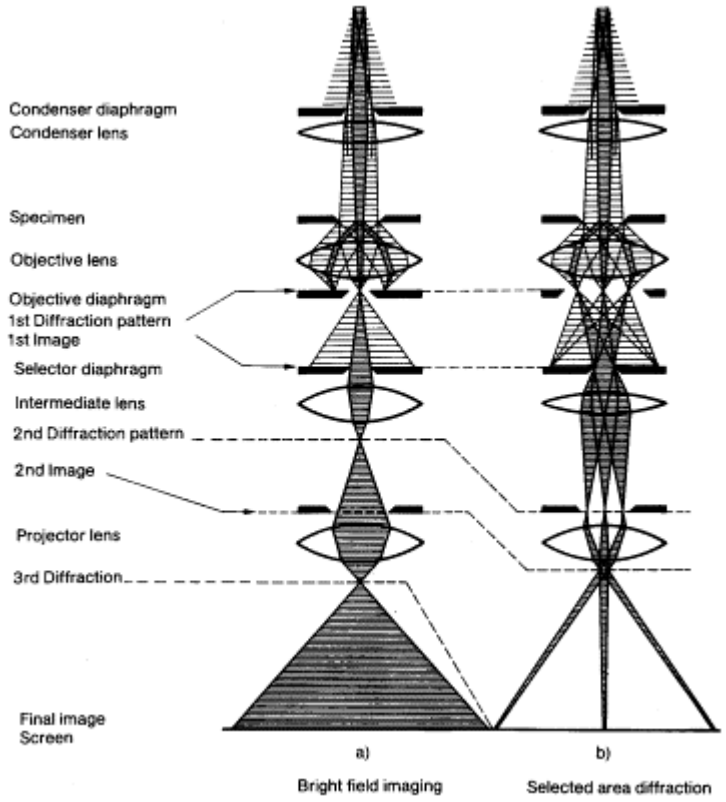

Fig. 23 *Transmission electron microscopy*[114]

TEM has a resolution of about 1 to 100 nm, and it can thus provide very detailed structural information on materials, even down to the molecular level. TEM specimen need to be very thin in order to transmit electron beams through the sample. Normally, the specimens are placed on copper grids or carbon-coated copper grids and viewed through the holes in the grid. The advantage of TEM is that it can be rapidly adjusted to provide an electron diffraction pattern from a selected area, facilitating the investigation of crystal structure and orientation and enabling particular morphological features to be identified.[115]

The quality of image depends on thickness of sample and on energy of the electron beams. Generally, increasing the thickness of a sample, or decreasing the energy of the electron beam, will induce more scattering events through more effective interactions between the electron beam and atoms of sample. This effect will enhance image contrast, since there is a larger deviation between the path lengths of transmitted and scattered electrons that reach the viewing screen.[111]

This method can be used for investigation of particle size and shape. Also it is very useful for studying of aggregation.

2.4.6 Photon correlation spectroscopy

Photon correlation spectroscopy (PCS) is a light scattering technique for studying the properties of suspensions and colloidal solutions. It is absolute, non-invasive and non-destructive method. Colloidal sized particles in a liquid undergo random Brownian motion owing to multiple collisions with thermally driven molecules on the liquid. The scattered light intensity from these diffusing particles will fluctuate in time, thus carrying information about the diffusion coefficient of the particles.[116]

This method can be used for measurement of sub-micron particle sizes, diffusion coefficients, viscosities, and molecular weights of polymers. The device measures a rate of diffusion of particles through the solution (liquid) and from this measurement, the particles size can be determined. The samples are illuminated by a laser beam and scattered light is investigated. Generally, with increasing particles size the intensity of light scattering decreases.

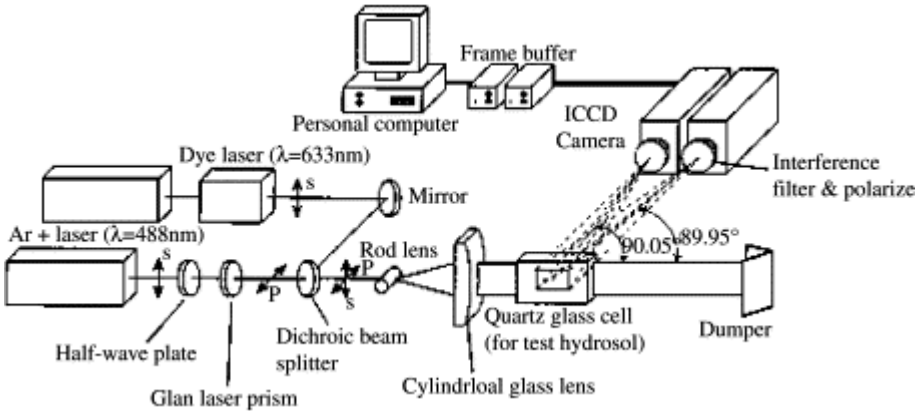

Fig. 24 *Principle of photon correlation spectroscopy*[116]

2.5 Superhydrophilic properties

When a drop of fluid is placed on the top of a perfectly smooth solid surface, there are two competing effects. The interactions with the solid substrate may make it energetically favourable for the drop to spread so that it wets the surface. However, spreading increases the area of contact between the fluid and the vapour. This increases the surface tension energy

between the drop and the vapour and can destabilize the wetting films. When the interaction with the solid surface (e.g., favouring the liquid-solid interface over the vapour-solid interface) dominates, a complete wetting occurs and when the surface tension term dominates, a partial wetting occurs (Fig. 25).[117]

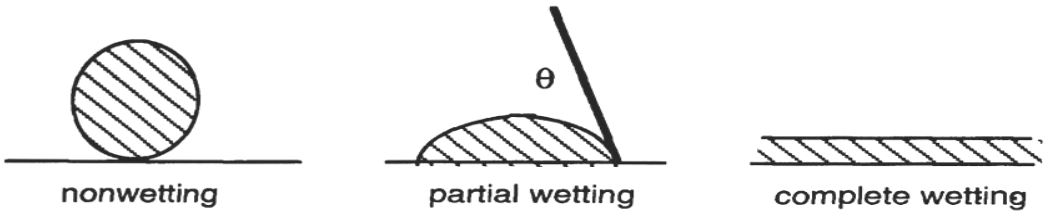

Fig. 25 *Illustration of a droplet placed on a solid substrate*

Wetting is characterized by contact angle θ which is specified for any given system. The shape of the droplet placed on the solid surface is determined by the Young's equation (17), where γ are surface tensions between three phases. This equation relates the surface tension between the solid surface, liquid droplets, and surrounding air to the contact angle between the water / air interface and the solid (Fig. 26).

$$\gamma_{sv} - \gamma_{sl} = \gamma_{lv} \cdot \cos\theta \tag{17}$$

Water droplets consequently assume a cap-like shape when sitting on a solid substrate. Smaller contact angle means flatter droplets and larger water surface. Large contact angles bring about reducing areas at the liquid / solid interface, and the substrate is not wetted as easily.[118]

Two extreme situations can happen, when the contact angle either tends to zero, we call this surface superhydrophilic, or when the contact angle approaches 180°and this situation occurs when the surface is superhydrophobic. Water coming into contact with a superhydrophilic surface spreads out and forms a thin film, while on the superhydrophobic surface, water forms into spherical bead-like drops, minimizing the solid / liquid contact area.

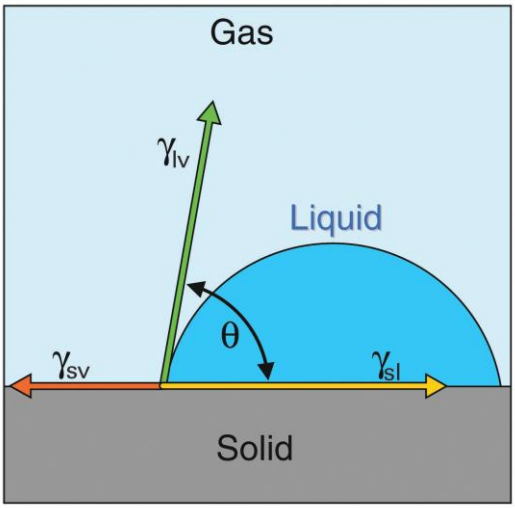

Fig. 26 *Wetting of solid surface according to Young's equation*

The photoinduced superhydrophilicity of TiO_2 thin films in which H_2O droplets are able to spread out to form H_2O layers under UV light irradiation was discovered in 1997.[119] It was found that if a TiO_2 film is prepared with a certain percentage of SiO_2, it acquires superhydrophylic properties after UV illumination. In this case, electrons and holes are still produced, but they react in a different way. The electrons tend to reduce the Ti(IV) cations to the Ti(III) state, and the holes oxidize the O^{2-} anions. In the process, oxygen atoms are ejected, creating oxygen vacancies. Water molecule can then occupy these oxygen vacancies, producing adsorbed OH groups, which tend to make the surface hydrophilic. The longer the surface illuminated with UV light, the smaller the contact angle for water becomes.[1]

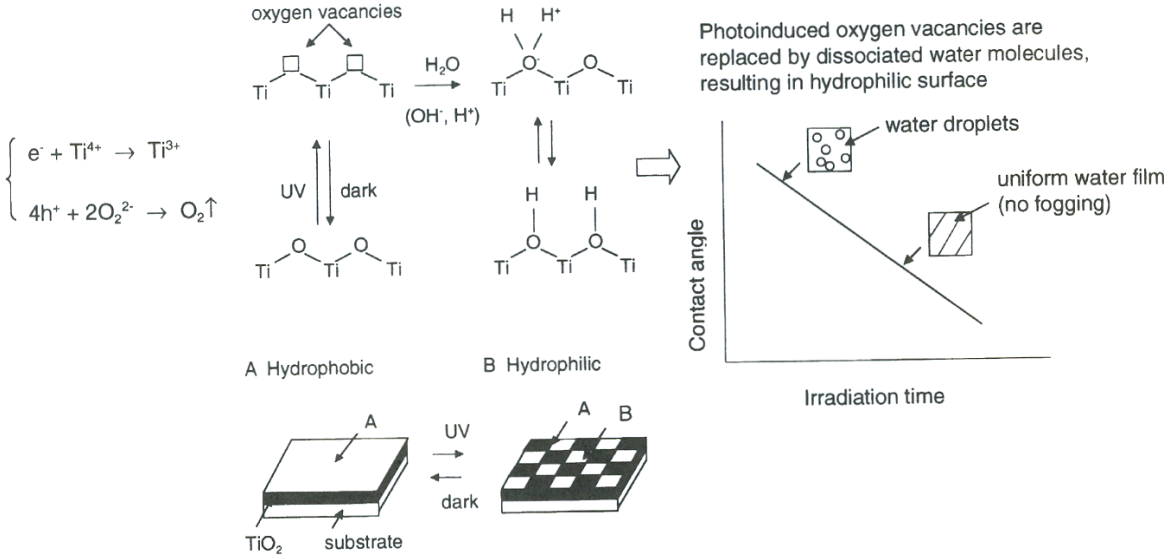

Fig. 27 *Mechanism of photo-induced hydrophilicity*

2.6 Photodegradation of water pollutant

Wastewater treatment is a very important for the removal of organic pollutants. Large amount of organic pollutants consumed in the industries are being released into the eco-system and constitute a serious treat to the environment. As chemical and agricultural wastes, these contaminants are frequently carcinogenic and toxic to the aquatic system because of their aromatic ring structure, optical stability and resistance to biodegradation. In past decades, the traditional physical techniques for the removal of organic pollutants from wastewaters have included adsorption, biological treatment, coagulation, ultrafiltration and ion exchange on synthetic resins.[120, 121] Those methods have not always been effective and they may not actually break down the pollutants in wastewater. For example, adsorption technology does not degrade the contaminants, but essentially transfers the contaminants from one medium to another, hence, contributing the secondary pollution. Moreover, such operations are expensive because the pollutants are treated before the adsorption process while the adsorbent medium has to be regenerated for reuse.[120] Traditional biological treatments are often ineffective in removing and degrading pollutants because the molecules, being mostly aromatic, are chemically and physically stable. Hence, biodegradation of organic pollutants is usually incomplete and selective.[122] In fact, some of the degradation intermediates may be more toxic and carcinogenic than the original pollutants.

Heterogeneous photocatalysis has been successfully used in the oxidation, decontamination or mineralization of organic and inorganic contaminants in wastewater without generating harmful by-products. A large amount of chemical substrates that have already been subjected to photodegradation experiments in water with or without auxiliary oxidants or photocatalyst. Many authors presented extensive lists of organic compounds that have been treated according to H_2O_2-UV, O_3-UV and TiO_2-UV procedures. Richard and Grabner[123] published work concerning the photodegradation of phenol and of its derivates in aqueous solution. Phenolic compounds are systematically introduced into the environment via several house-hold and industrial activities. A lot of fungicides, insecticides are based on this structural element. Hence, this class of organic compounds represents big toxicological risk because most of them are water soluble and highly toxic. They were detected in ground water reservoirs. Photocatalytic degradation of phenol derivates represents an alternative method for biological detoxification.[14]

2.6.1 Formic acid

Carboxylic acids occur in natural waters at varying concentrations depending on origin, aqueous solubility, and biological activity. Formic acid has become the most investigated organic molecules on single-crystalline surface. The absorption of formic acid on TiO_2 surface is one of the best examined organic systems at this point.

During the degradation of formic acid, this compound undergoes direct mineralization to water and carbon dioxide without the creation of any stable intermediate species.[124, 125, 126] Moreover, it also represents a possible final step in the photodegradation of more complex organic compounds.[127]

2.6.2 Organic dye

Dyes have relatively large photoabsorption (extinction) coefficients and therefore measurements of their concentrations in solutions are easy even if the concentrations are very low. However, the fact that dyes absorb visible light indicates that a photoreaction might be induced by visible-light photoabsorption (dye sensitization) as well as by photoabsorption of a photocatalyst. [128] Organic dyes are inappropriate as a model compound, particularly for testing visible light-induced photocatalytic activity. There are three reasons for its inappropriate:[17]

- Dye molecules absorb photons, especially in the visible light range, and thus photo-excited electrons may be injected into phootcatalytic particles.
- The absolute molar amount of dye contained in the reaction system can be much smaller than that of solid photocatalysts. The concentration of the dye in the solution should be relatively low since the absorption coefficient is large.
- The mechanism of dye degradation is so complicated that efficiency of the photocatalytic reaction, e.g., quantum efficiency, cannot be measured.

Advantage of using dye is:

- Measuring the consumption (decrease) of a dye during photo-irradiation requires only a spectrophotometer.

If dyes are used as model compounds, care must be taken in the interpretation of experimental results. Photocatalytic degradation of many organic compounds been reported, including noxious compounds such as polychlorobiphenyls (PCB), dioxin[129], dichlorodiphenyltrichloroethane (DDT)[130]. Among them the chlorophenolic compounds have been studied extensively, because these compounds are toxic, water-soluble and used for synthesis of other chemicals.

Many dyes are decolorized and ultimately mineralized by photocatalysis. In the degradation of azo dye, the degradation rate decreases in the order monoazo–diazo–triazo.[131] Three processes including oxidation and reduction are considered to occur simultaneously in the photocatalytic degradation of dye (Fig. 28). The photocatalytic degradation of organic compounds is the first process. Spectral sensitization is the second process. One moiety of dye molecule serves in last process as the electron acceptor, suppressing recombination between electron and positive hole.[1]

1. Oxidation

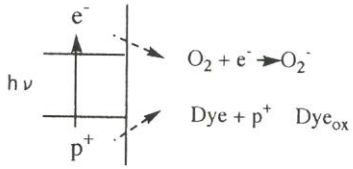

2. Electron injection

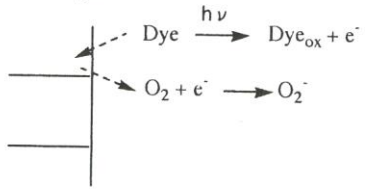

3. Oxidation and reduction

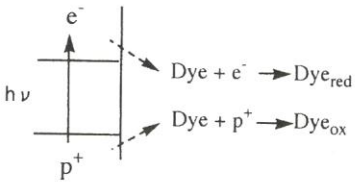

Fig. 28 *Photocatalytic degradation mechanism of dye*

3 AIM OF THE EXPERIMENTAL WORK

The aim of this work is to prepare the thin layers of titanium dioxide on the solid substrates. The preparation of TiO_2 thin layers are performed by two different methods; by materials printing and by chemical vapour deposition. TiO_2 for material printing is prepared by two methods; by sol-gel and by hydrothermal treatment. Photocatalytic activity of all prepared TiO_2 is investigated and the most active samples are evaluated.

Sol-gel method:

Titanium tetraisopropoxide (TTIP) is used as a precursor, acethyl acetone (AcAc) as a chelating agent, and ethanol is used as a solvent in sol-gel preparation. The sol deposition is realized by inkjet material deposition. Different amount of PEG are added to each prepared sol. PEG is used as anti-cracking agent. The influence of different sol loading on physical properties and final photocatalytic activity of prepared TiO_2 thin films is examined.

Hydrothermal treatment:

Titanium oxochloride ($TiOCl_2$) is used as a precursor, KOH as a precipitation agent and water is used as solvent. Hydrothermal synthesis is performed under various conditions. The influence of process temperature and time of hydrothermal treatment on final physical properties of prepared sols is studied. Subsequently, the best conditions of preparation for final activity are evaluated. These sols are deposited onto the substrates by material printing and again the photocatalytic activity of thin titania layers is evaluated.

Chemical vapour deposition

Titanium tetraisopropoxide (TTIP) is used as a precursor and nitrogen is used as carried and also dilution gas. Deposition is performed in cold-wall reactor. The final photocatalytic activity of thin titania layers is evaluated and compared with photocatalytic activity of titania thin film prepared by hydrothermal treatment.

4 EXPERIMENTAL SECTION

4.1 Chemicals

Reactants for preparation of TiO_2 films by sol-gel process:

- Titanium (IV) isopropoxide (p.a.), Fluka, Germany
- Absolute ethanol (p.a.), Penta, Czech Republic
- Acetyl-acetone (p.a.), Lachema, Czech Republic
- Polyethylenglycole 1500 (p.s.), Merck, Germany
- Sulphuric acid (p.a.), Lachema, Czech Republic
- 2,6-dichloroindophenol (A.C.S. reagent), Aldrich, Germany

Reactants for preparation TiO_2 thin films by hydrothermal synthesis:

- Titanium oxochloride
- Potassium hydroxide
- Chloride acid
- Formic acid
- Deionized water
- Tween 20
- Abesone
- CTAB
-

Reactants for preparation of TiO_2 films by chemical vapour deposition:

- Titanium(IV) isoprpoxide (97%), Aldrich, Germany

4.2 Used equipments

- Viscosimeter AVMn (Anton Paar)
- Densitometer DMA4500 (Anton Paar)
- NanoCalc-2000 (Micropack, Germany)
- Inkjet printer Epson R220
- Experimental printer FUJIFILM Dimatix
- Microscope Nikon Eclipse E200
- Camera Nicon D70
- Veeco Di CP-II machine (Dymek, Japan)
- Microscope ATM/STM 5500 (Pico Plus)
- Electron microscope MIRA II LMU, Tescan

- Electron microscope LEO43VP
- Perkin-Elmer Lambda 45 UV/VIS spectrophotometer with an integration sphere (RSA-PE-20, Lambsphere
- UV-VIS spectrophotometer Helios α, Spectronic Unicam
- UV-VIS spectrometer with integration sphere
- Fibre UV-VIS spectrophotometer
- X-ray diffractometer Panalytical X'Pert Pro MPD Current
- X-ray difractometer Empyrean, Panalytical
- X-ray diffractometer SEIFERT
- Contact Angle System OCA, DataPhysic
- Coulter N4Plus
- Transmission electron microscope JEOL JEM 2010
- Chromatograph Varian Prostar
- Magnetic stirring, Lavat MM7
- UV lamp OSRAM HQL 125 W
- Philips Metal-halide lamp HPA 400/30 SD
- Radiometer X 97, 315–400 nm, UV-3701-4, SN-14524, Gigahertz-Optik
- Peristaltic pump PCD 83
- Analytical scale Scaltec, SPB 32
- Calcination furnace

4.3 Sol-gel process

4.3.1 Synthesis of sol

Titanium(IV) isopropoxide (TTIP) was used as a precursor for preparation of TiO_2 by sol-gel method. Firstly, 40 cm^{-3} of absolute ethanol was mixed with 3.8 cm^{-3} of acetyl-acetone. The prepared mixture was added dropwise to 10.3 cm^{-3} TTIP under continuous stirring to control the hydrolysis and condensation reactions. This solution was maintained under stirring for a few minutes to obtain the complex chelate. Subsequently, 45 cm^{-3} of absolute ethanol with 0.69 cm^{-3} of water was added drop by drop to the prepared mixture to start the hydrolysis and condensation reactions. Different amounts of PEG with molecular weight of 1500 (0, 1, 4, 16 $g \cdot dm^{-3}$) were added to form the printing solutions. All prepared mixtures were stored in the darkness at the temperature 5 °C.

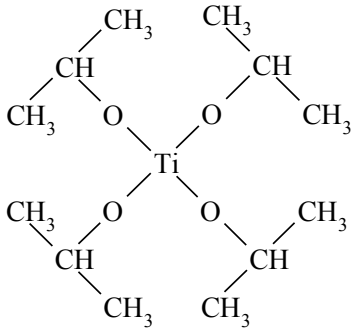

Fig. 29 *Used precursor; titanium(IV) isopropoxide*

4.3.2 Study of viscosity and density

We investigated viscosity and density of all prepared samples. There are important parameters for subsequent deposition by material printing. The viscosity of prepared solutions was measured by automatic viscosimeter AMVn and we observed a viscosity change as the function of present PEG amount. Densitometer DMA4500 was used for densitometry measurement and we observed the same dependence as in previous case. All measurement, viscosity as well as densitometry, were performed at the temperature of 25 °C.

Fig. 30 *Viscosimeter AMVn in combination of densitometer DMA4500*

4.3.3 Substrate pre-treatment

Soda-lime glass plates with size 50 mm × 50 mm × 1.1 mm were chosen as substrates for immobilization of TiO_2 thin layers. Firstly, these substrates had to be pre-treated in sulphuric acid with concentration 50%wt. for 120 minutes to avoid sodium ions diffusion to titania layer. These sodium ions would have caused a reduction of photocatalytic activity. Consequently, these plates were washed in a surfactant solution to remove a dust, grease and other residues, which might have collected during the storage of pre-treated glass plates and finally dried under the laboratory conditions.

4.3.4 Material printing

Sol application was carried out by the new method called material printing. A modified office inkjet printing Epson R220 was used for this purpose. Firstly, all original cartridges were removed and the ink tubing and printhead were purged by anhydrous propanol. This step secures removing of traces remaining aqueous ink. If the sol came in the contact with aqueous impurities, TiO_2 would start to precipitate, which can cause clogging of the printhead nozzles.

Afterwards, the prepared sols were filtered through 0.45 μm mesh size syringe filter into one of the ink cartridges, the others remained empty. This cartridge was installed to into the printer to the black ink position. Consequently, a series of head cleaning was performed to obtain a perfect nozzle check pattern. This check patterns had to be observed under UV-A light source because the sol is essentially color less when observed under daylight. Under UV-A light sol appeared yellow while the paper was bright blue because of the fluorescent brightening agents present in the paper.

Fig. 31 *Used inkjet printing Epson R220 with modified CD holder*

Subsequently, glass substrates were mounted into a modified CD holder (Fig. 31), fed into the printer and printed with "black only" drives setting. It means that only the ink from the "black" cartridge which is now filled by TiO_2 sol was utilized for printing. One of the main advantages of this technique of coating is the possibility to direct control the amount

of the deposited sol (i.e. the sol loading) by changing the grey–scale level of printed image (Fig. 32).

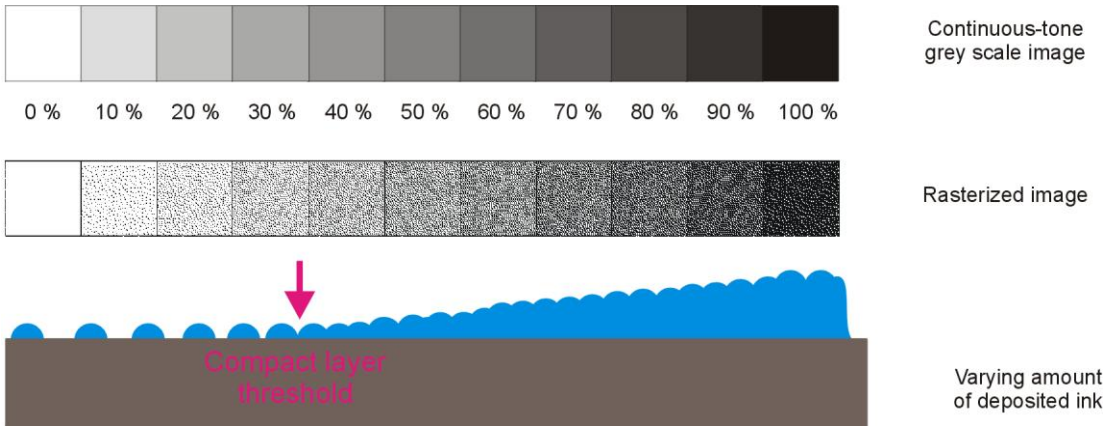

Fig. 32 *Layers build-up for different sol loading*[104]

In this figure (Fig. 32) we can observe the creation of printed layer. Different grey levels need to be converted into a halftone screen patter. In the case of inkjet printing, a combination of amplitude modulation screening and frequency modulation screening is used. Ink droplets of varying size are placed at different pitch. The printed substrate can be completely covered by sol because the printed droplets spread on the surface and have much larger diameters than diameter of eject droplets which roughly correspond to the nozzle diameter. In this work, we used three levels of sol loading (100%, 90% and 80%).

Before the printing we needed also choose from three modes of the printer operation available: "Slow, Medium and Rapid". For our purpose we chose mode "Rapid". In this mode, the printhead runs very quickly above the glass surface and it prints continuously in both directions. Because the motion of the printhead and the sol deposition is very fast, the evaporation of the printed solution takes after the printing phase is finished. Hence, in this way smooth and glossy layer of TiO_2 can be obtained.

All deposited glass plates were placed into an oven and dried at the temperature for 30 minutes and subsequently they were thermally treated in a calcination furnace at the temperature 450°C for 4 hours with the ramp of 3°C/min.

4.3.5 Characterization of TiO_2 thin layers

4.3.5.1 Thickness measurement

The thickness of prepared titania layers was determined by specular reflectance measurement using NanoCalc-2000. This method can be used for transparent as well as for semi-transparent films. The technique is based on the evaluation of how the layer interacts with light and we can measure the films with thickness in the range from 10 nm to 250 μm. The main advantages of this method are accuracy, high speed, simplicity, non–destructive

approach and no need of sample preparation. Each TiO_2 film was measured ten times and consequently, the average value was calculated.

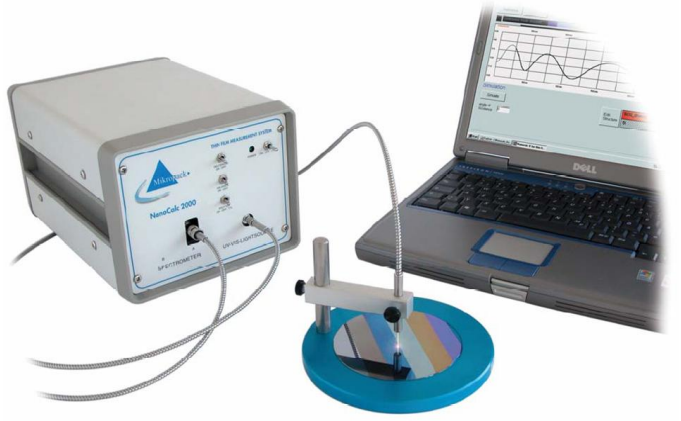

Fig. 33 *NanoCalc-2000 for measurement thickness of titania layers*

4.3.5.2 Optical microscopy

The quality of prepared layers was investigated by optical microscope Nikon Eclipse E200. The images were obtained from a digital camera Nikon D70 mounted on the optical microscope. The influence of the PEG and the sol loading on cracking intensity was evaluated from the optical images. The camera parameters were adjusted follows; exposure program of Aperture priority, ISO 400, chromatic temperature of 2800 K, white balance in auto mode. Microphotographs were obtained with magnification ten times.

4.3.5.3 Scanning electron microscopy

The surface topology was studied by scanning electron microscopy using electron microscope MIRA II LMU, Tesan. The size of primary crystals as well was film thickness was also evaluated by this method.

4.3.5.4 Atomic force microscopy

Apart from the scanning electron microscopy, there are others methods which can be used for the study of surface topology. One of them is atomic force microscopy. Topology of the samples was investigated by Veeco Di CP-II machine. Generally, AFM analysis can be performed in three different modes; contact, noncontact and tapping. Our analysis took place in tapping mode.

4.3.5.5 Photoinduced hydrophilicity

The photoinduced hydrophylicity was examined by the contact angle measurement of water droplets placed onto the titania layers. This determination was performed on the OCA20 by applying a sessile drop method. After the creation of droplet its evolution is recorded by a CCD camera and the contact angle was obtained by the processing the tangent method. The volume of the deposited droplets was 5 μL and the droplets were recorded in the 10 seconds after the creation. We studied freshly prepared glass as well as the glass stored

in the darkness for 10 days and we evaluated the changes in the hydrofilicity of these titanium dioxide thin films.

Subsequently, the photoinduced hydrophilic conversion was investigated using UV irradiation. A high pressure mercury lamp (OSRAM HQL 125 W) was used for this purpose and the intensity of irradiation was 15 W/cm^2. The contact angle of water droplets on the irradiated layers was measured in the 1, 3, 5 and 10 minutes. Every time five droplets were deposited and the average of found values was calculated.

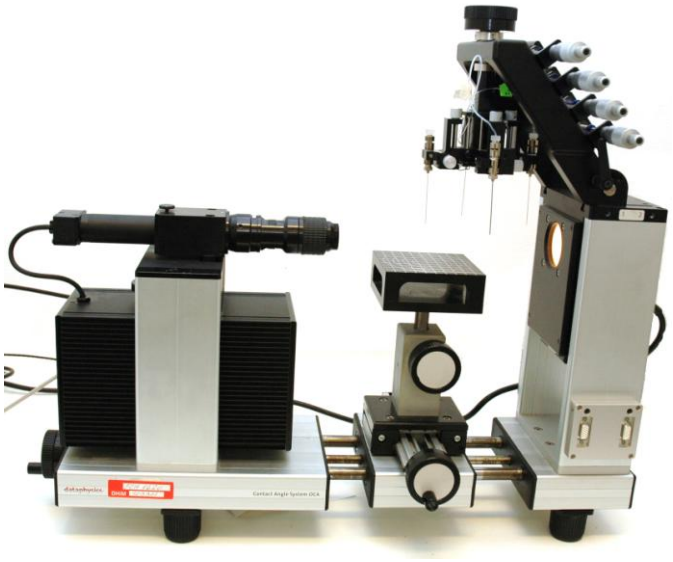

Fig. 34 *Apparatus for contact angle measurement OCA 20*

4.3.6 Photocatalytic activity

Photocatayltic activity was studied as a degradation rate of 2,6-dichloroindophenol (DCIP) with initial concentration 2×10^{-5} mol·dm^{-3}. The experiments were performed in a reactor consisting of two beakers, which were connected by peristaltic pump. Total volume of the degradated solution was 150 cm^3. The samples were placed in one of the beaker and the other beaker was used as a storehouse for DCIP solution (Fig. 36). UV irradiation was provided by the high pressure mercury lamp (Osram HQL 125W). The distance of the lamp from the samples was the same during all experiments. The intensity of irradiation was 10 W·m^{-2} and X97 irradiance meter with X9-7 probe was used for this measurement. The emission spectrum of used lamp is shown in Fig. 35.

Each sample was irradiated for 10 minutes to activate the photocatalyst before reaction. Immediately after the filling of a reactor by DCIP, the beaker was covered by a water cell to block IR radiation. Required amount of reaction solution (2 cm^3) was sampled every 5 minutes for UV-VIS analysis. Total duration of the experiments was 30 minutes. This time was enough for complete decolorisation of the reaction solution.

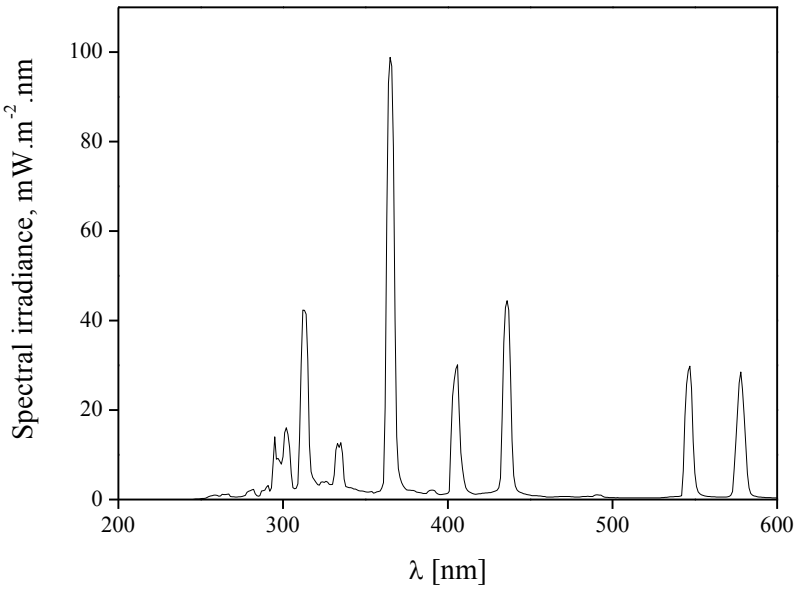

Fig. 35 *Emission spectrum of used UV lamp*

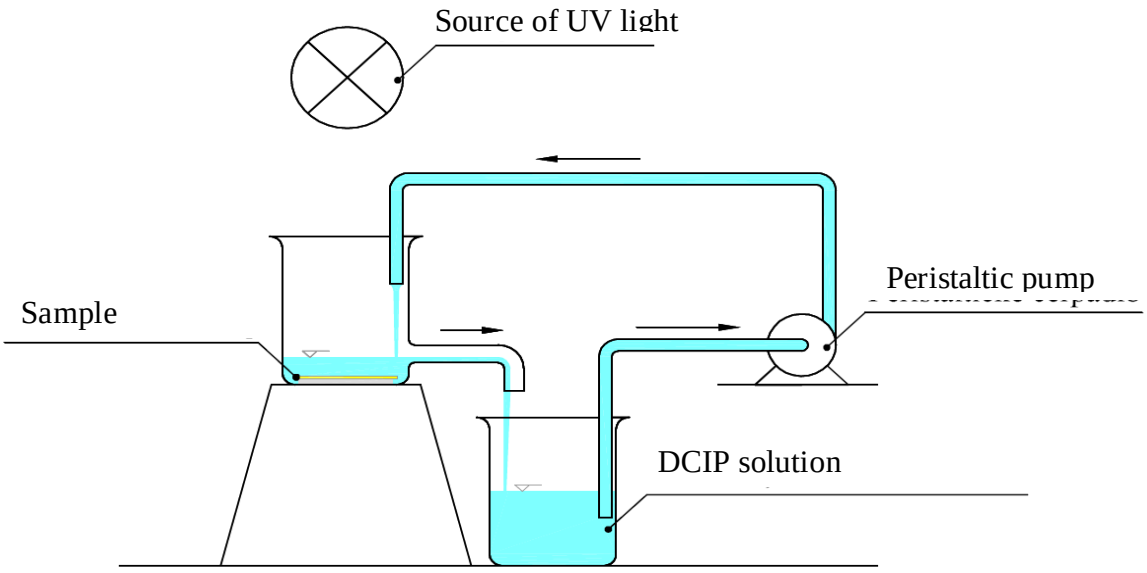

Fig. 36 *Arrangement of photocatalytic reactor*

4.4 Hydrothermal synthesis

The main goal of this work is to compare final properties, particularly the photocatalytic activity, of titanium dioxide prepared by different methods. In the first part, we dealt with printed thin films of TiO_2 prepared by the sol-gel method. Now, we concentrate on the preparation of colloidal titanium dioxide by hydrothermal synthesis. We studied the influence of different process conditions and different pH on physical properties and photocatalytic activity of prepared colloidal titania slurry.

4.4.1 Synthesis of colloidal TiO_2

Titanium oxo-chloride ($TiOCl_2$) was used as a precursor for preparation the colloidal suspension of TiO_2. This compound was added dropwise to an aqueous solution of KOH (with concentration 5 $mol \cdot dm^{-3}$) until neutral reaction of the resulting mixture. Consequently, the mixture was washed by deionised water to remove excess chloride ions. Prepared and washed mixture was diluted to 400 cm^3. We used 50 cm^3 of this solution with 50 cm^3 KCl (0.006M) for hydrothermal synthesis. This amount of potassium was evaluated in previous work as the best for photocatalytic activity. Finally, we added required amount of KOH (with concentration 1 $mol \cdot dm^{-3}$) to achieve the required basic pH (10) or HCl to reach acid pH (2). TiO_2 mixtures prepared by this way were hydrothermally treated under different conditions. We changed the time and temperature of the treatment. Synthesis took place for 6 hours, 24 hours or 48 hours and temperature of the process was 110 °C or 160 °C.

4.4.2 UV-VIS spectroscopy

Optical characterization of TiO_2 colloidal suspension was accomplished using UV-VIS spectrometer with an integration sphere with diameter of 5 cm. The system consists of two lamps. One of them was a deuterium lamp for UV region and the other a tungsten lamp for visible region. The measurement was performed in the range of 200–800 nm. The spectra of total and diffused reflectance and transmission were recorded under the following parameters: data interval of 1 nm, scan speed of 240 $nm \cdot min^{-1}$, smooth of 2 min, slit of 4 nm and lamp change at 326 nm. The measurement was performed in 0.1 cm cuvette. The principle of transmission a reflectance measurement is explained in Fig. 37.

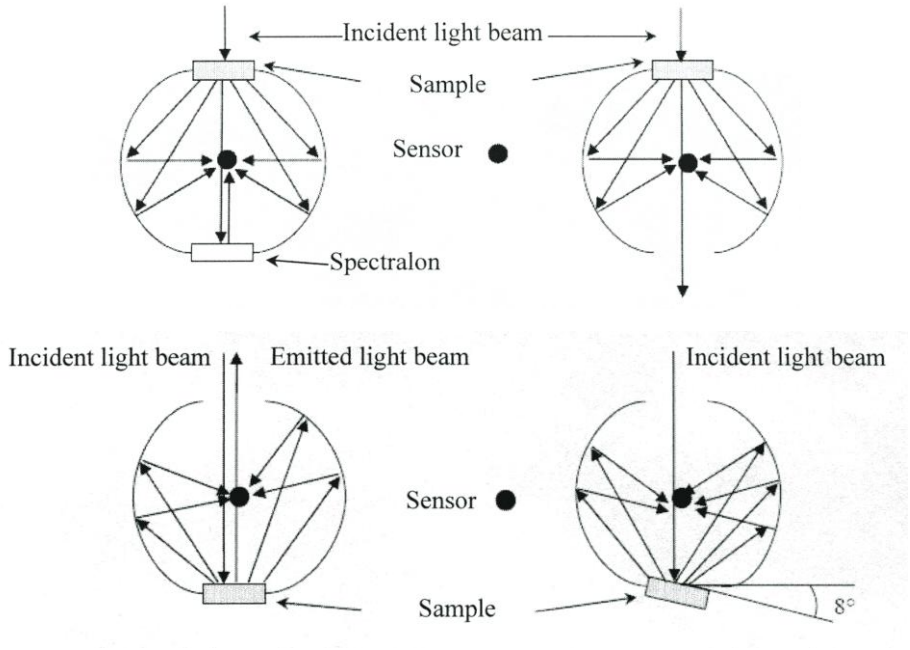

Fig. 37 *Principle of transmission and reflectance measurement, total and diffused transmission (top), diffused and total reflectance (bottom)*

- Total transmission: Opposite the sample there is a spectralon situated, the surface of which reflects transmitted light. Incident light beam goes through the sample which causes scattering of the beam. The sensor, placed in the middle of sphere, receives the sum of all transmitted light.
- Diffused transmission: Position of the sample is the same as in the previous case but contraty to the total transmission configuration there is no spectralon. It means that sensor receives diffused light beam collected by the sphere only.
- Total reflectance: During this measurement the sample is inclined at 8°which allows the inclusion of specularly reflected beam in the sphere. So the sensor receives the sum of all reflected beams (diffused and specular).
- Diffused reflection: In this case, sensor receives only the beams diffused by the reflection from the sample. Specular reflected beam is emitted by the orifice.

We measured the total transmission and total reflectance of all prepared samples and subsequently we calculated the absorptance of the TiO_2 according the following formula (18), where T (residual) represent the residual light of the source due to the dispersion..

$$A(\%) = 100 - T(\text{tot.}) - R(\text{tot}) - T(\text{residual}) \quad (18)$$

4.4.3 Gravimetric analysis

This method was used for the investigation of titania concentration in the solutions and also for the studying stability of these TiO_2 slurries. We took 5 cm^3 from each sample and

weighted it. Then this amount was dried to constant mass and we calculated the amount of TiO_2 in used volume.

Consequently, we also evaluated the stability of prepared samples by this method. We measured the concentration immediately after the sample's preparation and then after 1 day staying at rest. After this time we could observe certain concentration decreasing which was calculated. The extend of this decreasing provides us the information about the stability of prepared samples.

4.4.4 X-ray diffraction

The crystalline phase composition of prepared samples was investigated by single–crystal and powder X-ray diffractometer using CuKα as radiation source. The samples were examined in powder form. So for this purpose we took 5 cm^3 from all solution and this amount was dried to constant weight in an oven at the temperature 100 °C.

Subsequently, the crystallite size was calculated using Scherrer equation (19), where B is constant equal 0.94, λ is the wave length which is equal to 1.54 Å and β is the width of peak at a half of maximal height. The influence of different time, temperature and pH of process was studied.

$$d = \frac{\mathrm{B} \cdot \lambda}{\beta \cdot \cos\theta} \tag{19}$$

4.4.5 Photon correlation spectroscopy

Photon correlation spectroscopy is method used for evaluation of particle size. Coulter N4Plus machine was used for this purpose. The rate of particle diffusion through the solution was measured and the particle size was calculated from Einstein's equation (20) using an autocorrelation function.

$$D = \frac{\mathrm{k_B} \cdot T}{3 \cdot \pi \cdot \eta \cdot d} \tag{20}$$

In this equation k_B is Boltzmann's constant; T is temperature; η is dynamic viscosity and d is diameter of particle. This equation is usable for small spherical particle where we can consider solvent as continuous environment.

The samples were illuminated by a laser beam and light scatter was examined. This method is not usable for concentrated solution due to a high absorption. Nevertheless, the concentrations of our TiO_2 colloidal solutions were not higher than 4 %wt so we were able to use this method.

4.4.6 Transmission electron spectroscopy

Transmission electron microscopy (TEM) was used for analysis of crystallite size as well as their shape of prepared TiO_2. For this purpose we used a JEOL JEM 2010 microscope operated at 200 kV, equipped with a LaB_6 tip. The samples were prepared by simply putting a drop of the solution containing the particles on a holey-carbon thin film supported on a microscopy copper grid.

4.4.7 Band gap energy

The band gap of the prepared TiO_2 was evaluated from diffused reflectance measurement. For this purpose we used fiber UV-VIS spectrometer equipped with two lamps, deuterium lamp for UV region and halogen lamp for VIS area. The optical path consists of several optical fibers where six of them are connecter with lamp and one with CCD detector. Reflectance was measured in the range of wavelength from 200 nm to 800 nm and barium sulfate was chosen as a reference. We can calculate the molar absorption coefficient using the results from this analysis according the following formula (21) which is derived from Kubelka-Munk theory.

$$\alpha = \frac{\sqrt{(1-R)^2}}{2R} \tag{21}$$

We examined direct as well as indirect transitions. For direct transition, the dependence of $(\alpha \cdot h \cdot \nu)^2$ on $(h \cdot \nu)$ is constructed where $(h \cdot \nu)$ is a photon energy. On the other hand, $(\alpha \cdot h \cdot \nu)^{1/2}$ as a function of photon energy was constructed for indirect transition, and we estimated the exactly band gap energy from extrapolation to $\alpha = 0$.[20]

4.4.8 Photocatalytic activity

Photocatalytic activity of titania colloidal solutions was investigated as the degradation rate of formic acid (FA). This compound was chosen because of direct mineralisation to H_2O and CO_2 without the creation of any stable intermediate species.[125, 126, 132, 133] Moreover, it also represents a possible final step in the photodegradation of more complex organic compounds.[134]

The photocatalytic experiments took place at ambient temperature in a pyrex reactor (Fig. 38) with 50 cm^3 of reaction solution under constant stirring. The concentration of TiO_2 in the reaction solution was 1 $g \cdot dm^{-3}$ and the final concentration of FA in the solution was 100 ppm. Firstly, the reaction solution was placed to darkness for 30 minutes under continuous stirring in order to reach adsorption equilibrium of FA on TiO_2 surface. In the certain time steps of photocatalytic degradation, 1 cm^3 of the reaction solution was sampled for HPLC analysis. The total reaction time was 60 minutes. The photocatalytic activity of prepared TiO_2 was compared with commercial TiO_2 (P25, Degussa). The intensity

of radiation used during the photocatalytic testing was 7.209 $mW \cdot cm^{-2}$ in the UVA region 2.044 $mW \cdot cm^{-2}$ in the UVB region and no radiation of the UVC region was presented.

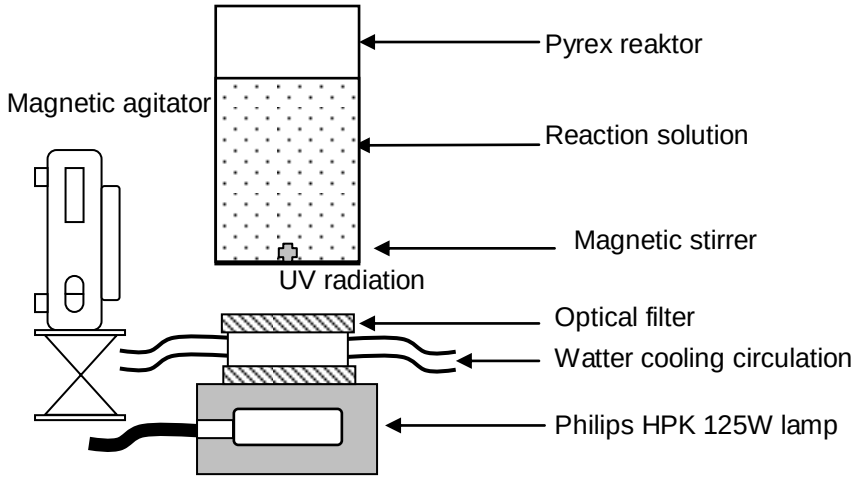

Fig. 38 *Experimental setup for photocatalytic experiments*

4.5 Printed layers of TiO_2 prepared by hydrothermal synthesis

4.5.1 Preparation of printed titania thin films

From previous study (5.2.3), we discovered that the solutions of TiO_2 prepared in acid environment were more stable than the same samples prepared in basic pH. That was the reason why we chose exactly these samples for the next work. The coating process demands stability of printing mixture and it was assured by using acid pH. The stability of colloidal suspension increases with decreasing pH. Hence we prepared the samples of TiO_2 in pH 1. The process was the same as in the previous case i.e. $TiOCl_2$ was added to 480 $cm^3$of KOH to neutral reaction. Consequently, this mixture was centrifugated for 15 times and finally we added 3 cm^3 KOH to final amount $3 \cdot 10^{-4}$ mol and required amount of HCl to set pH 1. Solutions were treated for different times (6, 24, and 48 hours) and we used two process temperatures (110 °C and 160 °C).

Coating deposition was performed in a novel way utilizing specialized experimental printer FUJIFILM Dimatix. Soda-lime glass plates of size $50 \times 50 \times 1.1$ mm were chosen as the substrate for immobilization of titania thin layers. The glass plates had to be pre-treated before the deposition in sulphuric acid in order to prevent sodium ions diffusion which would cause a reduction of photocatalytic activity.[135] Subsequently, the plates were washed in a surfactant solution to remove dust, grease and other residues.

TiO_2 colloidal solution was used for the formation of printing mixture which consisted of 1 cm^3 mentioned TiO_2 slurry, 1 cm^3 HCl, 1 cm^3 acyl benzene sulfonic acid (Abesone), and 1 cm^3 water, respectively. Abesone is an anion-active surfactant which was used in our case as a stabilizing agent of TiO_2 colloidal particles. HCl was added in order to maintain acid pH after the addition of water. H_2O was added to reach required viscosity of printing mixture. The prepare mixture was necessary to sonicated for five minutes and filtered through a 0.45 μm mesh size syringe filter before filling the cartridge.

The printed head contained 16 nozzles and it was attached to the filled tank and mounted into the Dimatix printer. The temperature of nozzle was set to 40 °C. The printer settings optimization is very important to obtain satisfactory results. Viscosity is just one of the few properties that predict the suitability of sol solution for inkjet printing deposition. Wetting ability of sol, which is generally low, needs to be mentioned as a relevant factor in layer preparation. Wettability is closely associated with changing nozzle span. Too large nozzle span leads to a banding structure of layers. The nozzle span was 20 μm, the nozzle shift was 4.5°.

In this part of study we investigated the influence of the film's thickness, for this purpose we prepared samples with one and two layers. We also compared the properties of thin films created from the TiO_2 by hydrothermal synthesis under the different conditions. Finally all deposited substrates were placed to calcinations furniture and dried during temperature increasing up to 500 °C with a ramp 3 °C/min. Glasses with TiO_2 layer were subsequently dried at this temperature for 30 minutes.

The amount of deposited TiO_2 was analyzed by gravimetric measurement. It means that the substrate was weighted before and after the titania deposition and we calculated the final mass of created layers from the difference.

4.5.2 X-ray diffraction

X-ray powder diffraction of TiO_2 was performed using X-ray diffractometer Empyrean, Panalytical. The powder was prepared by drying of the TiO_2 solutions at temperature 50 °C to constant mass. The crystallite phase of prepared TiO_2 as well as their percentage representation was investigated.

4.5.3 Optical properties

The optical properties of prepared thin films were studied by optical microscope Nikon Eclipse E200. The records were obtained form a digital camera Nikon D70 mounted on the optical microscope. The influence of a film thickness on homogeneity and presence of cracks was evaluated from recorded images. The camera parameters were adjusted follows; exposure program of Aperture priority, ISO 200, white balance in auto mode. The samples were measured in reflected light because of layers opacity. Used magnification was 20×.

4.5.4 Scanning electron microscopy

Topology of TiO_2 layers prepared as well as homogeneity of these films was studied by SEM. Imaging was performed by the LabSensNano laboratory (The Faculty of Electrical Engineering and Communication, Brno University of Technology). Scanning electron microscope MIRA II LMU, Tescan, was used for this purpose and all prepared films were analyzed by this technique.

4.5.5 Atomic force microscopy

Atomic force microscope Veeco Di CP-II was used for examine prepared samples. By this method we studied and compared topology and roughness of all monolayers. The analysis was carried out in tapping mode.

4.5.6 Photoinduced superhydrophilicity

The supperhydrophilic properties of TiO_2 deposited glass plates can be characterized by the measurement of water drop contact angle on the titania surfaces. This analysis was performed on the OCA20 by applying a sessile drop method. Immediately after the drop deposition its development was recorded by a CCD camera and the contact angle same as in previous case (4.3.5.5) was obtained by the software processing using the tangent method.

The total volume of deposited droplets was 5 μL and the droplets were recorded in the 10 seconds after the formation.

The hydrofilic properties were studied on all prepared samples. Each TiO_2 thin film was irradiated by UV light with intensity 10 mW/cm^2. Philips Metal-halide lamp HPA 400/30 SD was used as light source. We examined the angle decreasing during 30 minutes caused by UV irradiation. The final contact angle in certain time was calculated as the average of three measurements.

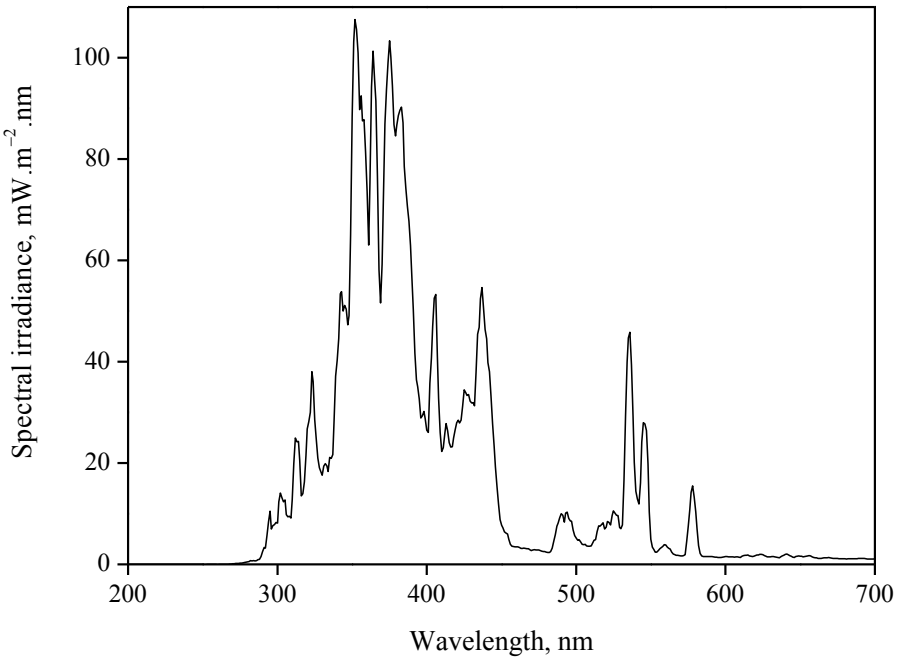

Fig. 39 *Emission spectrum of used metal-halide lamp Philips HPA 400/30 SD.*

4.5.7 Photocatalytic activity

The photocatalytic activity of these printed layers of TiO_2 was examined by monitoring the degradation rate of 2,6-dichloroindophenol. The experiments were performed in a flow reactor with a rotary sample holder. Each sample was placed on this holder and it was irradiated by UV light with intensity 7.5 mW/cm^2 for 10 minutes to activate TiO_2 photocatalyst. Philips Metal-halide lamp HPA 400/30 SD was used as the light source. The intensity was measured by Radiometer X 97

The initial concentration of 2,6-DCIP was $2 \cdot 10^{-5}$ mol·dm^{-3} and total volume of this solution used for one measurement was 70 dm^3. Immediately after 10 minutes of irradiation, aqueous solution of 2,6-DCIP was poured to the reactor and the reactor chamber was immediately covered by a transparent PE foil to prevent solution evaporation. A peristaltic pump maintained a continuous flow of DCIP solution and the surface of active TiO_2 layers was constantly watered.

Spectra Suite Ocean Optics software of fibre spectrometer provided on-line data collecting every 1 minute. The maximum of absorption peak is occurred at wave length 600 nm so

the concentration decreasing was studied at this wave length. The total time of the degradation reaction was 40 minutes.

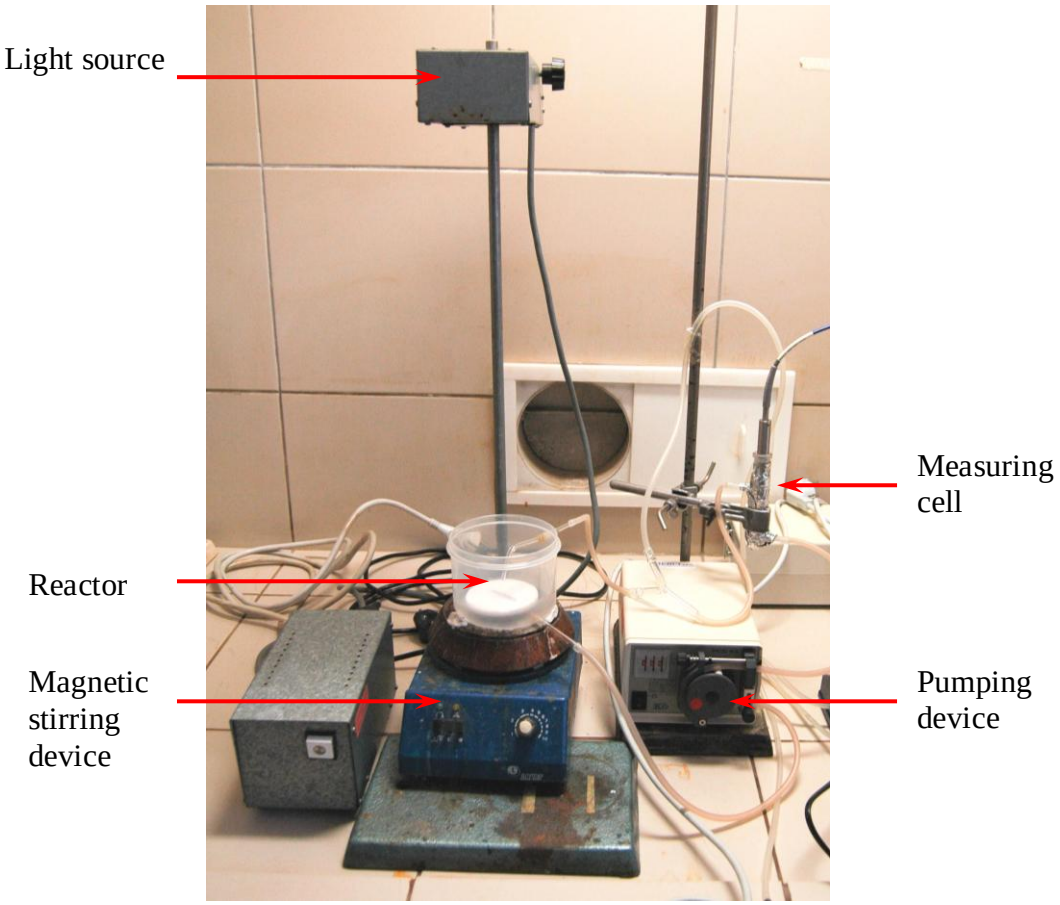

Fig. 40 *Arrangement of photocatalytic reactor and light source*

4.6 Chemical vapour deposition

4.6.1 Preparation of titania thin layers

Apart from the material printing, also chemical vapour deposition was chosen as a technique for the preparation of thin TiO_2 layers. Glassy carbon was used as substrate and silicon was chosen as a reference. Each substrate was pre-treated before the deposition. Glassy carbons were polished (Fig. 41) by Si-paper with different roughness (Si-P1000, Si-P1200, Si-P2400 and Si-P4000; respectively). Afterwards these polished substrates were ultrasonicated in absolute ethanol for 5 minutes and dried by Ar stream. Silicon was only washed in absolute ethanol and dried by Ar stream.

Titanium (IV) isopropoxide (TTIP) was used as the precursor, similarly in the case of sol-gel. The whole process was performed in a vertical cold wall CVD reactor (Fig. 42); it means that only the substrate was heated not the whole chamber where the substrate was placed. Vacuum was created in the first step of deposition. Consequently, a susceptor with substrates (Fig. 41), gas lines and water bath with precursor were heated to require temperatures. N_2 was used as carrier and dilution gas.

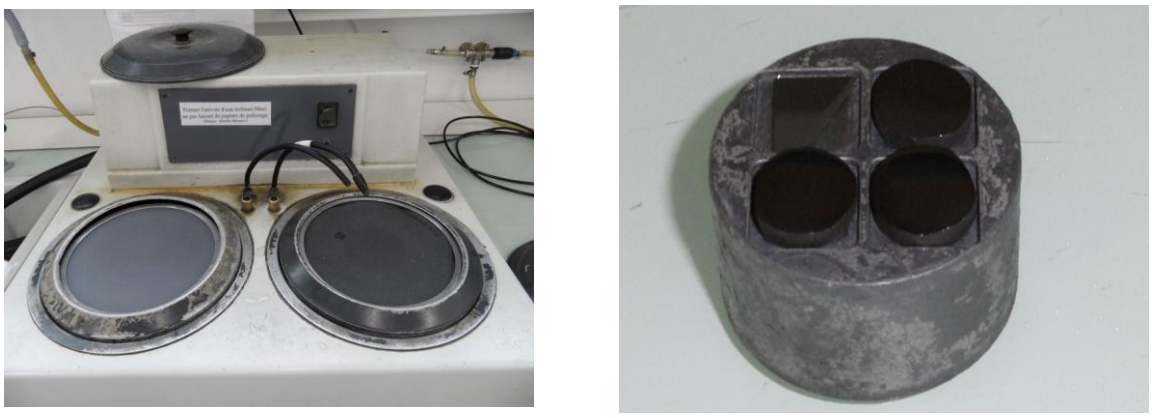

Fig. 41 *Machines for polishing the substrates (left) and susceptor with substrates (right)*

Temperature, pressure and duration of process are the main parameters which very significantly influence the final properties of prepared layer. Temperature affects the final crystallite phase and size of created titania grains. Pressure influences the deposition rate and subsequently the thickness of prepared layers. Duration of the process has mostly an effect on layers thickness. Our coating process was performed at temperature 350 °C, pressure 20 Torr and total time of all depositions was 3 hours. All samples were prepared during two depositions. The differences between these depositions were in the time for vacuum creation in the system and in the age of the precursor. The parameters of all performed deposition reaction are summarized in Table 3.

Table 3 *Parameters of all CVD*

CVD	First	Second
Samples	GC-1 Si-1	GC-2; GC-3; GC-4; Si-2
Distance from shower head to susceptor (mm)	55	55
T of gas lines (°C)	70	70
T of bath (°C)	37	37
Pressure (Torr)	20	20
Duration (min)	180	180
Carrier gas flow (%)	80.6	81.2
Dilution gas flow (%)	90	97.1
Susceptor T (°C)	380	380
Age of precursor	3 months	2 weeks
Time of creation vacuum (h)	1.5	2.0

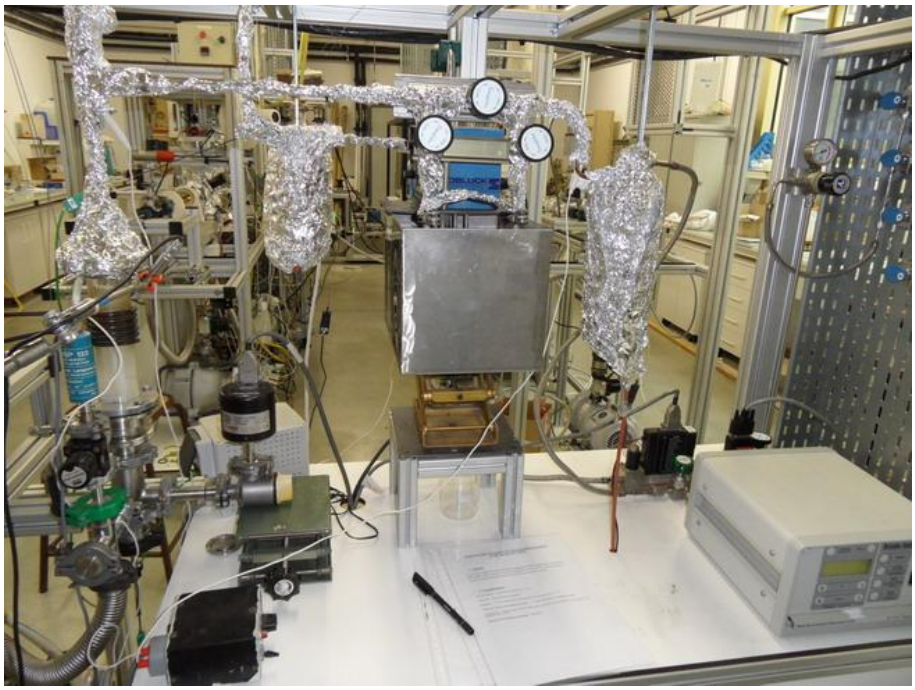

Fig. 42 *Used CVD reactor*

4.6.2 Gravimetric analysis

Gravimetric analysis was performed for investigation of titania amount on the substrates. The weight of substrates was measured before and after the deposition and from the difference of the values the final amount of deposited TiO_2 was calculated.

4.6.3 X-ray diffraction

The crystallite phase of prepared TiO_2 was evaluated by XRD measurement. Analysis was performed using difractometer SEIFERT. The measurement was carried out with fixed position of sample and source while the detector was moving. The analysis took place on TiO_2 thin films.

4.6.4 Scanning electron microscopy

Scanning electron microscopy (SEM) analysis was performed on LEO43VP microscope. Morphology as well as layers thickness were studied in this analysis. We compared samples prepared during different CVD.

4.6.5 Atomic force microscopy

This analysis was used for investigation of surface morphology especially for the evaluation of roughness. The measurement was took place using atomic force microscope ATM/STM 5500 (Pico Plus) in tapping mode. Used type of a tip was SiN with frequency of oscillation from 200 to 400 kHz.

4.6.6 Photocatalytic activity

Photocatayltic experiments were performed in a flow reactor (4.5.7) on a rotary sample holder as well as in previous case. Photocatalytic activity was again evaluated as a degradation rate of DCIP. Before the experiment, each sample was irradiated for 10 minutes under the light source with required intensity to activate titania photocatalyst. The total volume of used DCIP was 80 cm^{-3}. The initial concentration of DCIP was 2.10^{-5} $mol \cdot dm^{-3}$ and as the UV light source was used Philips Metal-halide lamp HPA 400/30 SD. Its emission spectrum is shown in Fig. 39. The experiments run under the same conditions as in case 4.5.7. However two intensities of irradiation (7.5 $W \cdot cm^{-2}$ and 10 $W \cdot cm^{-2}$) were used for comparison of their effect on final samples activity. Each sample was measured twice and subsequently the average value of rate constant was calculated. The final time for all experiments was 40 minutes.

The photocatalytic activity of these titania layers was compared with the results for hydrothermal printed layers. Reactivity of TiO_2 was calculated for 1 gram of photocatalyst. The activity of these samples could not be compared with results for sol gel method because arrangement of experiments was different and also different source of light with varied intensities were used.

5 RESULTS AND DISCUSSION

5.1 Sol-gel process

In this part of study we investigated the influence of added amount of PEG and sol loading on final physical properties and photocatalytic activity. PEG was used as anticracking agent and all sols were prepared according the procedure describing above (4.3.1). All layers of TiO_2 were prepared by the sol-gel process and deposited by new technique called material printing onto pre-treated soda-lime glasses. We used three different types of sol loading (100 %, 90 % and 80 %)

5.1.1 Study of viscosity and density

The prepared sols were characterized by examination of their viscosity and density. The viscosity was measured during seventeen days because it was the maximal time for their storage before their deposition. Changes in rheological properties of prepared coating mixture were studied during this time. We discovered that the viscosity changed negligible. These results indicate that all sols can be stored at the temperature of 5 ℃ for the time without any significant change of their rheological properties.

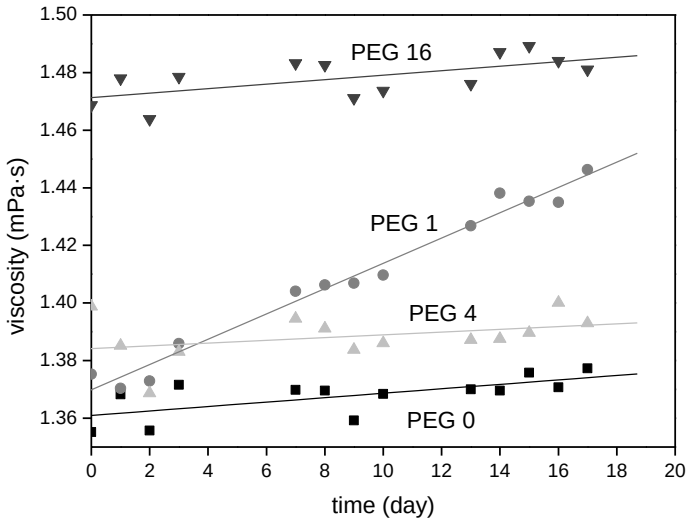

Fig. 43 *Changing of the viscosity during seventeen days¨*

The density of prepared coating mixture was measured by densitometer DMA4500. After the comparison we discovered that density increases with increasing amount of added PEG to the samples. The exact values are summarized in the following table (Table 4).

Table 4 *Density of prepared sols*

Type of sol	Density (g/cm^{-3})
PEG 0	0.8193
PEG 1	0.8196
PEG 4	0.8206
PEG 16	0.8263

5.1.2 Study of the thickness

The thickness of all prepared thin films was studied using NanoCalc-2000. We investigated the influence of added amount of PEG and sol loading on final thickness value. We observed insignificant difference between the samples PEG 0 and PEG 1. On the other side, there is the notable decreasing in the thickness for PEG 16 apparently caused by the removal of the organic matrix.

We discovered that viscosity is changing with the addition of PEG in the previous study. This variation of viscosity would have a significantly influence in spin-coating or in dip-coating. Nevertheless, the observed change of the viscosity does not affect the film thickness of the inkjet printed layers. Within the studied viscosity range, the drops are formed in the same way, their amount as well as their volume are constant, so also the thickness of the printed layers has to be independent on the viscosity (but influenced by the organic matrix fraction content).

We also confirmed that with increasing sol loading the thickness of prepared TiO_2 films increase. This result was supposed because when we have sol loading 100 % it means that we had to use more droplets during the printing. And because also in case of 80 % sol loading we created homogeneous layer it means that thickness had to be smaller than case of 100 % sol loading. Received results are shown in Fig. 44.

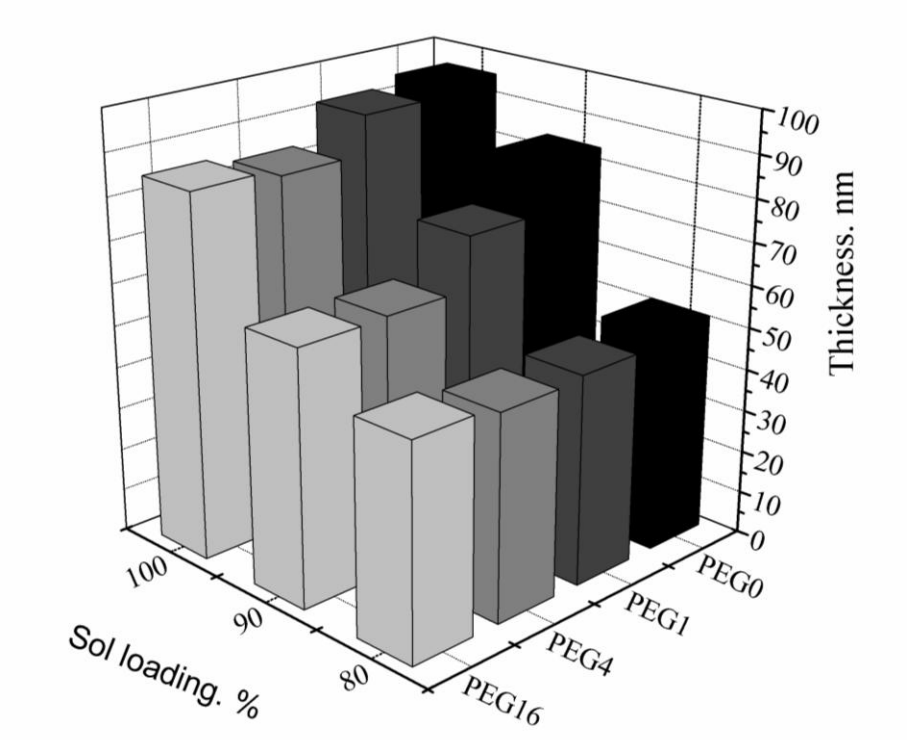

Fig. 44 *The influence of PEG' s amount and sol loading on final thickness of thin layers*

5.1.3 Optical microscopy

The quality of prepared titania films was studied by optical microscope in polarized light, with the magnification 10×. We found out that all prepared layers adhered well to the soda-lime glass after the calcinations process and all were optically transparent.

	80 %	90 %	100 %
PEG 0	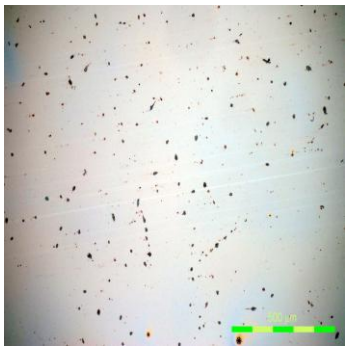	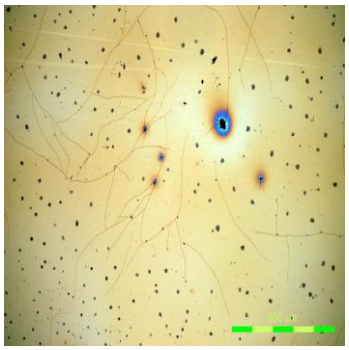	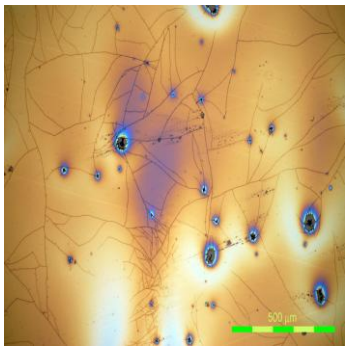
PEG 1	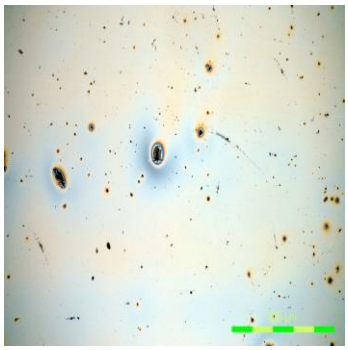	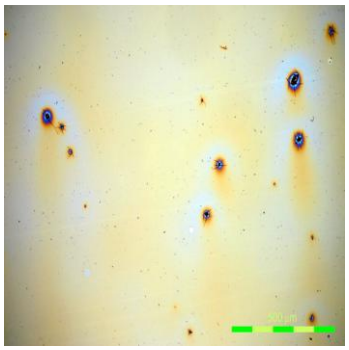	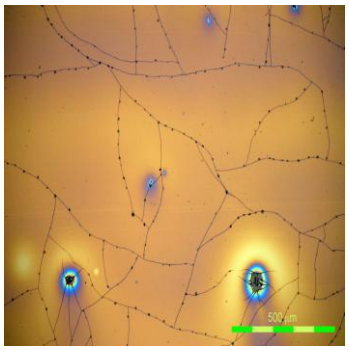
PEG 4	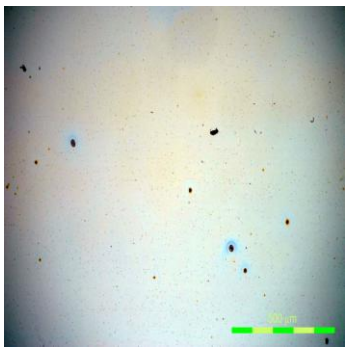	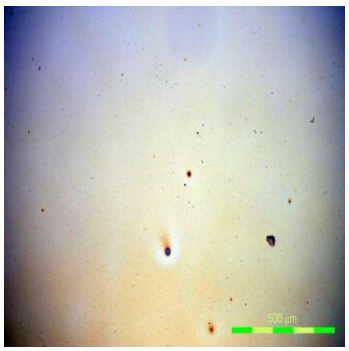	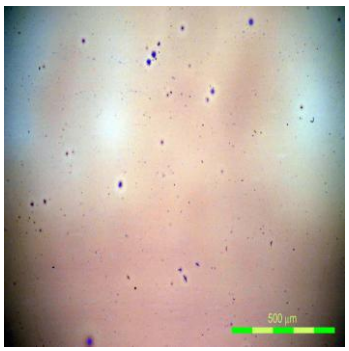
PEG 16	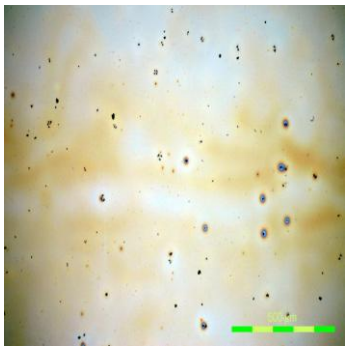	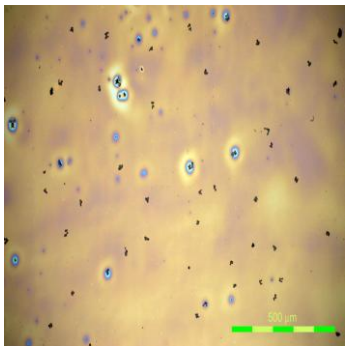	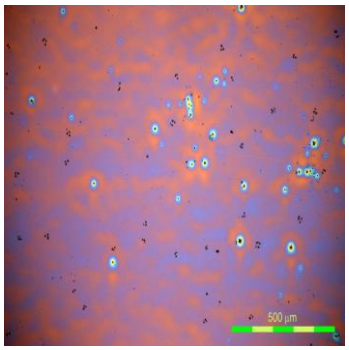

Fig. 45 *The influence of the sol loading and amount of PEG on the cracking intensity*

The influence of sol loading and PEG content on the optical properties of prepared layers was examined. After the comparison of different sol loading we found out that with decreasing film thickness (decreasing sol loading) the cracks are less frequent. In case of 80 % sol loading, there were no cracks present in the structure (Fig. 45). This cracking is caused by a tensile stress, which arises during the thermal treatment of layers.

The added PEG to the sol induced a gradual suppression of cracking. After the reaching concentration 4 $g \cdot dm^{-3}$ all cracks disappeared (Fig. 45). This phenomenon was observed in all prepared samples. We supposed that the free volume created by PEG decomposition enables a stress-free arrangement of titania crystallites created during the calcinations step and in this way the formation of cracks is suppressed.

5.1.4 Scanning electron microscopy

SEM analysis was performed using microscope MIRA II LMU, Tesan. The SEM images (Fig. 46) give us a detailed look at appearance of the printed layer at the nanoscale. We can roughly estimate the size of primary crystallites to be approximately in the range of 30–50 nm. We can also clearly see that the way the primary cracks develop at the nanoscale is different: with the addition of PEG, the primary nanocracks are shorter and more frequent. We assume this contributes to better relaxation of tensional stresses occurring during the calcination of the layer and thus prevent the formation of larger microcracks.

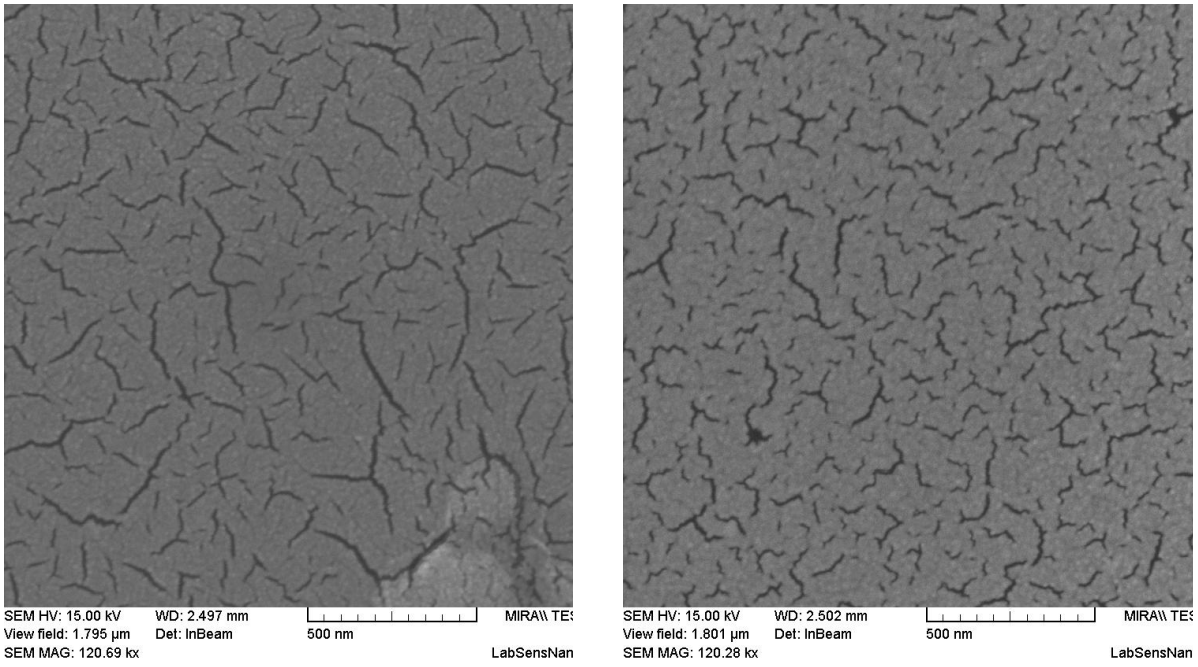

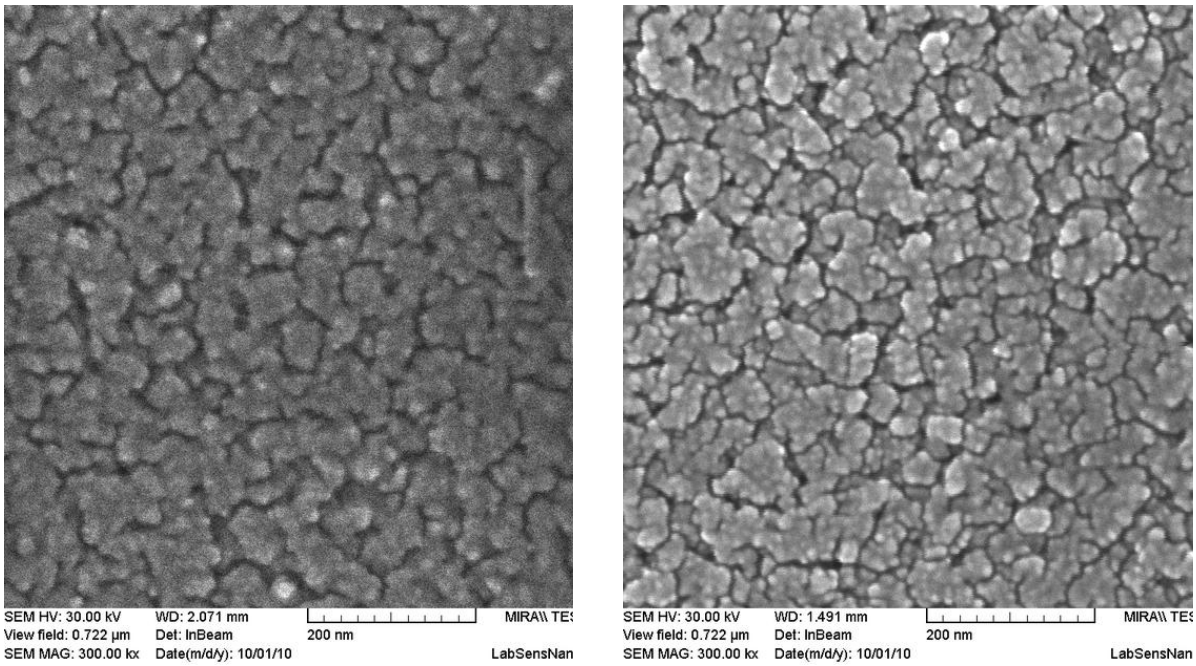

Fig. 46 *SEM images of titania layers*

5.1.5 Atomic force microscopy

The surface topology of prepared layers was studied by AFM analysis. Using this method, the influence of added PEG amount on the final roughness of prepared films was investigated. We calculated the root mean square roughness (R_q) during this analysis. The root mean square roughness is the root mean square average of the roughness profile ordinates calculated according the following formula (22), where *Z(x)* is profile ordinates of roughness profile (Fig. 47). The mean roughness is the arithmetic average of the absolute values of the roughness profile ordinates.[136]

$$R_q = \sqrt{\frac{1}{L}\int_0^L Z^2(x)dx} \tag{22}$$

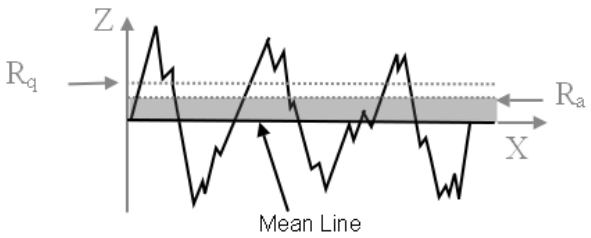

Fig. 47 *Roughness profile*[136]

We compared the sample without PEG (PEG 0) and the sample with the highest amount of PEG (PEG 16). We discovered that PEG causes an increase of surface roughness (surface

roughness of the sample PEG 0 was 0.28 nm; surface roughness of PEG 16 was 0.41 nm). The obtained records are shown in the following figure (Fig. 48).

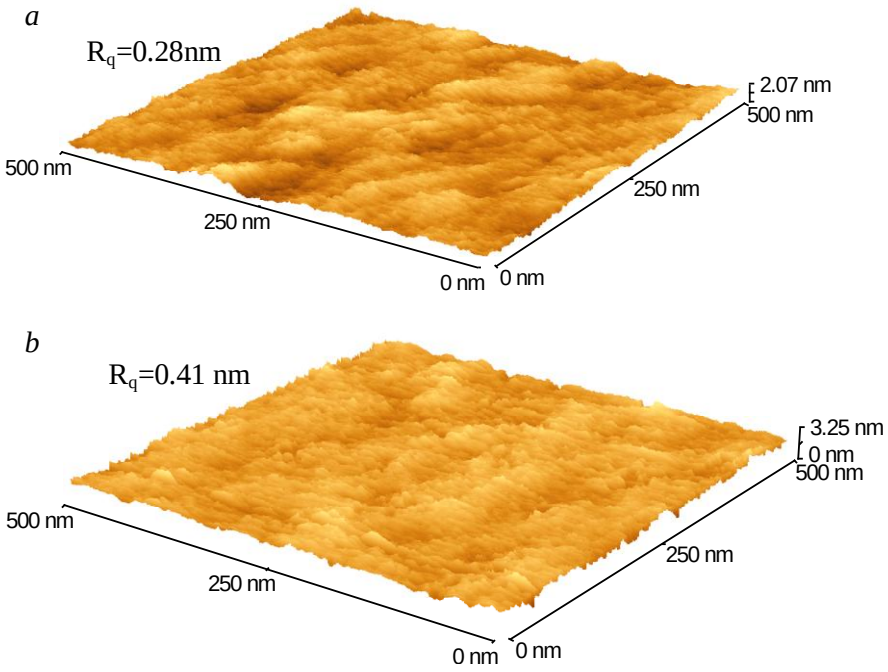

Fig. 48 *Comparison of the roughness; a) PEG 0; b) PEG 16*

5.1.6 Photoinduced hydrophylicity

The hydrophilic properties of prepared layers were evaluated by measuring water contact angle as a function of the incident UV light exposure dose. Firstly, we studied the freshly prepared films. It means the films which were not older than 24 hours. We discovered that all these films showed superhydrophilic character (Fig. 49). Superhydrophilic layers are considered those contacts angles of which are lower than 5°.

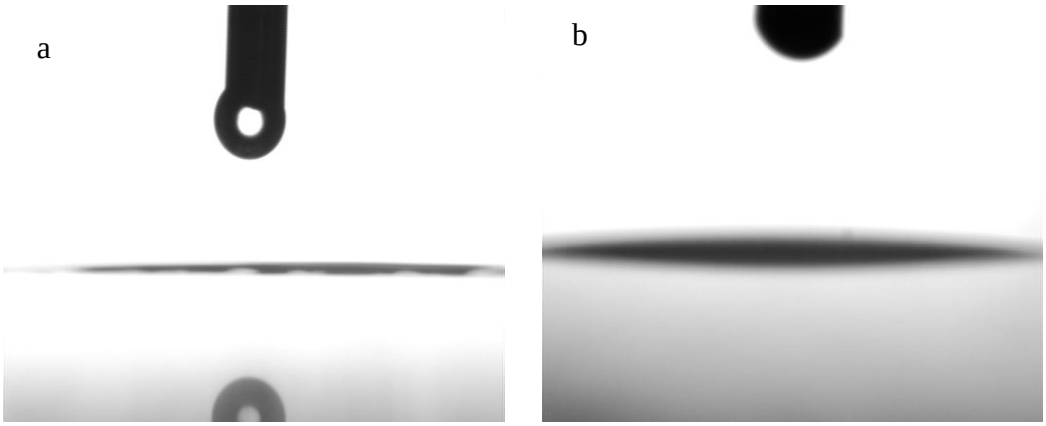

Fig. 49 *Water droplets placed onto the freshly prepared layers; a) PEG 0; b) PEG 16*

Afterwards titania samples were stored in darkness for 10 days. After this time, quite a high increasing of contact angle could be observed. All contact angles were higher than 50°. Nevertheless, after the irradiation of these layers by UV light with intensity of irradiation

15 W/m^2 all samples converted to hydrophilic nature again within 10 minutes. This could be explained in two ways. One of them is that by UV illumination the holes are transferred to the surface, creating oxygen vacancies most likely at the two coordinated bridging sites, which are suitable for dissociative water adsorption. Photoproduced electrons are also transferred to the surface Ti^{4+}, forming Ti^{3+} followed by the electron transfer to adsorbed oxygen molecules.[137, 138]

But on the other side, recent communication by Yates and co-workers suggest that photoproduced hydrophilic behavior on TiO_2 does not involve the production of surface oxygen vacancy defect sites, enhanced surface Ti-OH coverage on defect sites, or the modified surface bonding of bridging OH groups. They explain the hydrophilic properties as the production of the critical surface condition at the perimeter of a water droplet, which covers a hydrocarbon coated TiO_2 surface. And they discovered that gas phase O_2 is necessary to cause the photoinduced hydrophilicity effect.[139]

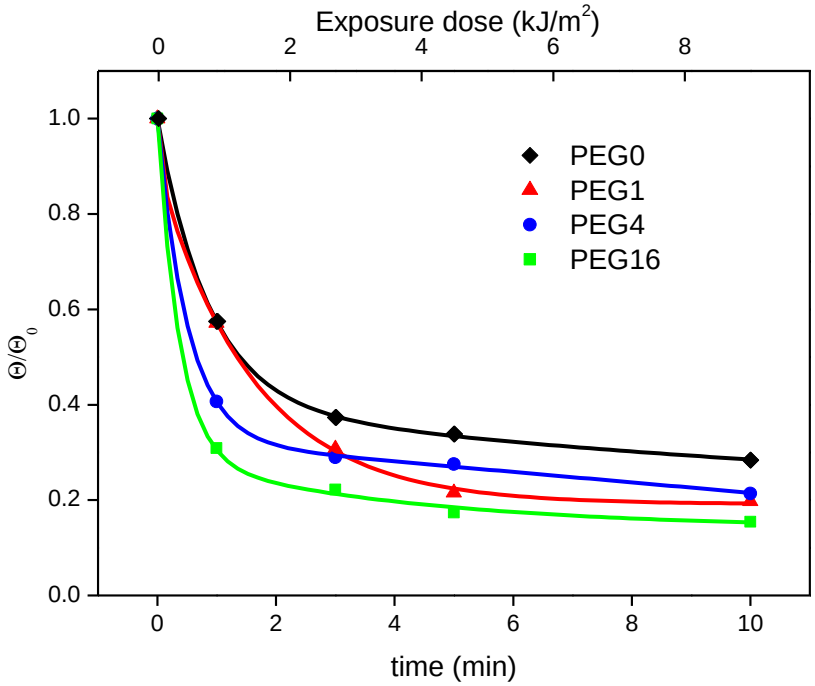

Fig. 50 *Decreasing of water contact angle after 10 minutes of irradiation*

In this study we discovered that the conversion from hydrophobic to hydrophilic properties was faster with increasing of PEG amount in the sol (Fig. 50). It could be caused by a smaller hydroxyl group content and smaller surface roughness for PEG 0 so in this case water could not so easily enter the interior region of the thin films. In part 5.1.5 we found out that with increasing amount of PEG the roughness of titania surface increase so also larger surface area. The coating films with larger surface area are more easily attacked by the water vapour to produce more hydroxyl groups. Hydroxyl groups existing in the coating films are attributed to the chemically adsorbed H_2O and also some H_2O is physically adsorbed on the surface of TiO_2 coating films.

Generally, with the increasing of chemically adsorbed hydroxyl groups on the surface, van der Waals forces and hydrogen bonds interactions between water and hydroxyl groups will be

increased. Water can easily spread across the surface and the hydrophilic character will be enhanced. [140]

5.1.7 Photocatalytic activity

The photocatalytic activity was evaluated as a degradation rate of DCIP realized in bath reactor. The first step of the degradation is dechloration accompanied by discoloration. Then, the oxidation of carbon skeleton follows, leading to the creation of short carboxylic acids. Finally, these acids undergo decarboxilation and are totally cleaved. [141, 142] DCIP was chosen due to its very easy detection in VIS range and a very low absorption at 360 nm wavelength.

DCIP solutions of known concentration were prepared to create a calibration curve. Absorption characteristic were measured in range 400–800 nm. We observed that the absorption maximum corresponds to 600 nm (Fig. 51). The calibration curve was obtained as a dependence of maximum absorbance on the molar concentration of the solution. The linear function was calculated as $y = 14601x$ with $R^2 = 0.999$.

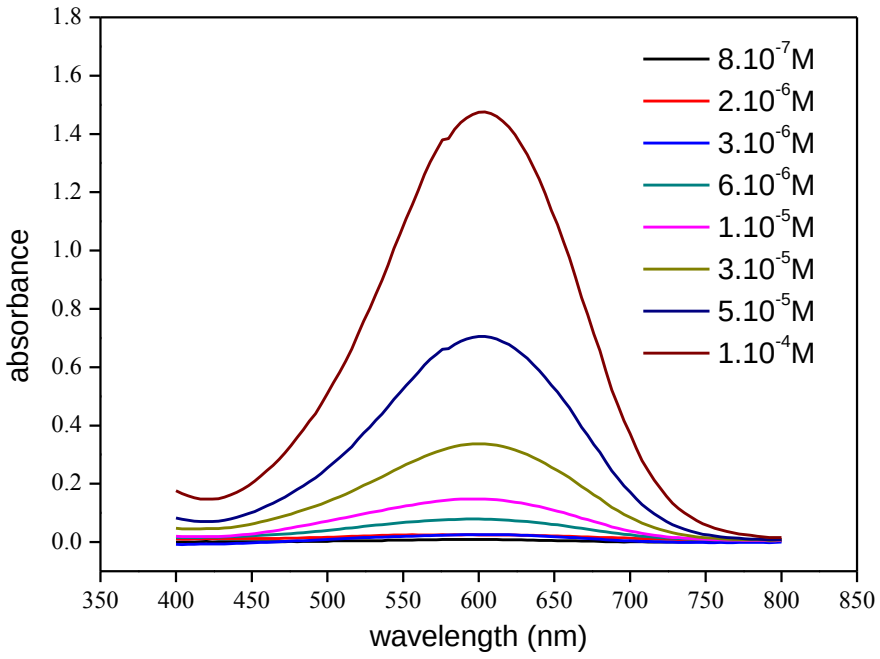

Fig. 51 *VIS absorption spectrum of DCIP*

We discovered that a dependence of logarithm of concentration on time is linear (Fig. 52) so it means that photochemical degradation of DCIP runs according to first order kinetics. The oxidation reaction of the DCIP is much more complicated process than the first order reaction described by the equation (5). On the other hand the determination coefficient calculated for all studied samples was more than 0.98, which means that the selected reaction model was correct. The degradation reaction is than characterized by a formal rate constant.

An experiment with the blank (without photocatalyst) was carried out and final value of direct photolysis was subtracted from the final measurement values to obtain the net photocatalytic efficiency. The rate constant was calculated according to the equation (23),

where the rate constant is equal to the slope of the straight line. It was observed that not only photocatalytic degradation of DCIP on the TiO_2 surfaces with the rate constant $\bar{k}_i$ as an average of three measurements occurred. Also direct degradation of the dye appeared under the set irradiation conditions. That is why the average rate constant $\bar{k}_0$ for the direct degradation out of two measurements was calculated. The rate constant k_0 describes a degradation reaction of the DCIP without any TiO_2 layer present in the reactor. The final formal rate constant was calculated as $\left(\bar{k}_i - \bar{k}_0\right)$ for each sample. The standard deviation of the formal rate constants was calculated according to the equation (24).

$$\ln\left(c_{A0}/c_A\right) = f(t) \tag{23}$$

$$\Delta\left(\bar{k}_i - \bar{k}_0\right) = \left(\bar{k}_i - \bar{k}_0\right)\sqrt{\left(\frac{\Delta\bar{k}_i}{\bar{k}_i}\right)^2 + \left(\frac{\Delta\bar{k}_0}{\bar{k}_0}\right)^2} \tag{24}$$

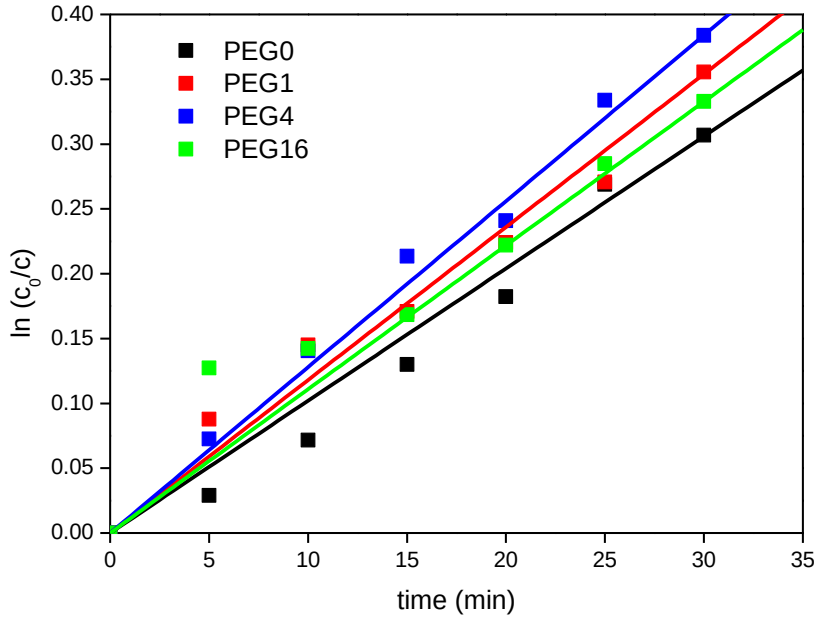

Fig. 52 *Dependence of logarithm of concentration on time*

We compared the influence of PEG and sol loading on final photocatalytic activity of prepared TiO_2 in this part of study. We discovered that samples with PEG have higher activity than the sample without PEG (Fig. 53). This can be accounted for the higher roughness of the thin layers surface, which is created by the present of PEG (5.1.5).

Consequently, we investigated the influence of sol loadings on the titania photocatalytic reactivity. We found out that the samples with 100% sol loading were the most photocatalytically active (Fig. 53). It can be explained by presence of higher amount of photocatalysts with increasing sol loading.

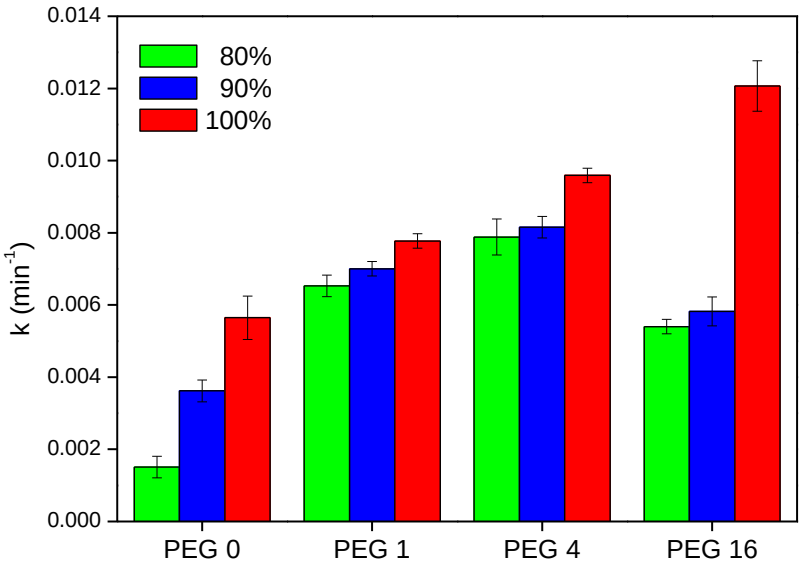

Fig. 53 *Photocatalytic activity of prepared TiO_2*

5.2 Hydrothermal synthesis

5.2.1 Preparation of TiO_2 colloidal solution

Twelve samples were prepared by hydrothermal synthesis with varying process conditions, especially pH, temperature or duration of process. Subsequently, the physical properties of prepared solutions were examined by UV-VIS spectroscopy, XRD analysis, Photon correlation spectroscopy, Transmission electron microscopy. Finally, the photocatalytic activity was evaluated as the degradation rate of formic acid.

5.2.2 UV-VIS spectroscopy

Total transmission and total reflectance were measured using UV-VIS spectroscopy. Consequently, the final absorption was calculated according the formula (18). The results from this analysis are shown in Fig. 54. As we can observe the absorption maximum is situated in all samples nearly in the same position, closely 323 nm.

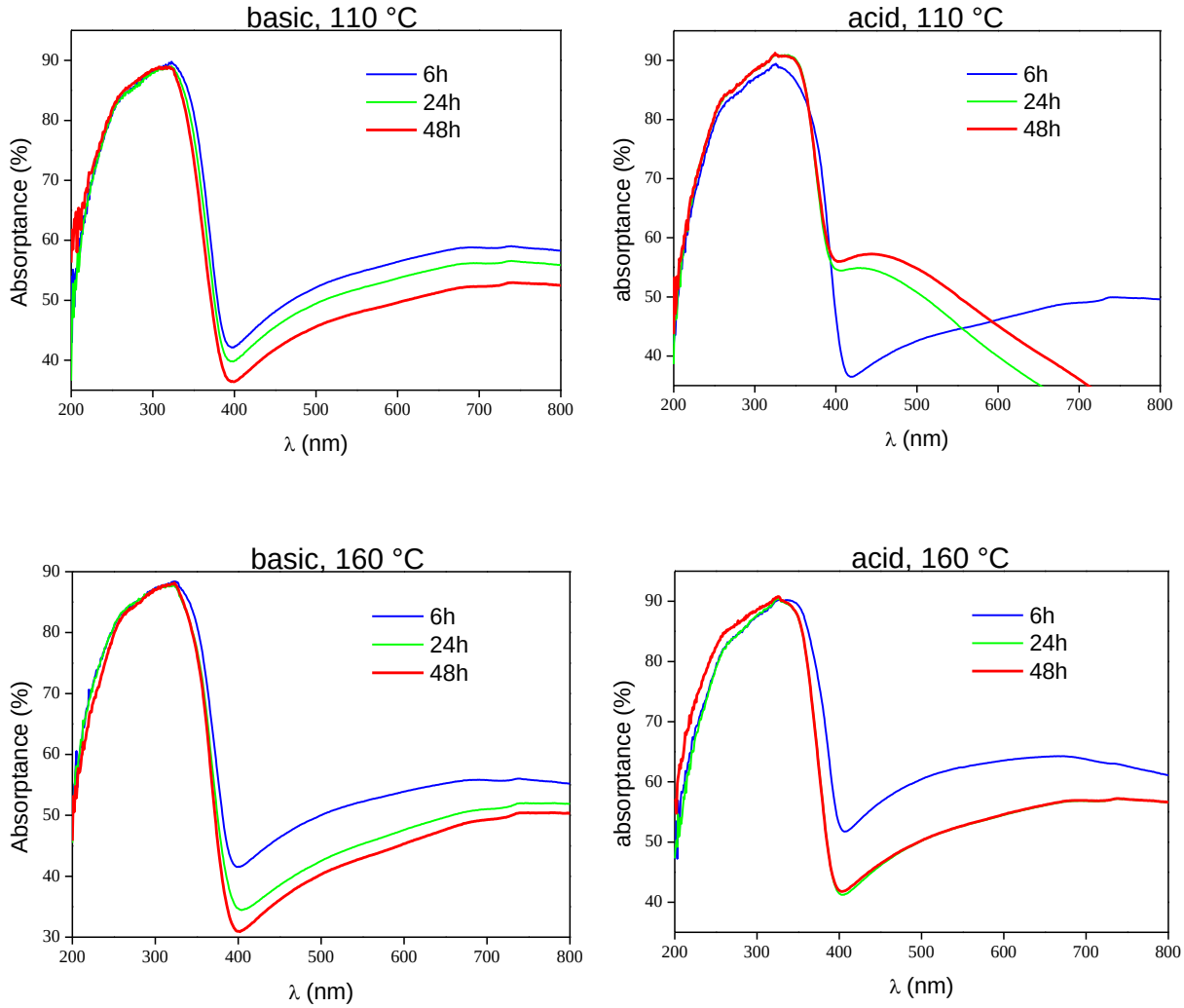

Fig. 54 *Absorptance calculated from transmission and reflectance measurement*

For better understanding of the relationship between the optical properties and the photocatalytic activity, the average UV absorption ($\bar{A}_{UV}$) of titania colloidal solutions was determined. We expected that TiO_2 with higher ($\bar{A}_{UV}$) are more photocatalytic active. The values of ($\bar{A}_{UV}$) were calculated from the sum of integrated absorptance in the range of wavelength from absorptance minimum to the absorptance value at 290 nm divided by the difference of these wavelength values[143] (25). All received results are summarized in Table 5.

$$\overline{A_{UV}} = \frac{\int_{\lambda(A\min)}^{290} A(\lambda)d(\lambda)}{100\left(\lambda_{(A\min)} - 290\right)} \tag{25}$$

We can observe, higher values for acid titania slurries indicate that these samples should be more active than the same samples prepared in basic pH. After the comparison of different temperature of hydrothermal synthesis we discovered that higher values were reached for temperature 110 °C in acidic samples. We consequently discovered that the samples prepared at this temperature were more stable (Fig. 55). In the case of basic pH, higher average absorption was observed in for 160 °C. Again these solutions were more stable and we supposed that also they should be more active.

Table 5 *Wavelength of minimal and maximal absorption and average UV absorption of colloidal suspensions of TiO_2*

pH	Temperature	Time	λ_{Amin} (nm)	λ_{Amax} (nm)	Average UV absorption
Acid	110 °C	6 h	420	326	0.864
		24 h	406	325	0.830
		48 h	406	325	0.833
	160 °C	6 h	407	328	0.838
		24 h	403	325	0.766
		48 h	403	325	0.769
Basic	110 °C	6 h	399	323	0.720
		24 h	398	323	0.694
		48 h	400	316	0.679
	160 °C	6 h	400	323	0.722
		24 h	404	323	0.702
		48 h	402	323	0.681

5.2.3 Gravimetric analysis

Firstly, the concentration of prepared samples was examined gravimetrically. All obtained results are summarized in Table 6. When we compared received values, we discovered that the concentration of the samples decreased with increasing time of hydrothermal synthesis. We also found out that more concentrated solutions were prepared in basic environment.

Table 6 *Comparison of concentration*

pH	Temperature	Time	Concentration (% wt.)
Acid	110 °C	6 h	0.59
		24 h	0.53
		48 h	0.52
	160 °C	6 h	1.22
		24 h	1.03
		48 h	0.82
Basic	110 °C	6 h	3.12
		24 h	2.04
		48 h	1.99
	160 °C	6 h	1.45
		24 h	1.53
		48 h	0.70

We investigated the stability of prepared colloidal solution after 1 day of leaving in a rest using gravimetric analysis. The obtained results are shown in Fig. 55. We discovered that with increasing time of hydrothermal treatment the stability of TiO_2 particles increases except the samples prepared at 110 °C in basic pH. These slurries had constant stability. This result can be explained by decreasing of particle size with increasing time of hydrothermal treatment (Fig. 57) so the sedimentation was lower in the case of longer time.

After the comparison of different pH we found out that samples prepared in acidic environment were more stable. When we compared different temperatures, 110 °C in acid pH and 160 °C in basic pH was evaluated as better temperature for preparation hydrothermal titania solutions.

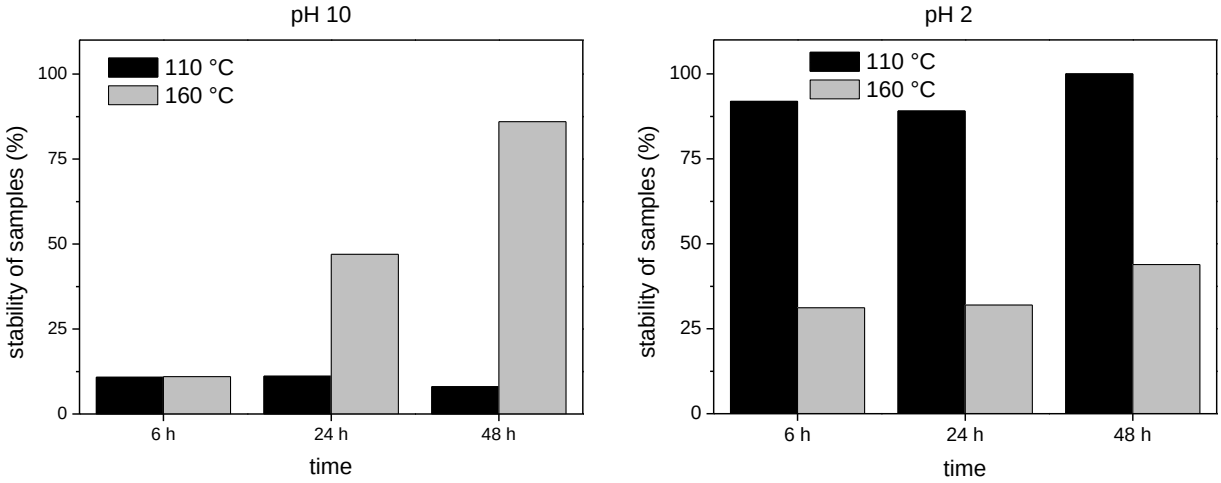

Fig. 55 *Stability of samples after 1 day*

5.2.4 Study of crystallinity and crystallite size

Crystalline phase in the sample was identified from X-ray powder diffraction pattern. Obtained spectra are shown in Fig. 56. After the results evaluation we discovered that all samples prepared in basic pH were pure anatase with the main peak in position around 25.2° (Fig. 56). This result is in a good agreement with our assumption because it is well known that basic pH support the creation of pure anatase phase.[144]

When we evaluated the spectra obtained for TiO_2 prepared in acid pH we discovered that in all cases except the sample prepared at 110 ℃ and treated for 6 hours, we received a mixture of anatase and rutile. In the mentioned case we obtained a mixture of rutile and anatase with main peak in the position 27.4°.This deviation could be caused by reaching lower pH than 2 after the addition of 0.9 cm^{-3} of HCl. We added still the same amount for HCl but for this sample we reached pH of only 1.7 instead of 2. This decreasing caused probably creation of rutile as the major phase. In other cases as well as in basic environment the dominant phase was anatase with the position of the main peak in 25.2° (Fig. 56).

We also found out that with increasing temperature the width of the main peak decreases. This dependence was observed in acidic as well as in basic environments. Also, this dependence was discovered for increasing pH at temperature 160 ℃. No similar dependence was presented for temperature 110 ℃. Generally it is known that narrow peak indicates higher crystallite size.

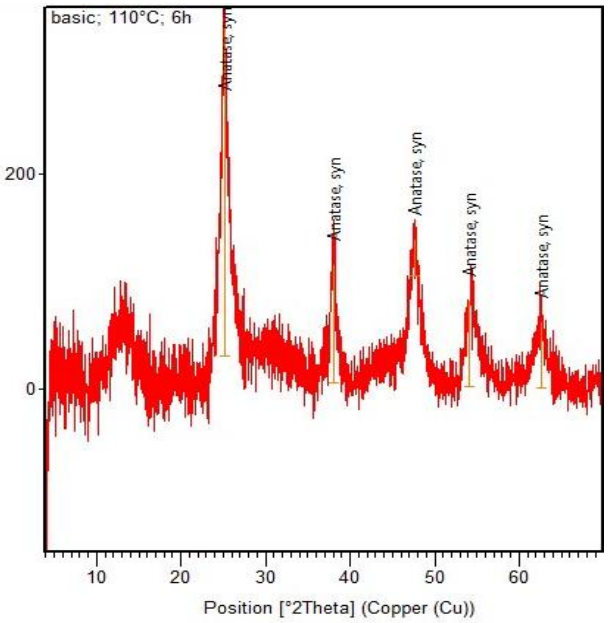
basic; 110°C; 6h
Anatase, syn
Anatase, syn
Anatase, syn
Anatase, syn
Anatase, syn
200
0
10
20
30
40
50
60
Position [°2Theta] (Copper (Cu))

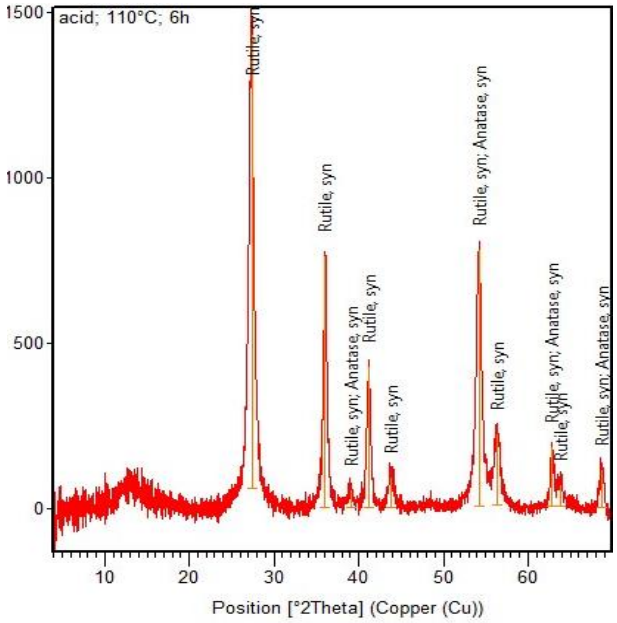
acid; 110°C; 6h
Rutile, syn
Rutile, syn
Rutile, syn; Anatase, syn
Rutile, syn
Rutile, syn
Rutile, syn; Anatase, syn
Rutile, syn
Rutile, syn
Rutile, syn; Anatase, syn
Rutile, syn; Anatase, syn
1500
1000
500
0
10
20
30
40
50
60
Position [°2Theta] (Copper (Cu))

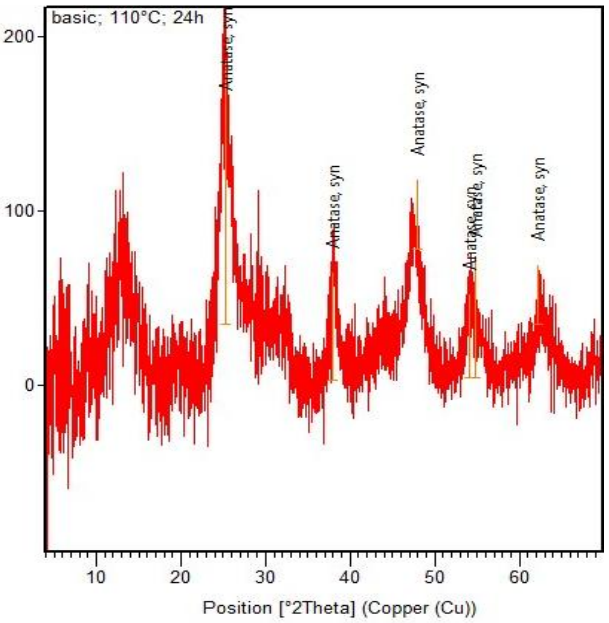
basic; 110°C; 24h
Anatase, syn
Anatase, syn
Anatase, syn
Anatase, syn
Anatase, syn
200
100
0
10
20
30
40
50
60
Position [°2Theta] (Copper (Cu))

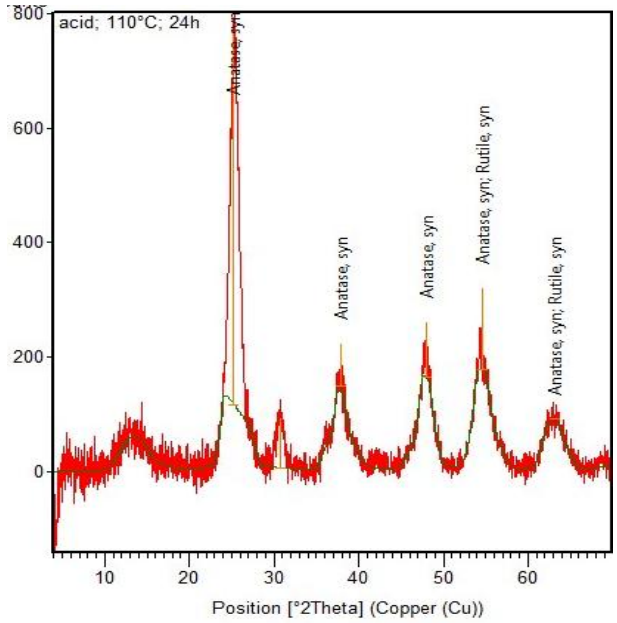
acid; 110°C; 24h
Anatase, syn
Anatase, syn
Anatase, syn
Anatase, syn; Rutile, syn
Anatase, syn; Rutile, syn
800
600
400
200
0
10
20
30
40
50
60
Position [°2Theta] (Copper (Cu))

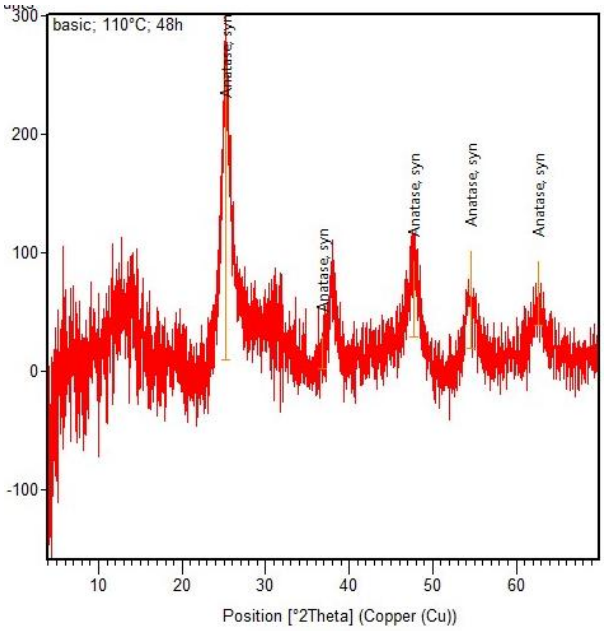
basic; 110°C; 48h
Anatase, syn
Anatase, syn
Anatase, syn
Anatase, syn
Anatase, syn
300
200
100
0
-100
10
20
30
40
50
60
Position [°2Theta] (Copper (Cu))

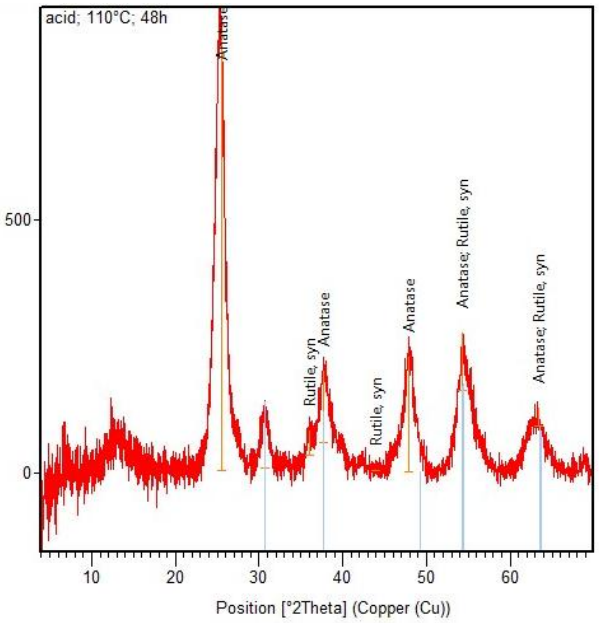
acid; 110°C; 48h
Anatase
Rutile, syn
Anatase
Rutile, syn
Anatase
Anatase; Rutile, syn
Anatase; Rutile, syn
500
0
10
20
30
40
50
60
Position [°2Theta] (Copper (Cu))

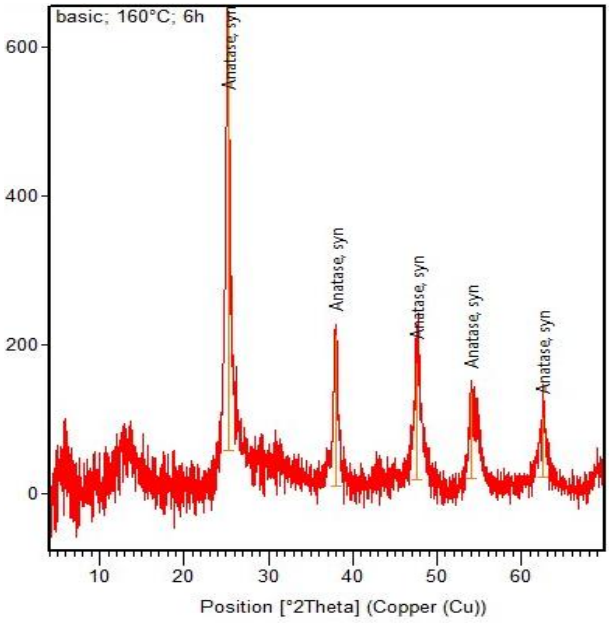
basic; 160°C; 6h
Anatase, syn
Anatase, syn
Anatase, syn
Anatase, syn
Anatase, syn
600
400
200
0
10
20
30
40
50
60
Position [°2Theta] (Copper (Cu))

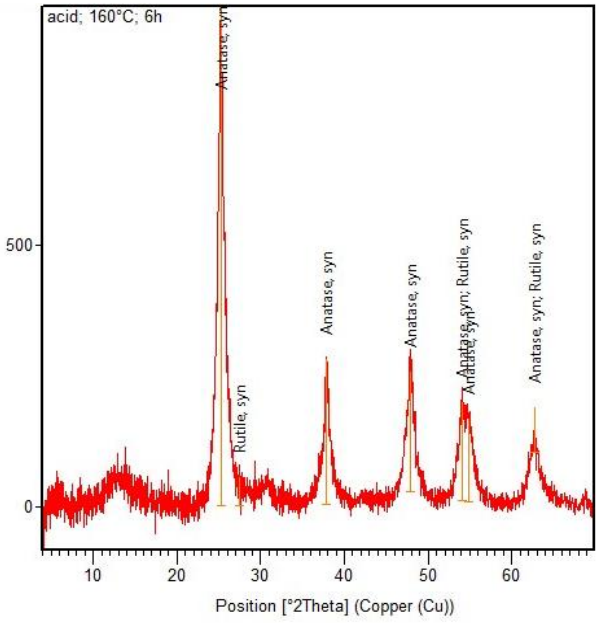
acid; 160°C; 6h
Anatase, syn
Rutile, syn
Anatase, syn
Anatase, syn
Anatase, syn; Rutile, syn
Anatase, syn; Rutile, syn
500
0
10
20
30
40
50
60
Position [°2Theta] (Copper (Cu))

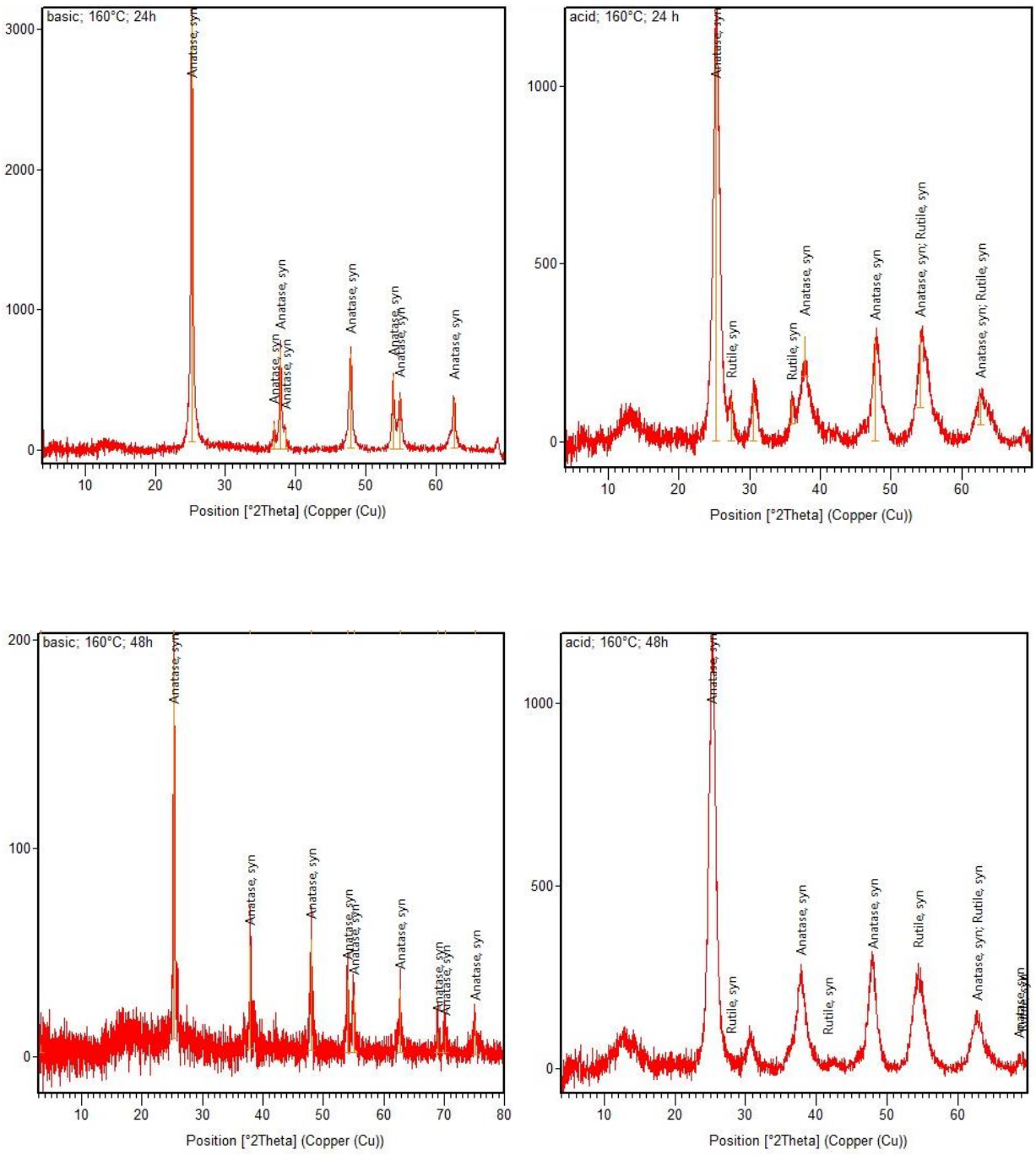

Fig. 56 *XRD spectra for all studied TiO_2 solutions*

Using the Scherrer equation (19) we could calculate the mean crystallite size. The obtained results are summarized in table (Table 7). We found out that the crystallite size decreases in the acidic environment with increasing time. However, we could observe no such dependence between the time of hydrothermal treatment and the crystallite size in the basic environment.

After the comparison of samples prepared in same pH but with using different temperature we discovered that with increasing temperature the crystallite size increases as well. This result is in a good agreement with the previously published data.[42, 145]

Table 7 *Crystalllite size*

pH	Temperature	Time	Crystallite size (nm)
Acid	110 °C	6 h	23
		24 h	14
		48 h	9
	160 °C	6 h	31
		24 h	30
		48 h	26
Basic	110 °C	6 h	14
		24 h	9
		48 h	14
	160 °C	6 h	20
		24 h	42
		48 h	37

5.2.5 Evaluation of particle size

The analysis of particle size was performed by photon correlation spectroscopy techniques. All prepared samples were studied by this analysis. Obtained results are summarized in Table 8. When we compared these results with results from XRD analysis we discovered that results do not correlate. However we needed only the information if the particles were not higher than 450 nm what is the limit for printing technique. By this method we discovered that aggregates in our solutions were not higher than 200 nm so there slurries were usable for material printing.

Table 8 *Particle size*

pH	Temperature	Time	Particle size (nm)
Acid	110 °C	6 h	147
		24 h	63
		48 h	12
	160 °C	6 h	3
		24 h	15
		48 h	30
Basic	110 °C	6 h	158
		24 h	78
		48 h	16
	160 °C	6 h	19
		24 h	24
		48 h	41

5.2.6 Transmission electron microscopy

Transmission electron microscopy was used for particle size comparison of the TiO_2 prepared at temperature 160 °C. The aggregation of particles can be observed by this method. TiO_2 colloidal systems created at 160 °C was chosen because for these samples we discovered increasing of particle size with increasing time of hydrothermal treatment. This result was in disagreement with the results from XRD analysis. We supposed that this increasing could be caused by particles aggregation.

We could not observe any dependence between crystallite size and time of hydrothermal treatment for basic solutions by XRD analysis. However, we received quite difference results from this electron microscopy analysis. We found out that with increasing duration of the hydrothermal treatment the crystallite size decrease (Fig. 57). It is the same dependence which we observed in the acidic environment by XRD analysis. By this method we also confirmed that really in the case of longer time of hydrothermal treatment we saw higher particles aggregation. This aggregation might be the main reason why we recorded such high value of particle size by photon correlation spectroscopy. Indeed, the particles were smaller than 15 nm actually for time 48 hours.

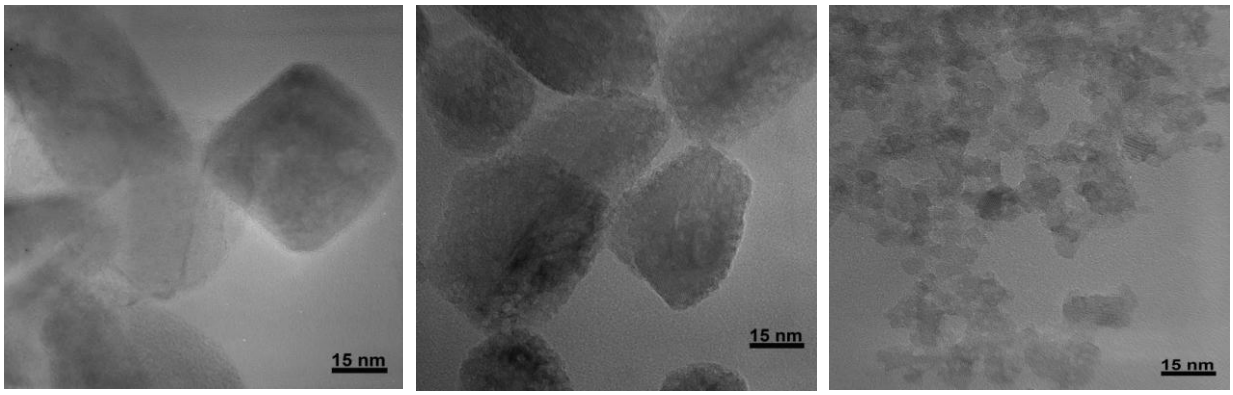

Fig. 57 *TEM images for basic samples prepared at 160 °C; left- 6h; middle-24h; right-48h*

Subsequently, we used this method for investigation of TiO_2 crystallinity. We compared the particles shape of samples prepared in acidic and in basic pH. We discovered that in basic solutions, strictly cubic particles were present (Fig. 58). This result confirmed the result from XRD analysis where we found out that these TiO_2 were pure anatase because cubic shape is typical for anatase phase.[146]

In the case of acidic environment, we could observe also rods apart from the cubic shape (Fig. 58). This shape confirms the presence of rutile phase.[147] So we affirmed that the samples prepared in pH of 2 consist of anatase and rutile mixture. These results are consistent with the results of XRD analysis.

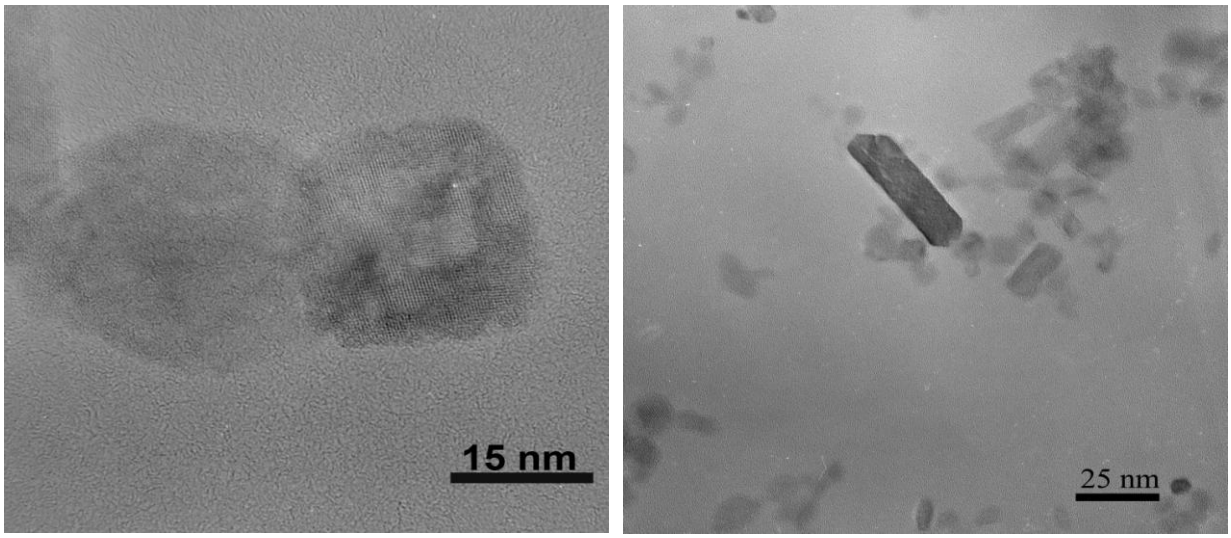

Fig. 58 *TEM images samples prepared in basic pH (left) and in acid pH (right)*

5.2.7 Band gap energy

Absorption coefficient was calculated according equation (21) and consequently used to establish the type of band-to-band transition in these TiO_2 nanoparticles. The dependence of molar absorption coefficient was recorded as a function of the photon energy for direct (Fig. 59) as well as for indirect transition (Fig. 60). Subsequently, the extrapolation for value $\alpha = 0$ was performed from which the band gap energy was found. Generally, it is known that band

gap energy of TiO_2 in anatase phase is 3.23 eV and rutile phase 3.03 eV. Obtained results are summarized in table (Table 9).

Table 9 *Band gap energy for direct and indirect transition*

pH	Temperature	Time	Band gap energy (eV)	
			Direct	Indirect
Acid	110 ℃	6 h	3.56	3.03
		24 h	3.42	3.04
		48 h	3.43	3.08
	160 ℃	6 h	3.56	3.17
		24 h	3.43	3.12
		48 h	3.48	3.17
Basic	110 ℃	6 h	3.52	3.17
		24 h	3.54	3.19
		48 h	3.51	3.16
	160 ℃	6 h	3.64	3.25
		24 h	3.65	3.24
		48 h	3.66	3.29

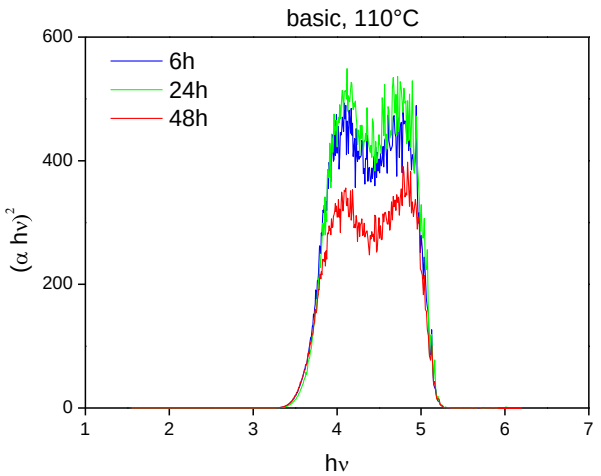

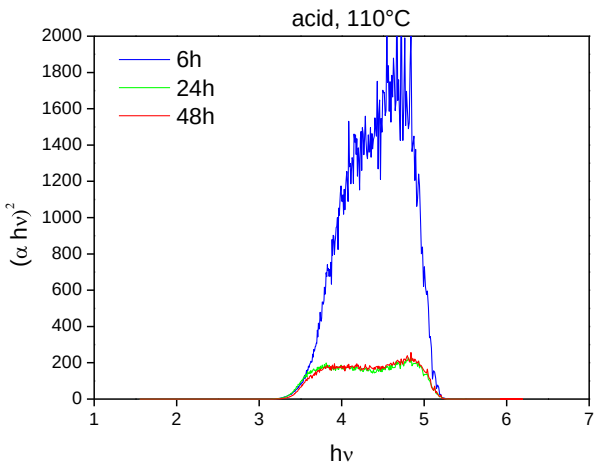

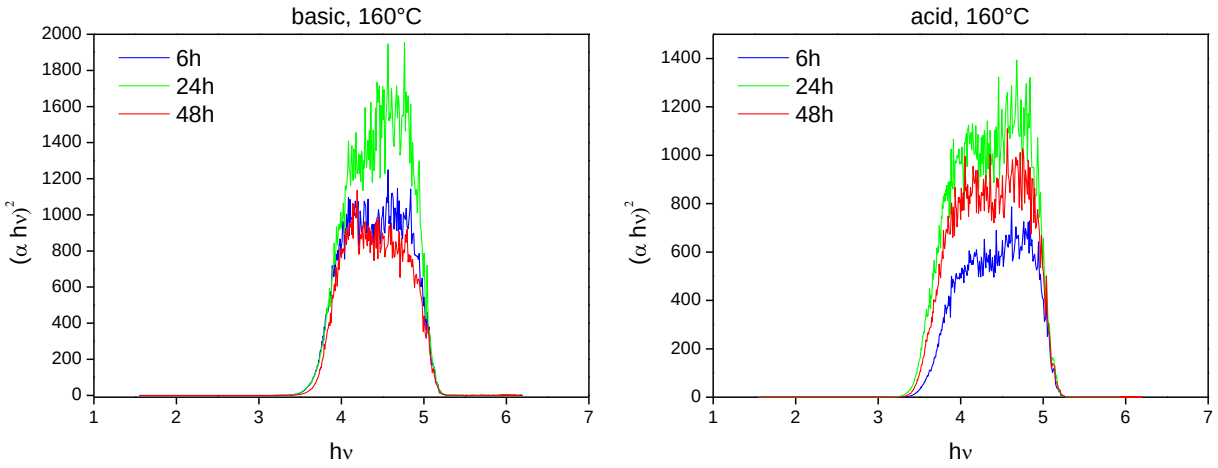

Fig. 59 *Evaluation of band gap energy from direct transition*

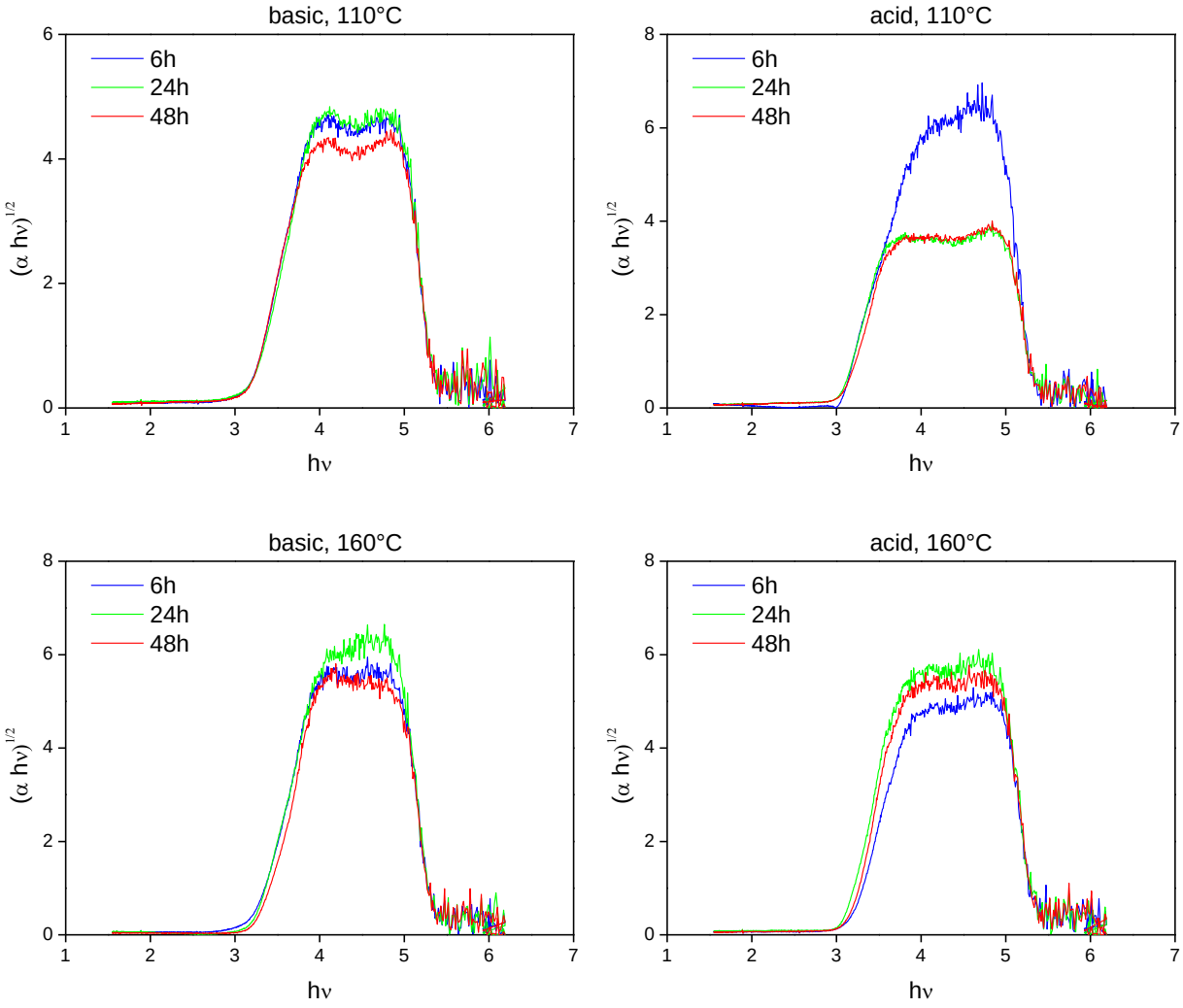

Fig. 60 *Evaluation of band gap energy from indirect transition*

We discovered that all prepared TiO_2 were indirect semiconductors from this analysis. After the comparison of individual samples, we found out that TiO_2 prepared in basic pH had their band gaps around value of 3.23 eV what is typical for anatase phase. On the other side we can observe the blue shift for acid samples. It can be caused by presence of rutile phase.

5.2.8 Photocatalytic activity

The photocatalytic activity was evaluated by the degradation rate of formic acid. We compared the rate constant of prepared TiO_2 and evaluated the best conditions of hydrothermal treatment for final activity. We investigated the decreasing of FA concentration because of UV radiation by HPLC analysis. A record of this analysis is shown in the Fig. 61. It is the dependence of peak intensity (mAU) on the retention time (min). In this figure we can observe decreasing of FA peak (in the position 11.4 min) which characterized the decreasing of FA concentration. There is also noticeable peak in the position 4.7 min that correspond to the injection peak. The concentration of FA was calculated from the height of the peak. For this purpose it is necessary to perform a calibration (Fig. 62). A linear function was calculated as $y = 0.0039x$ with $R^2 = 0.998$.

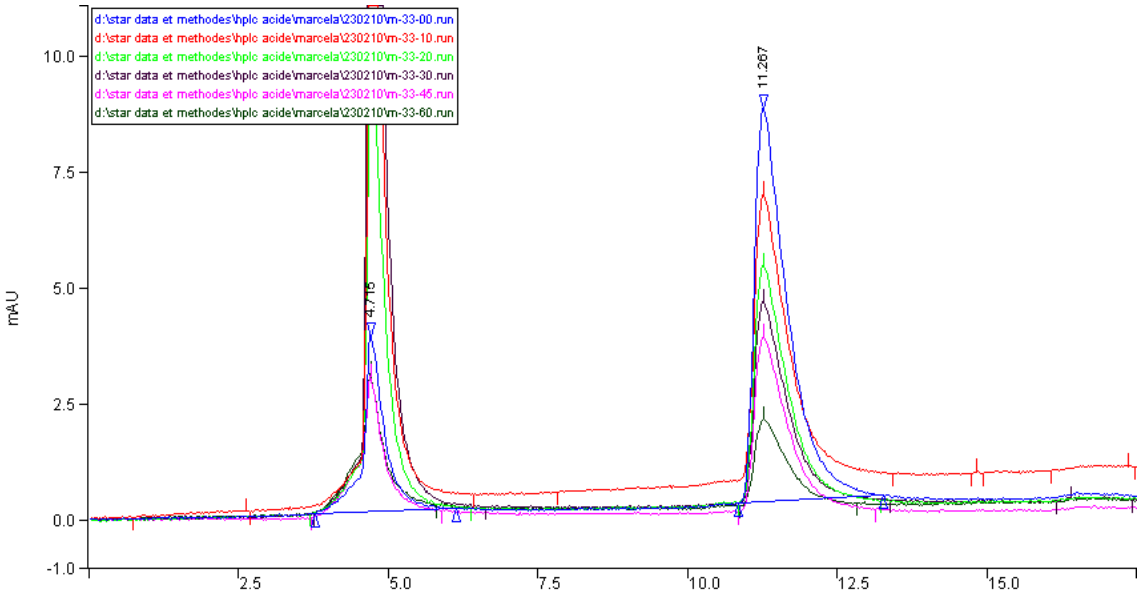

Fig. 61 *Record of HPLC analysis; acid sample; 160°C; 6 hours*

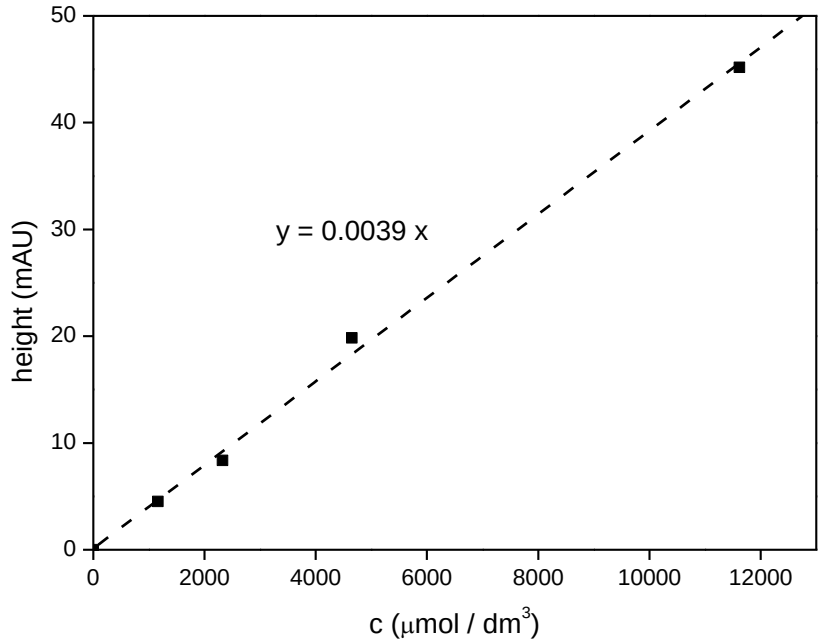

Fig. 62 *Calibration curve of formic acid*

We examined the decreasing of relative concentration as a function of time. We discovered that the profile of time-dependent photocatalytic reactivity is linear within the studied range (Fig. 63), so we conclude that our degradation reactions run according to the zero kinetics model. Subsequently, we calculated the rate constants (k) and their standard errors (SE) for all prepared samples. The comparison of received results is shown in Fig. 64.

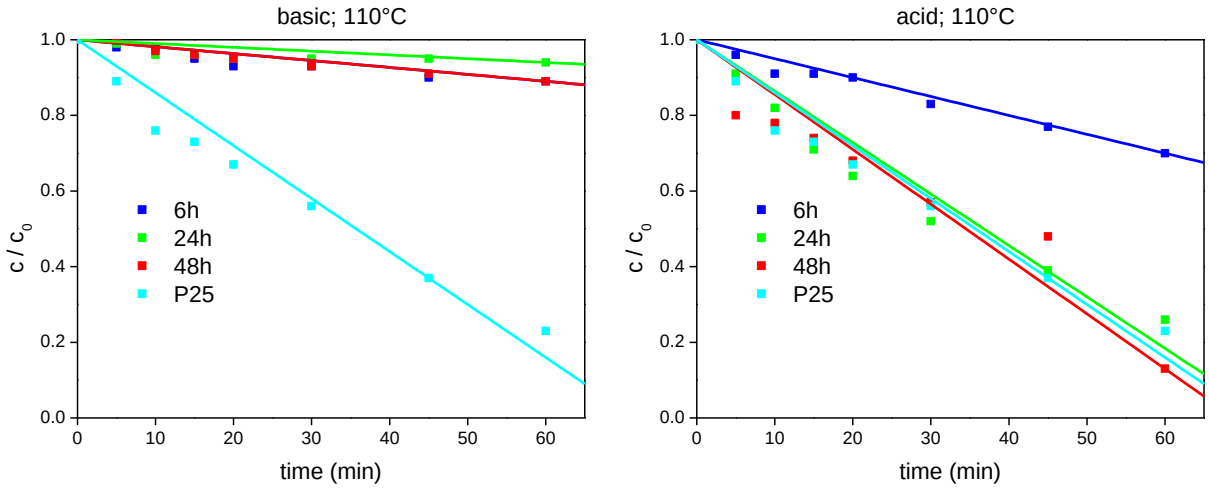

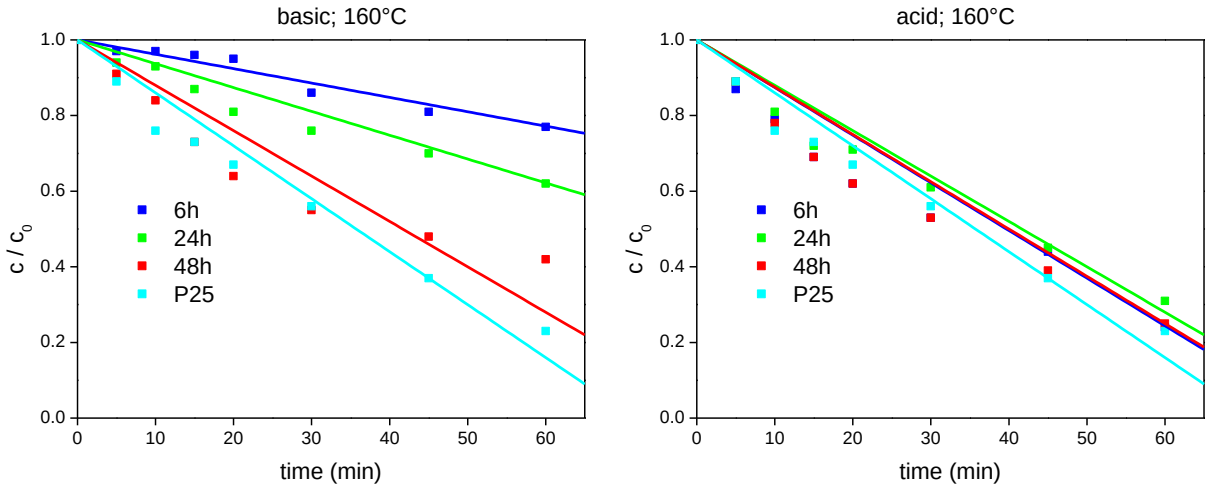

Fig. 63 *FA concentration decreasing during degradation process*

We discovered that the higher photocatalytic activity was reached for samples prepared in acid pH from this investigation. This phenomenon was observed for both used temperatures. This result was expected because in these solutions we found higher values of absorptions (Table 5). Also we found out that with increasing pH we received higher particle size (Table 8). And it is well known that the bigger particles have smaller specific surface areas which lead to lower photocatalytic activity. The other factor which can contribute to lowering of TiO_2 activity was the reduction of rutile phase with increasing pH. It is discovered that mixture of anatase and rutile has higher photocatalytic activity than pure anatase. Finally, the stability of prepared colloidal solutions can also contribute to results photocatalytic activity and we discovered that higher stability was observed for the samples prepared in acid pH than the basic samples.

After the comparison of process temperature we could observe differences between the basic and acidic titania solutions. We discovered that the photocatalytic activity decreases with increasing treatments temperature in acidic environment. This result can be explained by increasing crystallite size with increasing process temperature (Table 7) which means that the specific surface area decreases entailing the decreasing of TiO_2 activity. We also found that samples prepared in acid pH at higher temperature had a lower absorption and smaller stability which also leads to lower photocatalytic activity.

In the case of basic pH, we observed the opposite dependence. It means that with increasing process temperature the activity of prepared samples increased. We found out that TiO_2 solutions prepared at temperature 160 °C showed higher stability and absorption of UV light. We also discovered higher band gap energy for these samples (Table 9) which can contribute to lower probability of recombination and consequently to higher activity.

When we studied the influence of treatment time on the final photocatalytic activity, we discovered that in acidic environment at lower temperature the photocatalytic activity increases with increasing duration of hydrothermal treatment. This dependence was not observed at 160°C. This phenomenon can be explained by crystallite size. As was written in previous part, (5.2.4) the crystallite size decreases with increasing treatment time at

temperature 110 °C what leads to higher specific surface area and consequently to higher photocatalytic activity. The differences between the crystallite sizes in case of 160 °C was not so significant what correspond to similar value of photocatalytic activity.

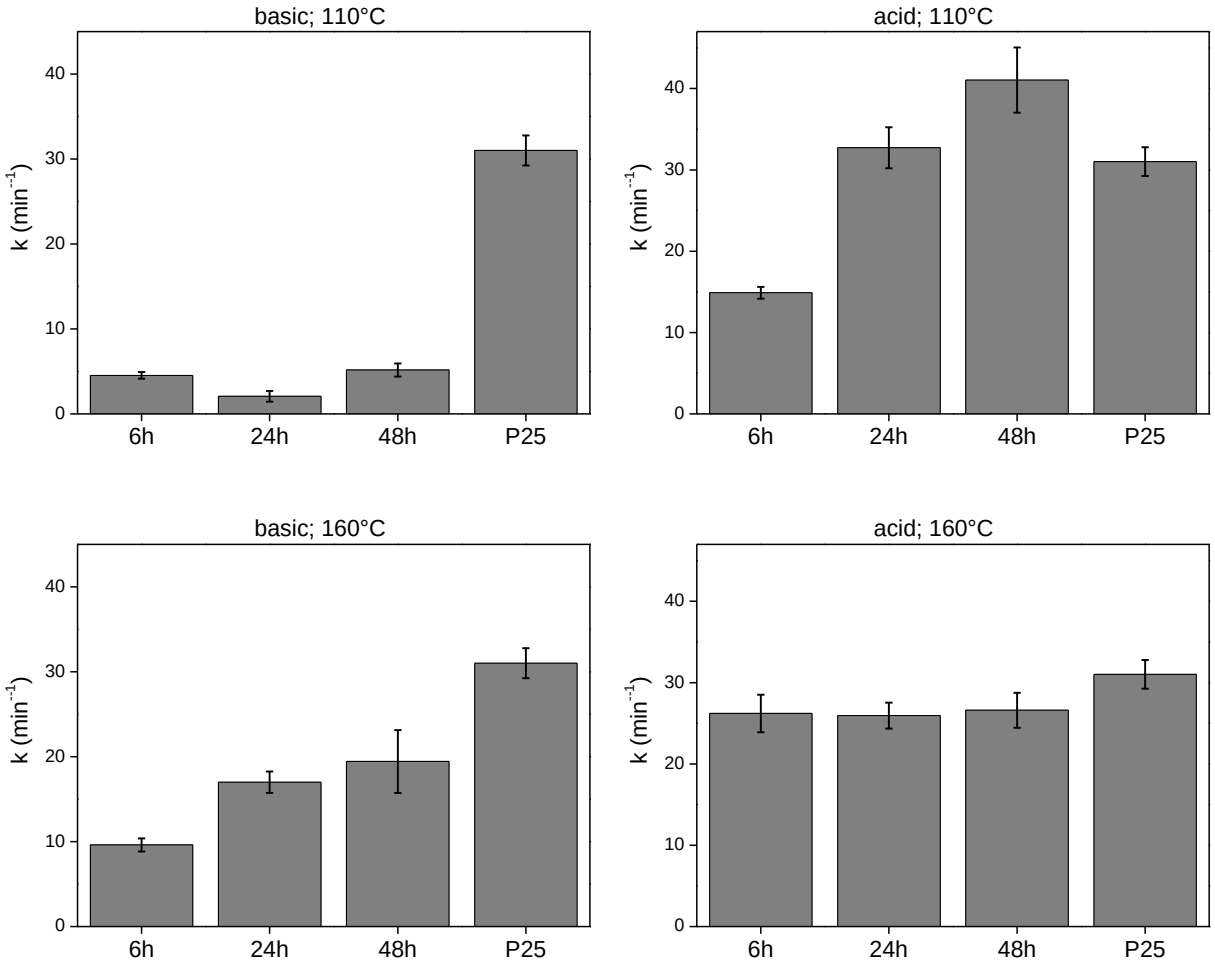

Fig. 64 *Comparison of rate constants k (·10^{-6} min^{-1})*

In basic pH at temperature 160 °C we also observed the increasing of photocatalytic activity. We suppose that decreasing of particle size discovered in section 5.2.6 contributed to this enhance. At the temperature 110 °C, the photocatalytic activity for this kind of samples is again similar.

According to this analysis, the best samples were prepared in acid pH at 110 °C. After the comparison of these samples with commercial TiO_2 (P25) we discovered that our best samples (acidic, 110 °C, 24 hours and 48 hours) were comparable with P25.

In this part of work we discovered that the process conditions have the significant influence on the photocatalytic activity and also on the final physical properties of prepared samples. We discovered that acid solutions had better physical properties and also better final photocatalytic activity. Therefore these samples were chosen for further investigation.

5.3 Printed layers of TiO_2 prepared by hydrothermal synthesis

5.3.1 Preparation of thin titania films

The colloidal solutions of TiO_2 were prepared by hydrothermal synthesis under the different conditions. These samples were used for formation of printing mixtures. Soda-lime glass substrates were coated using experimental printer FUJIFILM Dimatix.

Different surfactants were used as stabilization agents. Firstly, we tried the neutral (Tween 20) (Fig. 65). We observed decreasing of aggregation using this compound but this decreasing was not sufficient. It means that still quite high amount of TiO_2 particles remained in the mesh size syringe filter. Consequently, we tried one anion active surfactant (Abesone) (Fig. 65) and one cation active surfactant (CTAB) (Fig. 65). We observed that only in case of anion active surfactant the aggregation of colloidal particles was completely removed.

Cation active

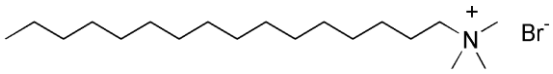

Anion active

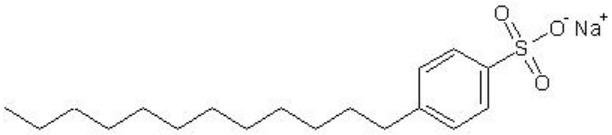

Neutral

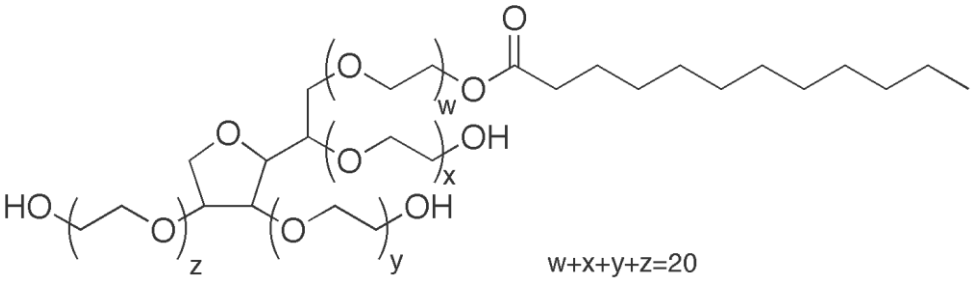

Fig. 65 *Used surfactant; CTAB (left); Abesone (right); Tween 20(bottom)*

We prepared TiO_2 one- and two-layers samples by material printing. This part of study focuses on investigation of thickness influence on final physical properties and photocatalytic activity of the prepared samples. TiO_2 thin films were fixed on the substrate drying at temperature 550 °C for 30 minutes.

The amount of deposited titania particles was evaluated by gravimetric measurement. The obtained results are summarized in table (Table 10). We discovered that in the case of double-layers, the amount increased twice. It means that deposition rate during whole printing

process was constant because printing of double-layer takes twice more time than in case of one-layer.

Table 10 *Results from gravimetric analysis*

Sample			Amount of TiO_2 (g)
110 °C	6 h	1 layer	0.0015
		2 layers	0.0028
	24 h	1 layer	0.0012
		2 layers	0.0023
	48 h	1 layer	0.0015
		2 layers	0.0030
160 °C	6 h	1 layer	0.0011
		2 layers	0.0022
	24 h	1 layer	0.0011
		2 layers	0.0026
	48 h	1 layer	0.0007
		2 layers	0.0020
P25		1 layer	0.0006
		2 layers	0.0014

5.3.2 XRD analysis

The X-ray diffraction patterns of the systems allowed us to identify the crystal phase in TiO_2 systems. All studied powders were pure rutile. This result indicates that the final crystallite phase is mostly dependent on used pH, on temperature and time of hydrothermal synthesis in less extent. All investigated samples were prepared at pH 1 in contrast of the previous work (5.2.4) where TiO_2 was prepared at pH 2. This pH decreasing brought about change of TiO_2 crystallite phase from mixture of anatase and rutile to pure rutile (Fig. 66). This result is in good agreement with published data of Yin et al.[148] where they published that pure rutile is obtained at lower temperature of hydrothermal synthesis using pH around 1.

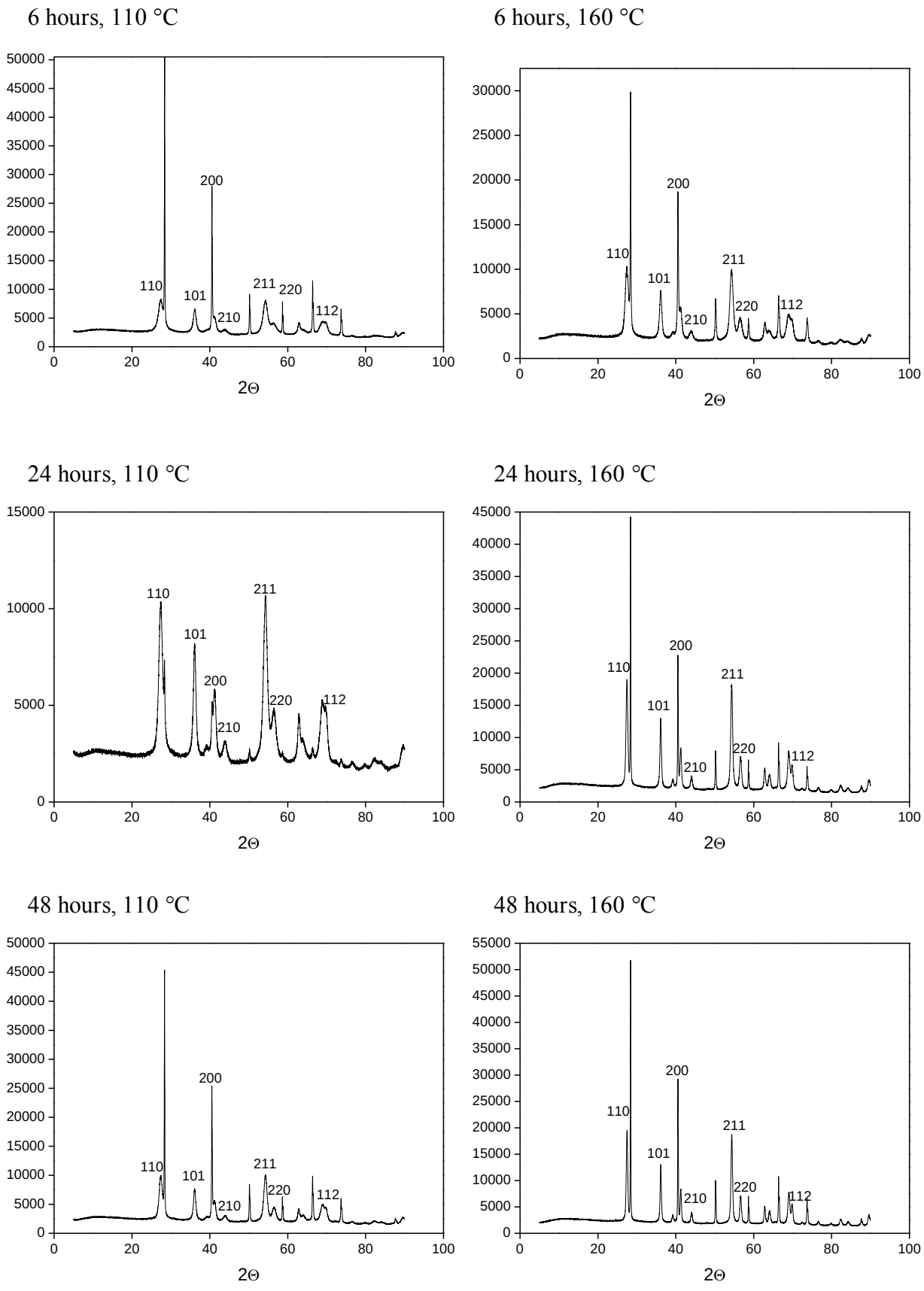

Fig. 66 *XRD records*

5.3.3 Optical microscopy

The quality of prepared layers was examined using Nikon Eclipse E200 optical microscope connected with a digital camera Nikon D70. The used magnification was 20× which were necessary for our purpose because the aim of our study was to compare the homogeneity of prepared films.

All TiO_2 films deposited onto soda-lime glass plates showed milk color and they adhered to the glass substrate after the drying process. We studied the influence of different thickness on final homogeneity and appearance of prepared samples. We discovered that all double-layers were darker that was caused by higher thickness and higher presence of TiO_2 nanoparticles. We also found out that more homogeneous samples were double-layer samples. We suppose that was caused again by higher amount of TiO_2 in the layers. When we compared the samples prepared by the sol-gel method where we had used ordinary printer Epson R220 (4.3.5.2) and these samples prepared by material printer Dimatix we discovered that in these samples there were not presented any cracks. In the case of layers prepared by the sol-gel method we had to use PEG for removing these cracking (Fig. 45).

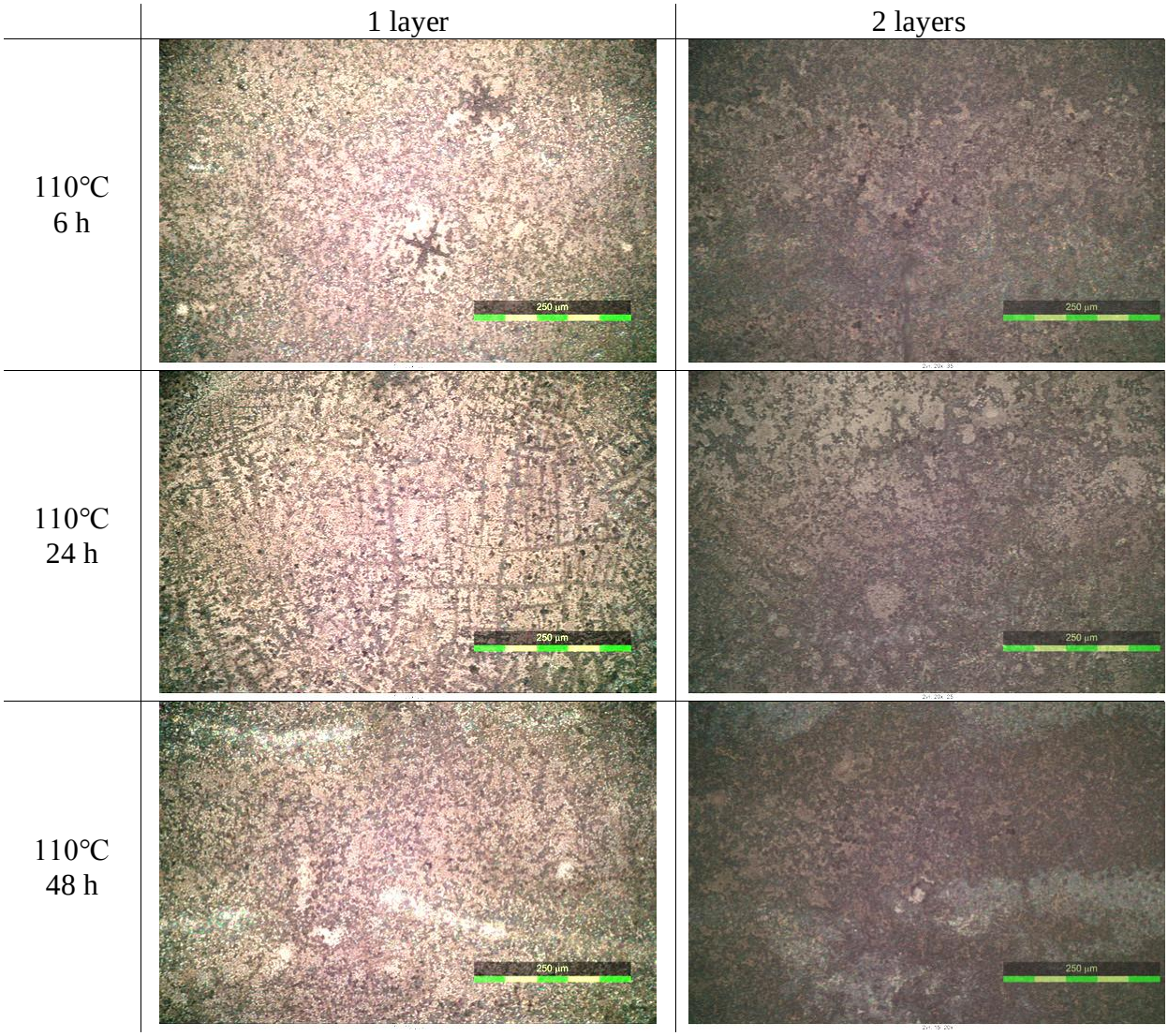

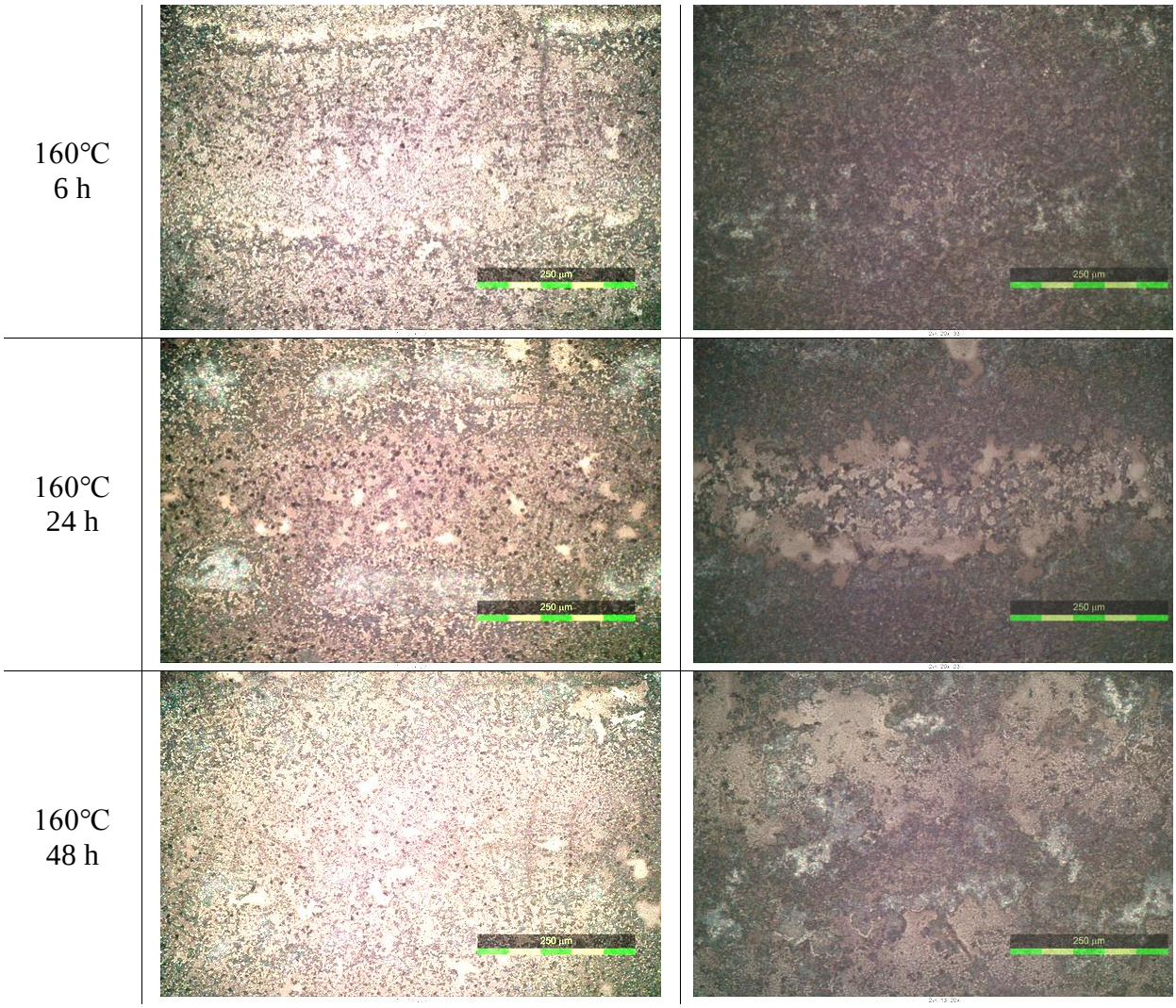

Fig. 67 *Images from optical analysis*

5.3.4 Scanning electron microscopy

The morphology of printed layers was examined by SEM method. The grains size of TiO_2 and the homogeneity of prepared layers were compared for samples synthesized under different conditions. This analysis confirmed that used time of hydrothermal treatment had an enormous influence of final morphology of printed layers

Results form this analysis indicated that with increasing time of hydrothermal treatment the homogeneity of printed layers increased (Fig. 68). It is in a good agreement with the results from TEM analysis (5.2.6). The grain size of each sample was evaluated and we found out that the grain size decrease with increasing time of treatment (Fig. 68). These results were observed for both used temperatures.

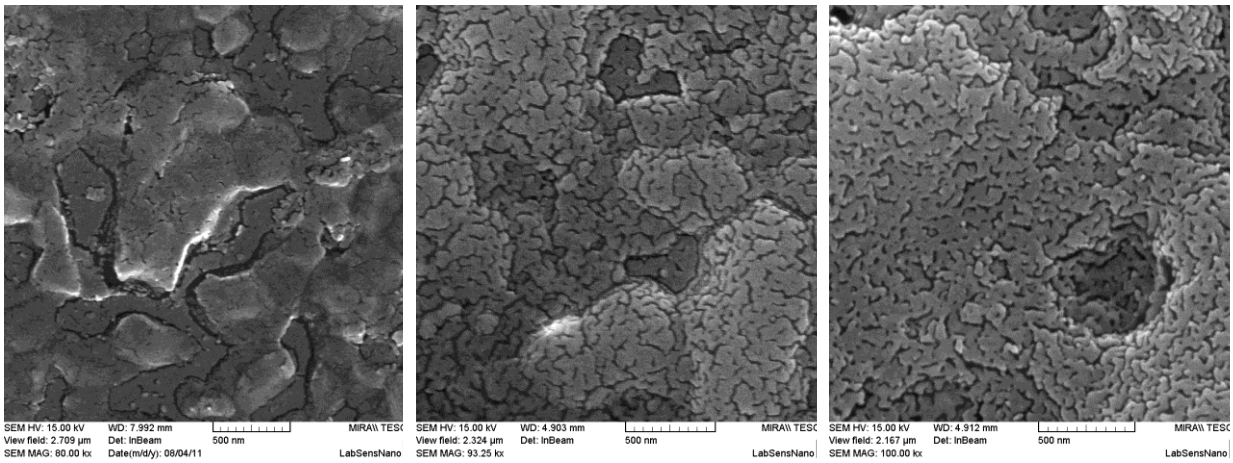

Fig. 68 *Printed layers of titania synthesized at 110°C for different time; 6 h (left); 24 h (middle); 48 h (right)*

5.3.5 Atomic force microscopy

We confirmed the result from SEM measurement by AFM analysis where we observed that with increasing time of hydrothermal treatment the grain size decreases (Fig. 69). The comparison of grain sizes was carried out from scans across 1 μm^2 area. Apart from the evaluation of grain size, we also examined the roughness of prepared layers. We can observe obtained results in Table 11. We discovered that roughness (R_q) of prepared samples increases with increasing time of hydrothermal treatment

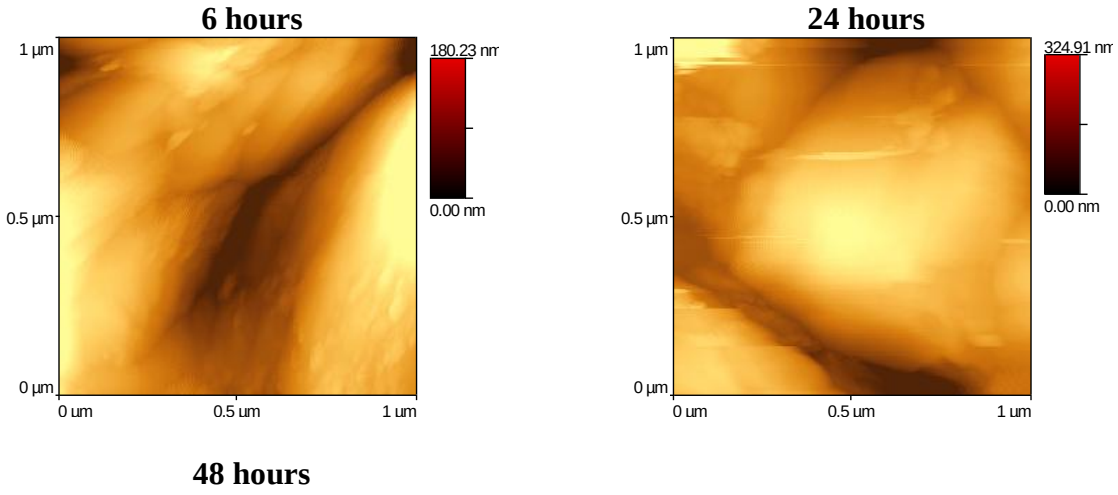

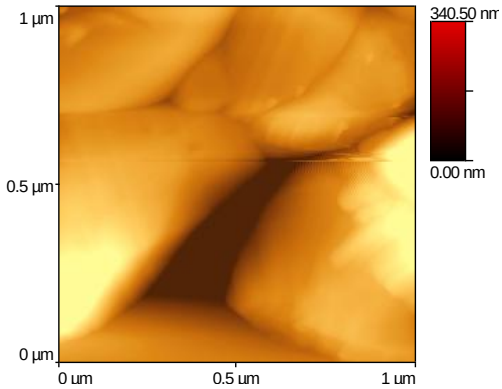

Fig. 69 *Images from AFM analysis*

Table 11 *Roughness of titania printed layers*

Temperature	Time (hours)	R_q (nm)
110 °C	6	40
	24	84
	48	91
160 °C	6	60
	24	53
	48	105

5.3.6 Photoinduced hydrophilicity

Contact angle measurement by the method of sessile drop was carried out for the evaluation of hydrophilic properties of TiO_2 thin films. The analysis was performed during 30 minutes and we discovered that this time was not sufficient for reaching superhydrophylic properties for some samples. As a superhydrophilic surface we consider such surface where the contact angle of deposited drop is lower than 10°. All obtained values are summarized in the tables (Table 12, Table 13).

We found out that the contact angle decreasing was nearly the same for one-layers as well as for double-layers TiO_2 thin films in case of 6 hours and 24 hours (this result was observed for both treatment temperatures). The samples synthesized for the longest time had the smallest tendency change their hydrophobic properties. We observed the smallest decreasing of contact angle after 30 minutes of irradiation by UV light.

Table 12 *Contact angle after different duration of irradiation for one-layer samples*

		UV: 0 min	UV: 10 min	UV: 20 min	UV: 30 min	Δ (0–30) min
Exposure dose ($kJ \cdot m^{-2}$)		0	60	120	180	
110 °C	6 h	62	42	38	36	26
	24 h	39	25	20	14	25
	48 h	31	22	18	16	15
160 °C	6 h	50	40	33	30	20
	24 h	43	34	27	22	21
	48 h	62	56	50	48	14

Table 13 *Contact angle after different duration of irradiation for two-layers samples*

		UV: 0 min	UV: 10 min	UV: 20 min	UV: 30 min	Δ (0–30) min
Exposure dose ($kJ \cdot m^{-2}$)		0	60	120	180	
110 °C	6 h	40	22	19	16	24
	24 h	36	17	13	11	25
	48 h	35	22	17	15	20
160 °C	6 h	31	16	11	8	23
	24 h	29	12	10	8	21
	48 h	45	41	34	31	14

When we compared the results for one and two layers we discovered that for the same samples we obtained similar contact angle decreasing. After the absorption of quantum of light the electrons are generated in the conduction band and these electrons caused the reduction of Ti(IV) to Ti(III). Simultaneously in the valence band there were generated holes which oxidize the O^{2-} anions. During this process, oxygen atoms are ejected, creating oxygen vacancies. Water molecule can then occupy these oxygen vacancies, producing adsorbed OH groups, which tend to make the surface hydrophilic.

By comparing of contact angles decreasing for samples synthesized at different temperature we discovered that higher changes were reached for TiO_2 printed layers where titania colloid solution was prepared at lower temperature. This result was observed in all cases (for both thickness of layer and also for sample synthesized for different hydrothermal time).

5.3.7 Photocatalytic activity

The photocatalytic activity was evaluated as the degradation rate of DCIP in a flow reactor. The absorption maximum of DCIP was found at wave length 600 nm so the absorbance was recorded each minute at this value. The total time of reactions was 40 minutes because of complete decolonization of DCIP solution.

Subsequently the constant rates for examined samples were calculated. The influence of layers thickness was investigated. The activities of our samples were compared with the photocatalytic activity of common commercial TiO_2 (P25).

We discovered that logarithm dependence of relative concentration on time was linear for all prepared titania layers (Fig. 70). So we assumed that reaction runs according the first order kinetics within the studied range. The reaction rate constants (k), their standard errors (SE) and conversion degree were calculated (Table 14).

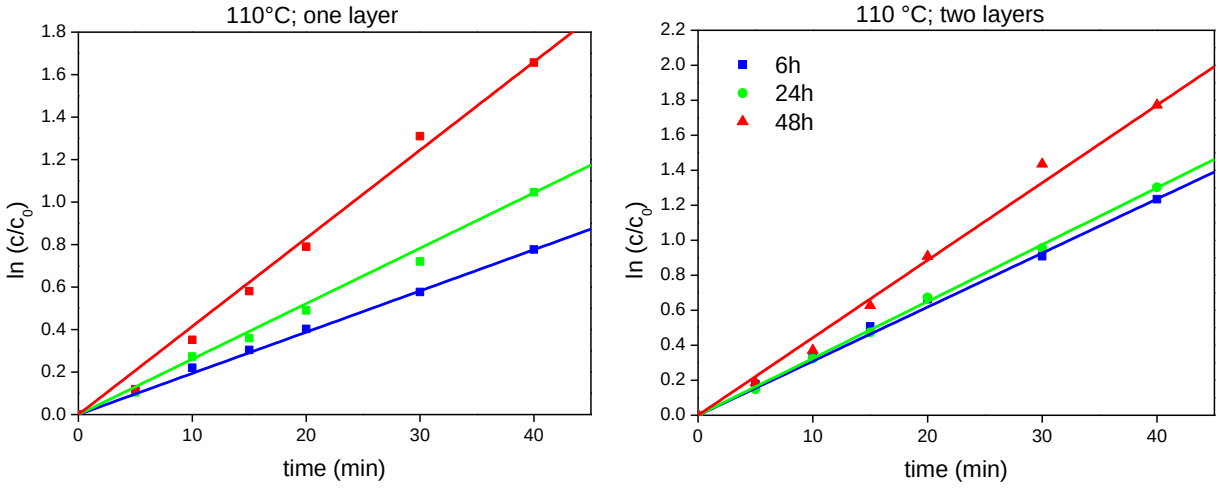

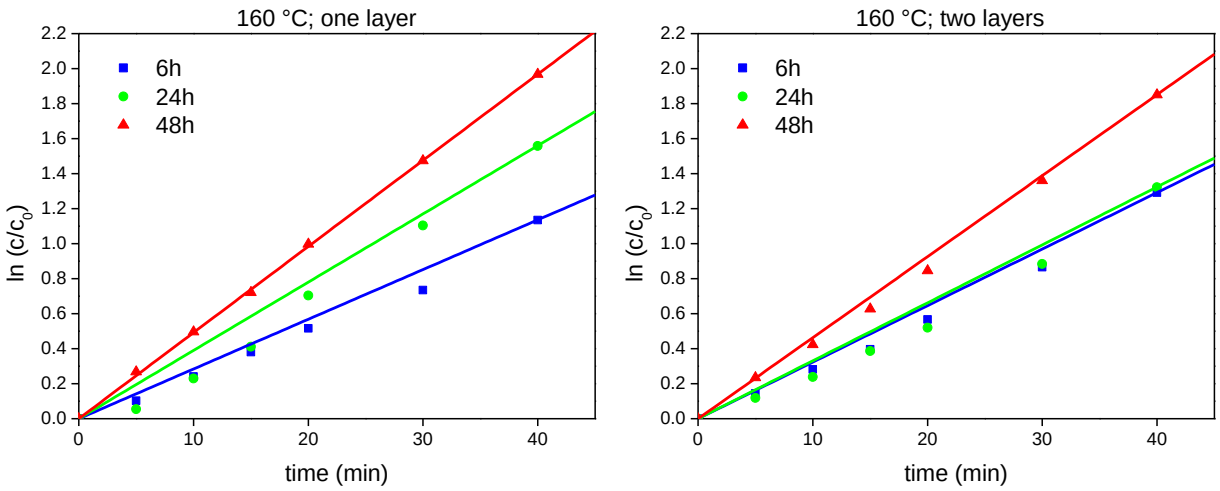

Fig. 70 *Confirmation of the first order kinetics*

The analysis was performed with intensity 7.5 $mW \cdot cm^{-2}$. We discovered from this measurement that double-layers samples were more active. This result was supposed because of higher presence of TiO_2 in the double-layers, i.e. more photocatalyst and so higher amount of photoactive sites.

Although the amount of deposited TiO_2 in case of double-layers increased twice (Table 10) we did not observe increasing of photocatalytic activity two times. It means that all titania particles didn't participate of photocatalytic degradation process. It could be cause by using insufficient intensity for activation of all photocatalysts. Also there could be the influence of a steric effect which could cause adsorption of lower amount of DCIP.

When we compared TiO_2 hydrothermally treated for different time we discovered that samples synthesized for longest time were the most active (Table 14). It could be caused by the decreasing of crystallite size with increasing of treated time which was found out in previous part of the study (Table 7) and also by SEM (5.3.4) and AFM (5.3.5) analysis. Smaller crystallite size leads to higher specific surface area and to increasing of photocatalytic activity.[149]

Table 14 *Formal 1st order rate constant, their standard errors and conversion degree for experiment took place using intensity 7.5 mW·cm^{-2}*

Sample			k (min^{-1})	SE (min^{-1})	Conversion degree (%)
110 °C	6 h	1 layer	0.0002	0.0001	51.0
		2 layers	0.0090	0.0005	66.4
	24 h	1 layer	0.0049	0.0003	61.6
		2 layers	0.0163	0.0009	74.9
	48 h	1 layer	0.0130	0.0007	69.6
		2 layers	0.0212	0.0012	79.2
160 °C	6 h	1 layer	0.0084	0.0005	68.6
		2 layers	0.0083	0.0005	67.4
	24 h	1 layer	0.0122	0.0008	72.8
		2 layers	0.0153	0.0009	76.3
	48 h	1 layer	0.0271	0.0015	83.1
		2 layers	0.0313	0.0017	86.0
P25		1 layer	0.0284	0.0017	84.5
		2 layers	0.0344	0.0019	87.7

Photocatalytic activities of all samples including P25 per 1 g of photocatalyst are shown in Fig. 71. The final standard error was influenced by the SE of partial measurement (calculation of constant rate and SE of weighting). Final standard error was calculated according the equation (26)[150]. When the considered values are independent *r* is equal to 0. When there is a total dependence *r* is equal 1. Because rate constant is dependent on the amount of photocatalysts only in a small range and consequently it is independent we considered *r* equals 0.

$$\left(\frac{S_{k/m}}{k/m}\right)^2 = \left(\frac{S_k}{k}\right)^2 + \left(\frac{S_m}{m}\right)^2 - 2r\left(\frac{S_k}{k}\right)\left(\frac{S_m}{m}\right) \tag{26}$$

We discovered that P25 is the best photocatalyst. Most of prepared samples had activity much lower than P25 only TiO_2 synthesized for 48 hours at 160 °C showed a comparable efficiency.

This difference between our TiO_2 and P25 was probably caused by the different phase of TiO_2. In case of P25 there was mixture of anatase and rutile however all our titania were pure

rutile. So this result was expected because it is well known that mixture of anatase and rutile is much more active than only pure anatase or pure rutile. So this supposition was confirmed in this part.

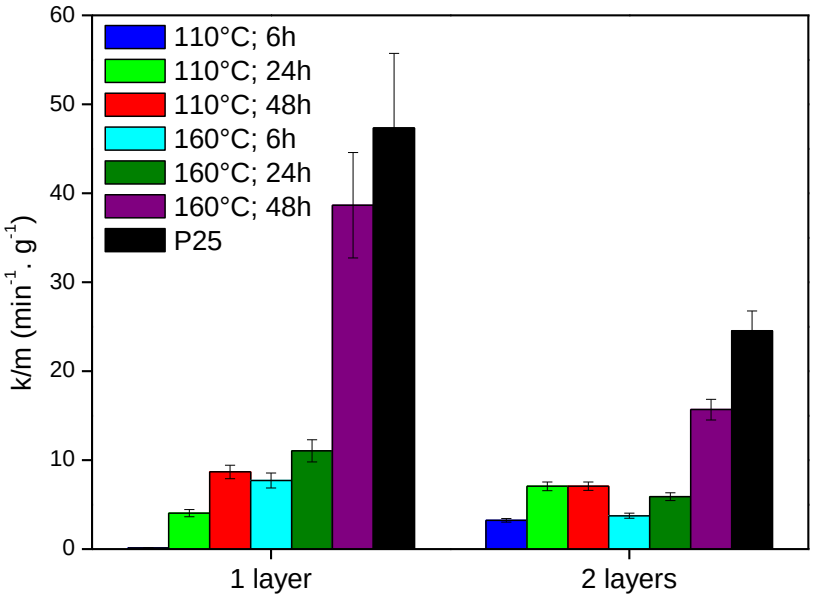

Fig. 71 *Photocatalytic activity per gram*

5.4 Samples prepared by CVD

5.4.1 Preparation of samples

Apart from the material printing, CVD method was used as a second technique for the preparation of thin TiO_2 films. The samples were prepared during two depositions cycles. The duration of vacuum creation and age of precursor were the parameters which were different (Table 3). Physical properties as well as photocatalytic activity of the titania layers was evaluated and we studied the influence of substrate positions and influence of different parameters of CVD on final properties. The position of substrates on susceptor is shown in Fig. 72.

Fig. 72 *Position of glassy carbon during CVD processes*

5.4.2 Gravimetric analysis

Gravimetric analysis was performed for each sample and deposited amount of TiO_2 was evaluated. We can observe the results from this analysis in Table 15. We discovered that in case of sample 1, higher amount of TiO_2 was deposited. This difference was probably caused because of different CVD process. Sample 1 was prepared in the first deposition where we used old precursor. Before the second deposition we had to change TTIP and the others samples were prepared with the new precursor. We supposed that this difference comes from using the new precursor.

Table 15 *Amount of deposited TiO_2 by CVD method*

Sample	Amount of TiO_2
GC-1	1.020 mg
GC-2	0.488 mg
GC-3	0.524 mg
GC-4	0.494 mg

5.4.3 XRD analysis

XRD analysis was used for the characterization of crystallite phase of prepared TiO_2 layer. Because used temperature has the main influence on crystallite phase that, we supposed the preparation of the same titania modification in all cases. We worked at temperature 350 °C in both cases (Table 3). We found out that all prepared titania were pure anatase. Obtained spectra are shown in Fig. 73.

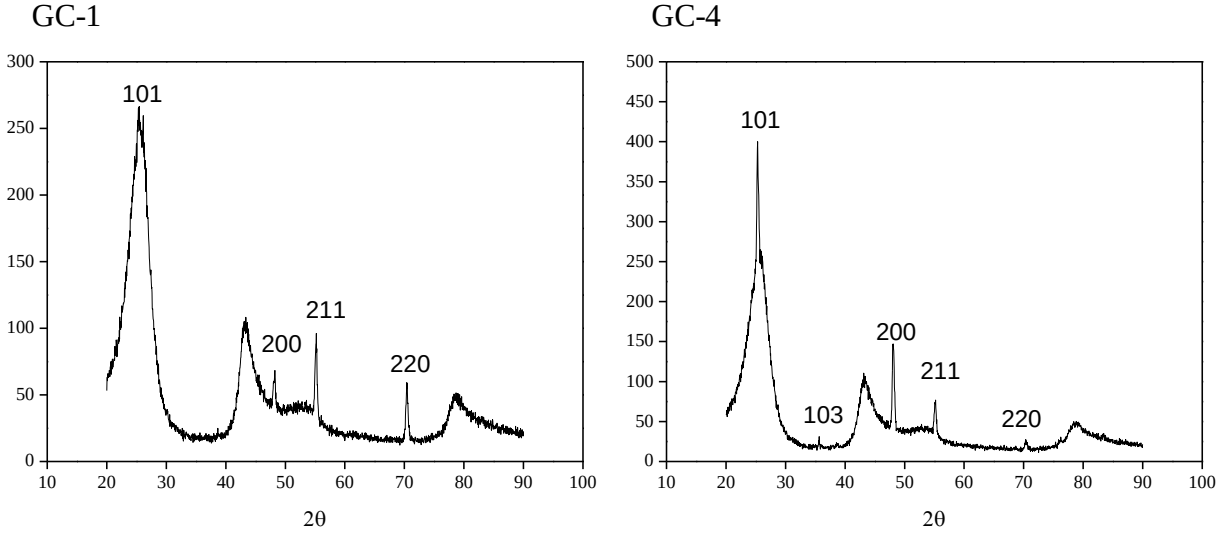

Fig. 73 *XRD spectra*

5.4.4 SEM analysis

SEM analysis was performed on LEO43VP microscope. The SEM images give us a detailed look at the appearance of the TiO_2 layers (Fig. 74). We can observe difference between the grain size of first sample (GC-1) and the others. This sample was prepared during a different CVD process (Table 3). The parameters which were changed in the second CVD were time for the creation of vacuum and the age of precursor. In the first case, the duration of vacuum creation was 1.5 hours in the second one there was 2 hours. It means that only small changes in the process parameters can influence the final properties of prepared layers. Also the age of TTIP could influence the morphology of prepare TiO_2 layer.

Consequently, the thickness of prepared TiO_2 layers was evaluated by a cross section analysis (Fig. 75). We discovered that thicker layers were prepared during the first CVD (around 2.6 μm). Thickness of the second films was evaluated around 2 μm.

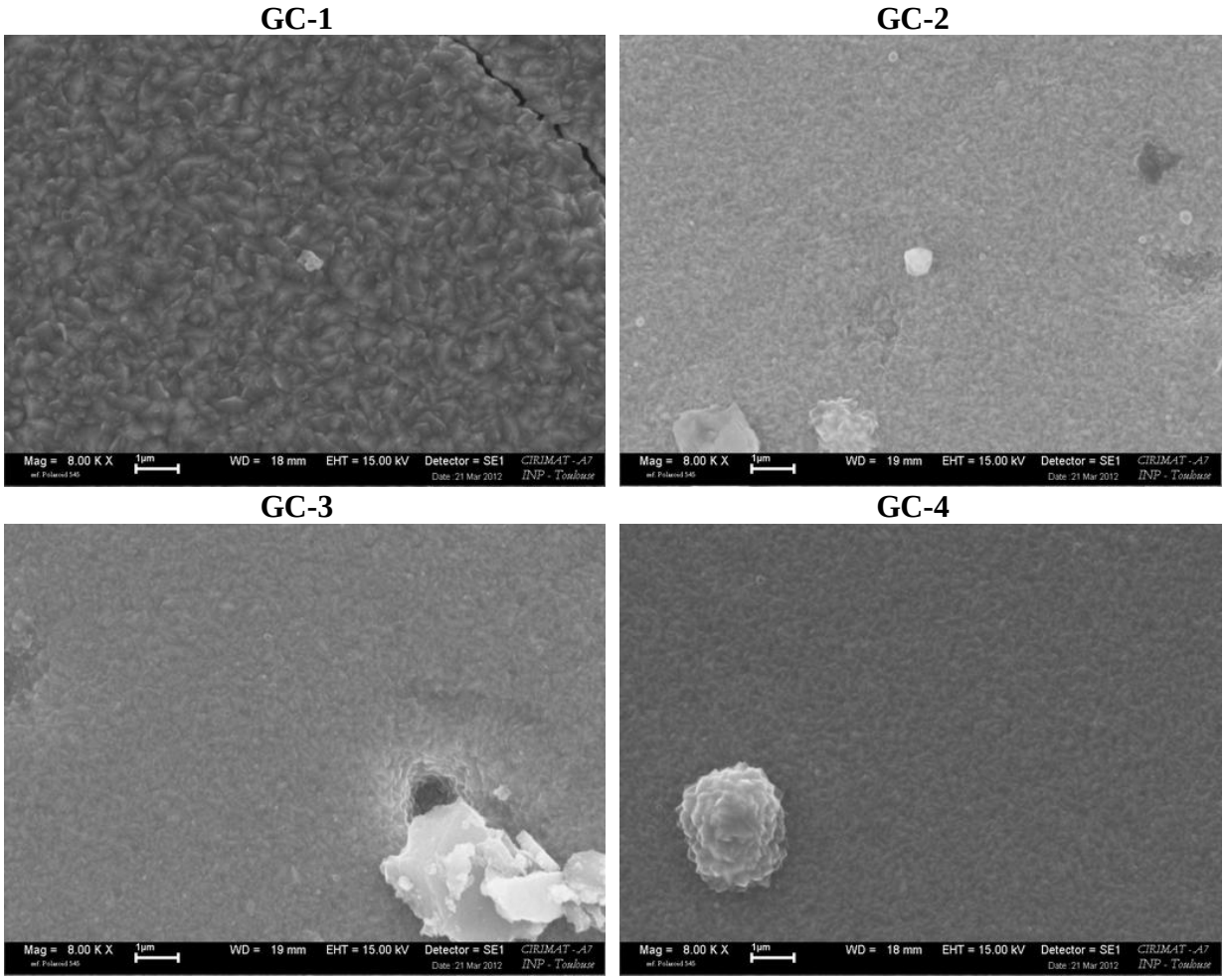

Fig. 74 *SEM images of titania surface*

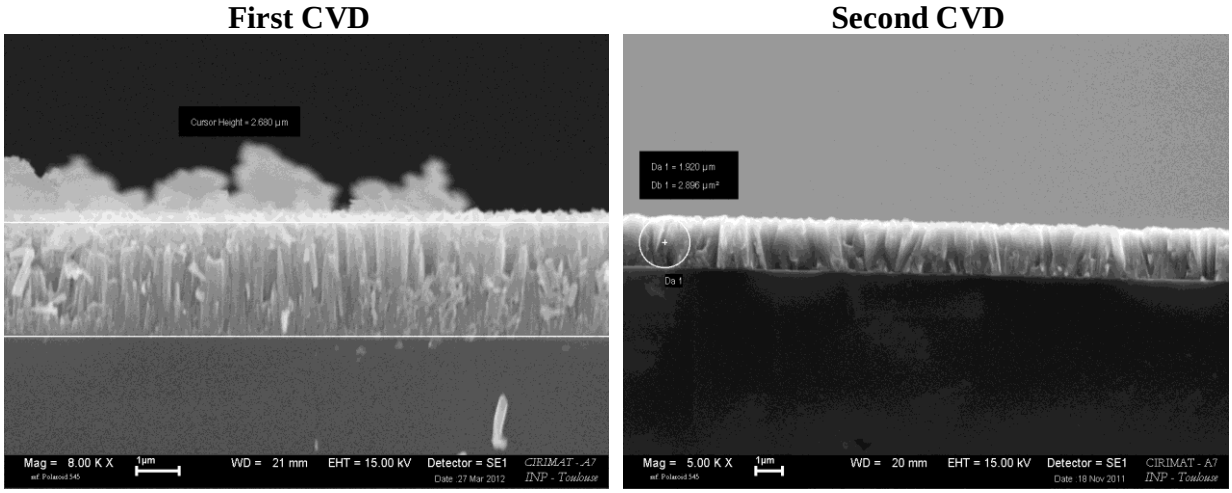

Fig. 75 *SEM images (cross section)*

5.4.5 AFM analysis

The topology and roughness of prepared layers was examined by AFM. We studied 1 μm^2 area and each sample was analyzed on five different places. Roughness was calculated as an average value from five records (Table 16). The mean roughness R_a (roughness average) was calculated according the following formula (27)[136], where *Z(x)* is the profile ordinate of roughness profile.

$$R_a = \frac{1}{L}\int_0^L |Z(x)|dx \tag{27}$$

Obtained results are summarized in the following table (Table 16). After the comparison of a grain size of sample GC-1 (sample prepared during first CVD process) and the other samples we discovered that this sample is consisting of bigger grains (Fig. 76). This result confirmed the result from SEM analysis (Fig. 74). We also observed higher roughness in this case (Table 16).

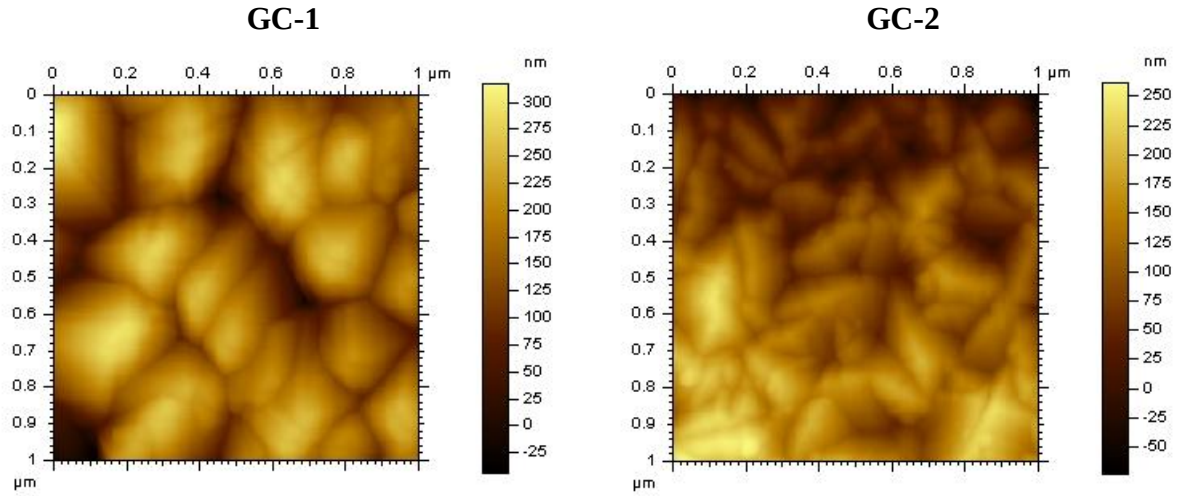

Fig. 76 *Images from AFM analysis*

Table 16 *Roughness of TiO_2 layers prepared by CVD*

Sample	R_a
GC-1	65.2 nm
GC-2	47.1 nm
GC-3	39.6 nm
GC-4	25.9 nm

5.4.6 Investigation of photocatalytic activity

The photocatalytic activity of prepared titania thin layers was examined as a degradation rate of DCIP in a flow reactor. The reactivity of samples was studied for two different intensities (7.5 W·cm^{-2} and 10 W·cm^{-2}). Consequently, the results for intensity 7.5 W·cm^{-2} were compared with the activity of hydrothermal process printed layers. As well as in the previous case, (5.3.7) we observed a linear dependence of relative concentrations logarithm on time also for these samples (Fig. 77). So this result indicates that reaction runs according the first order kinetics within the studied range.

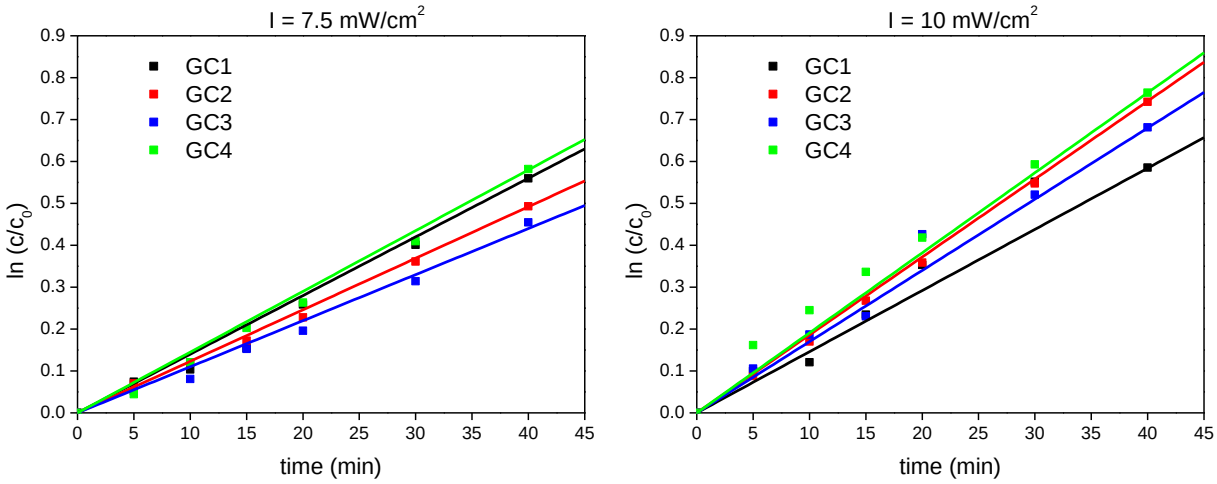

Fig. 77 *Linear dependence of logarithm of relative concentrations on time*

The formal 1st order rate constants (k) and their standard errors (SE) were calculated for both intensities and obtained results are shown in Fig. 78. As we can observe the photocatalytic activity of prepared samples increases with increasing intensity of irradiation. This result was expected because higher intensity can activate more photocatalysts so the degradation reaction runs faster.

In the case of intensity 7.5 mW·cm^{-2} the photocatalytic activity for all samples were similar however for 10 mW·cm^{-2} we could observe increasing reactivity of samples GC-3 and GC-4.

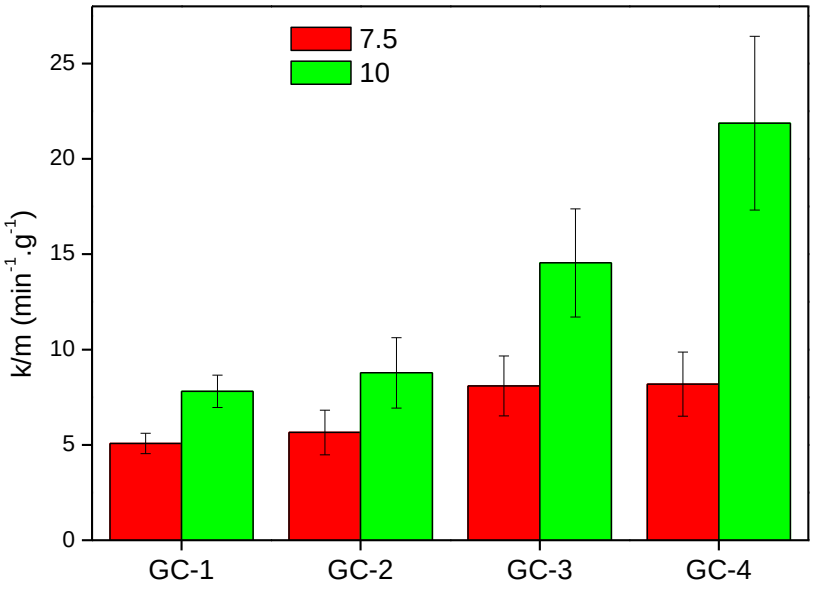

Fig. 78 *Comparison of photocatalytic activity for two intensities of irradiation*

Subsequently, the activity of TiO_2 layers prepared by CVD method was compared with the activity of samples prepared by material printing from hydrothermally treated sols. The rate constants had to be related to 1 gram of photocatalysts because the amount of deposited TiO_2 was in each case different. The results from this analysis are summarized in Fig. 79. We discovered that only the sol treated at 160 °C for 48 hours was more active and the others had a comparable activity.

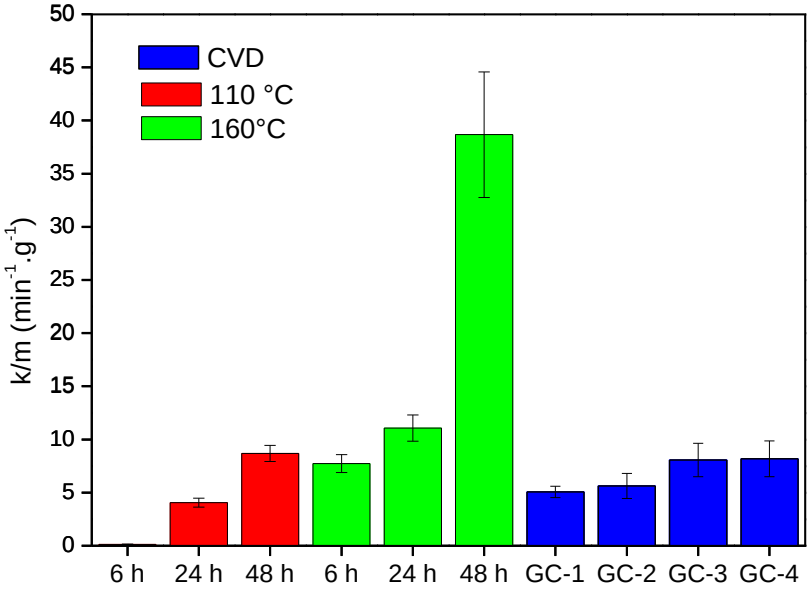

Fig. 79 *Comparison of photocatalytic activity for samples prepared by hydrothermal treatments and CVD method*

6 CONCLUSION

Two methods of thin layers depositions were used in this study; material printing and chemical vapour deposition. Two sols with different precursors (TTIP and $TiOCl_2$) and different preparation (sol-gel method and hydrothermal treatment) were used for material printing. All thin layers were deposited onto the soda-lime glass plates in this case. TTIP was used as a precursor during the CVD process and these layers were deposited onto glassy carbon substrates.

The layers prepared by sol-gel method were homogeneous and transparent. PEG was used as anticracking agent and we discovered that concentration of 4 $g \cdot dm^{-3}$ caused their complete disappearance. The thickness of prepared layers was investigated by specular reflectance measurement using NanoCalc-2000 and we found out that the thickness of titania films increased with increasing sol loading (5.1.2). The morphology of the layers was examined by SEM analysis (5.1.4) and the roughness was evaluated using AFM analysis (5.1.5). We discovered that with increasing amount of PEG the roughness increased. The sessile water drop method was used for studying photoinduced superhydrophilicity. We discovered that after storage the layers in darkness for 10 days all films obtained hydrophobic properties. Nevertheless, these properties were changed back to superhydrophilic after the irradiation by UV light with intensity 15 W/m^2 for 10 minutes.

We investigated the influence of process conditions on final properties for the hydrothermally treated sols. We discovered that temperature and duration of hydrothermal synthesis as well as pH of reaction have significant influence on final properties as stability of slurries (5.2.3), crystallite phase and size (5.2.4), and final photocatalytic activity (5.2.8). Acidic environment was evaluated as better so the other study continued only with sols prepared under this condition.

Consequently, acidic sols were deposited onto the soda-lime glass plates by material printing. We discovered that only anion-active surfactants could be used for preparation of stable printing mixture (5.3.1). All these layers had milky color. Crystallite phase was examined by XRD analysis and we discovered that we prepared pure rutile. This change of crystallite phase from mixture of anatase and rutile (5.2.4) to pure rutile (5.3.2) was caused by decreasing of pH from value 2 to 1. The morphology and grain size was evaluated by SEM (5.3.4) and AFM (5.3.5). We discovered that grain size decreased with increasing of treatment time. As well as for layers prepared by the sol-gel method, we studied the photoinduced superhydrophility for all prepared films. However, we found out that even 30 minutes what corresponded to exposure dose 180 kJ/m^2 was not sufficient to reach superhydrophilic properties in this case (5.3.6).

Apart from the material printing, the thin titania layers were deposited also by CVD. The samples were prepared during two processes and the parameters of the reactions were the same while the only differences were in age of precursors and in the time for vacuum creation. Crystallite phase of prepared layers was analysed by XRD method and in both cases we prepared pure anatase. This result was supposed because of the same temperature. The morphology and thickness of prepared layers were examined by SEM (5.4.4). The thickness

of the films prepared during the first process was higher than in the second. The topology and roughness of the samples was investigated by AFM (5.4.5).

The aim of this work was to investigate the photocatalytic activity of all prepared TiO_2, to compare different method and evaluated the best conditions or the preparation of the titania thin layers. In case of samples prepared by CVD method we examined the influence of different intensities and positions on the susceptor. We did not observe any significant difference between the photocatalytic activities of the samples for the same intensity. This result indicates that there is not any influence of the samples position and their efficiency. Then we found out that with increasing intensity of irradiation the activity of TiO_2 increase (5.4.6).

We compared the influence of treatment conditions and amount of layers on final activity in case of printed layers prepared by hydrothermal synthesis. We discovered that with increasing amount of layers the photocatalytic activity increases. As the best time for hydrothermal synthesis were evaluated 48 hours. When we studied the influence of temperature we observed higher activity for samples prepared at 160 ℃ but only in case of one layer. These results were not obtained for two layers. In this case we found out that photocatalytic activities were similar for samples treated for the same time (5.3.7).

The calculation of activity per gram was necessary for the comparison these two method of depositions. We discovered that activity of TiO_2 synthesized at 110 ℃ for 6 hours was very negligible with the others samples. So these conditions were not satisfactory. The activity of samples treated for times 24 and 48 hours at 110 C were comparable with the activity of samples prepared in CVD process. We evaluated as the best conditions for the preparation time 48 hours and temperature 160 ℃ (5.4.6).

The photocatalytic activity of titania prepared by sol-gel process could not be compared with the other results because the conditions of the experiment was different. We used different reactor (Fig. 36), different lamp (so different emission spectrum) and also different intensity of irradiation (1 mW/cm^2). We discovered from these experiments that activity increased with increasing sol loading. Also we discovered that with increasing amount of PEG the efficiency increased but only up to 4 $g \cdot dm^{-3}$. We observed decreasing of the activity in case of PEG 16 (5.1.7).

7 REFERENCES

[1] KANEKO, Masao. *Photocatalysis*: *science and technology*. Berlín: Springer, 2002, p. 9–28, 109–122, 157–172. ISBN 35-404-3473-9.

[2] PFAFF, Gerhard a Peter REYNDERS. Angle-Dependent Optical Effects Deriving from Submicron Structures of Films and Pigments. *Chemical Reviews*. 1999, vol. 99, no. 7, p. 1963–1982. ISSN 0009-2665.

[3] BRAUN, Juergen H., Andrejs BAIDINS, Robert E. MARGANSKI. TiO2 pigment technology: a review. *Progress in Organic Coatings*. 1992, vol. 20, no. 2, p. 105–138. ISSN 03009440.

[4] YUAN, Shuai, Wanhua CHEN, Shengshui HU. Fabrication of TiO2 nanoparticles/surfactant polymer complex film on glassy carbon electrode and its application to sensing trace dopamine. *Materials Science and Engineering: C*. 2005, vol. 25, no. 4, p. 479–485. ISSN 09284931.

[5] SALVADOR, A., M.C. PASCUAL-MART, J.R. ADELL, A. REQUENI, J.G. MARCH. Analytical methodologies for atomic spectrometric determination of metallic oxides in UV sunscreen creams. *Journal of Pharmaceutical and Biomedical Analysis*. 2000, vol. 22, no. 2, p. 301-306. ISSN 07317085.

[6] FUJISHIMA, AKIRA, KENICHI HONDA. Electrochemical Photolysis of Water at a Semiconductor Electrode. *Nature*. 1972, vol. 238, no. 5358, p. 37–38. ISSN 0028-0836.

[7] GRATZEL, M. Photoelectrochemical cells. *Nature*. 1972, vol. 414, 338–344. ISSN 0028-0836.

[8] MILLS, Andrew, Stephen LE HUNTE. An overview of semiconductor photocatalysis. *Journal of Photochemistry and Photobiology A: Chemistry*. 1997, vol. 108, no. 1, p. 1–35. ISSN 10106030.

[9] CHEN, Xiaobo, Samuel S. MAO. Titanium Dioxide Nanomaterials: Synthesis, Properties, Modifications, and Applications. *Chemical Reviews*. 2007, vol. 107, no. 7, p. 2891–2959. ISSN 0009-2665.

[10] LINSEBIGLER, Amy L., Guangquan. LU, John T. YATES. Photocatalysis on TiO2 Surfaces: Principles, Mechanisms, and Selected Results. *Chemical Reviews*. 1995, vol. 95, no. 3, p. 735–758. ISSN 0009-2665.

[11] DRESSELHAUS, M S, G DRESSLHAUS. Fullerenes and Fullerene Derived Solids as Electronic Materials. *Annual Review of Materials Science*. 1995, vol. 25, no. 1, p. 487–523. ISSN 0084-6600.

[12] ANDERSSON, Martin, Lars ÖSTERLUND, Sten LJUNGSTRÖM, Anders PALMQVIST. Preparation of Nanosize Anatase and Rutile TiO 2 by Hydrothermal Treatment of Microemulsions and Their Activity for Photocatalytic Wet Oxidation of Phenol. *The Journal of Physical Chemistry B*. 2002, vol. 106, no. 41, p. 10674–10679. ISSN 1520-6106.

[13] YU, Jimmy C., Lizhi ZHANG, Zhi ZHENG, Jincai ZHAO. Synthesis and Characterization of Phosphated Mesoporous Titanium Dioxide with High Photocatalytic Activity. *Chemistry of Materials*. 2003, vol. 15, no. 11, p. 2280-2286. ISSN 0897-4756

[14] OPPENLAENDER, Thomas. *Photochemical purification of water and air*. Weinheim: Wiley-VCH, 2003, p. 101–136. ISBN 35-273-0563-7.

[15] DIJKSTRA, M.F.J., H.J. PANNEMAN, J.G.M. WINKELMAN, J.J. KELLY, A.A.C.M. BEENACKERS. Modeling the photocatalytic degradation of formic acid in a reactor with immobilized catalyst. *Chemical Engineering Science*. 2002, vol. 57, no. 22-23, p. 4895-4907. ISSN 00092509.

[16] BENEDIX, R., F. DEHN, J. QUAAS, M. ORGASS. Application of titanium dioxide photocatalysis to create self-cleaning building materials. *Lacer*. 2005, vol. 5, p. 157–167.

[17] OHTANI, B. Photocatalysis A to Z–What we know and what we do not know in a scientific sense. *Journal of Photochemistry and Photobiology C: Photochemistry Reviews*. 2010, vol. 11, no. 4, p. 157–178. ISSN 13895567.

[18] GRAY, Kimberly A. Photocatalysis Group. *Civil and environmental engeneering* [online]. 2006 [cit. 2012-02-28]. Available: http://www.civil.northwestern.edu/EHE/HTML_KAG/Kimweb/Photocatalysis.html,

[19] LINSEBIGLER, Amy L., Guangquan. LU, John T. YATES. Photocatalysis on TiO2 Surfaces: Principles, Mechanisms, and Selected Results. *Chemical Reviews*. 1995, vol. 95, no. 3, p. 735–758. ISSN 0009-2665.

[20] MADHUSUDAN REDDY, K, Sunkara V MANORAMA, A RAMACHANDRA REDDY. Bandgap studies on anatase titanium dioxide nanoparticles. *Materials Chemistry and Physics*. 2003, vol. 78, no. 1, p. 239–245. ISSN 02540584.

[21] FUJISHIMA, A., K. HASHIMOTO, T. WATANABE. TiO2 Photocatalysis: fundamentals and applications. *Journal of Electrochemistry*. 1999, vol. 35, no. 10, p. 1137–1138. ISSN 1023-1935.

[22] LITTER, M. Heterogeneous photocatalysis Transition metal ions in photocatalytic systems. *Applied Catalysis B: Environmental*. 1999, vol. 23, no. 2-3, p. 89–114. ISSN 09263373.

[23] HERRMANN, J. Heterogeneous photocatalysis: fundamentals and applications to the removal of various types of aqueous pollutants. *Catalysis Today*. 1999, vol. 53, no. 1, p. 115–129. ISSN 09205861.

[24] CASTELLO, Geri K. *Handbook of photocatalysts*: *preparation, structure and applications*. New York: Nova Science Publishers, c2010, p. 455–476. Materials science and technologies series. ISBN 978-1-60876-210-1.

[25]LEE, S.F. *Wavelength selective photocatalytic dielectric elements on poly(tetrafluoroethylene) refractors and lamp covers to provide a self-cleaning surface for use on roadway lighting fixtures* [patent]. U.S., 2003, US 6599618 B1 20030729.

[26] EIAMCHAI, Pitak, Pongpan CHINDAUDOM, Mati HORPRATHUM, Viyapol PATTHANASETTAKUL, Pichet LIMSUWAN. Design and investigation of photo-induced super-hydrophilic materials for car mirrors. *Materials*. 2009, vol. 30, no. 9, p. 3428–3435. ISSN 02613069.

[27] PING, Huang. *Structure of a light-catalyst mechanism of an air cleaner* [patent]. Taiwan. U.S., 2003, US 20050089452.

[28] WANG, W.H. *Fluorescent lamp device capable of cleaning air* [patent]. Thaiwan. U.S., 2004, US 20040226813.

[29] BUTTERS, B.E. a A.L. POWELL. *Water treatment process for the reduction of THM and HAA formation* [patent]. U.S., 2004, US 2010-848016

[30] CASTELLO, Geri K. *Handbook of photocatalysts*: *preparation, structure and applications*. New York: Nova Science Publishers, 2010, p. 493–510. Materials science and technologies series. ISBN 978-1-60876-210-1.

[31] YU, Chun-Kang, Kan-Hung HU, Shing-Hoa WANG, Todd HSU, Huei-Ting TSAI, Chien-Chon CHEN, Shiu-Mei LIU, Tai-Yuan LIN, Chin-Hsing CHEN. Photocatalytic effect of anodic titanium oxide nanotubes on various cell culture media. *Applied Physics A*. 2011, vol. 102, no. 2, p. 271-274. ISSN 0947-8396.

[32] RAO, T.N., D.A. TRYK, A. FUJISHIMA. Applications of TiO2 photocatalysis. *Encyclopedia of Electrochemistry*. 2003, vol. 6, p. 536–561, ISBN 978-3-527-61042-6.

[33] ASTRUC, Didier. *Organometallic chemistry and catalysis*. Berlin: Springer, 2007, 608 s. ISBN 978-3-540-46128-9.

[34] MARTOVSKÁ, L., CHUCHVALEC, P.: *Kinetika a katalýza příklady a úlohy*, Ediční středisko, VŠCHT, Praha, 199, ISBN 978-80-7080-670-8 1.

[35] YAMAZAKI, Suzuko, Satoru TANAKA, Hidekazu TSUKAMOTO. Kinetic studies of oxidation of ethylene over a TiO2 photocatalyst. *Journal of Photochemistry and Photobiology A: Chemistry*. 1999, vol. 121, no. 1, p. 55–61. ISSN 10106030.

[36] ATKINS, Peter William. *Atkins' Physical Chemistry*. 7th ed. Oxford: Oxford University Press, 2002, 1149 s. ISBN 01-987-9285-9.

[37] SERPONE, Nick a Angela SALINARO. Terminology, relative photonic efficiencies and quantum yields in heterogeneous photocatalysis. Part I: Suggested protocol. *Pure and Applied Chemistry*. 1999, vol. 71, no. 2, p. 30–320. ISSN 0033-4545.

[38] KERISIT, Sebastien, Kevin M. ROSSO, Zhenguo YANG, Jun LIU. Computer Simulation of the Phase Stabilities of Lithiated TiO 2 Polymorphs. *Journal of Physical Chemistry C*. 2010, vol. 144, no. 44, p. 19096–19107. ISSN 1932-7447.

[39] BANFIELD, J.F., D.R. VEBLEN. Conversion of perovskite to anatase and titanium dioxide (B): A TEM study and the use of fundamental building blocks for understanding relationships among the titania minerals. *The American mineralogist*. 1992, vol. 77, no. 5–6, p. 545–557. ISSN 0003-004x

[40] GREENWOOD, N. N.; EARNSHAW, A.: *Chemistry of the elements*. 2nd ed. S.l.: Elsevier, 1997. ISBN 978-008-0501-093.

[41] YU, Jiaguo, Xiujian ZHAO, Qingnan ZHAO. Effect of surface structure on photocatalytic activity of TiO2 thin films prepared by sol-gel method. *Thin Solid Films*. 2000, vol. 379, no.1–2, p. 7–14. ISSN 00406090.

[42] YU, J, G WANG, B CHENG, M ZHOU. Effects of hydrothermal temperature and time on the photocatalytic activity and microstructures of bimodal mesoporous TiO2 powders. *Applied Catalysis B: Environmental*. 2007-01-15, vol. 69, no. 3–4, p. 171–180. ISSN 09263373

[43] ZABAN, A., S. T. ARUNA, S. TIROSH, B. A. GREGG, Y. MASTAI. The Effect of the Preparation Condition of TiO 2 Colloids on Their Surface Structures. *The Journal of Physical Chemistry B*. 2000, vol. 104, no. 17, p. 4130–4133. ISSN 1520-6106.

[44] Mindat.org. *Locality, mineral & photograph data* [online]. 1993 [cit. 2011-03-03]. Available: http://www.mindat.org/show.php?id=213&ld=1

[45] Mineralogie, Systematik und Nomenklatur. *Büro für angewandte Mineralogie* [online]. 2004 [cit. 2011-03-23]. Available: http://www.a-m.de/deutsch/lexikon/mineral/oxide.htm

[46] Handbook of Minerals Raman Spectra. *Laboratoire de Sciences de la Terre* [online]. 2000 [cit. 2011-04-27]. Available: www.ens-lyon.fr/LST/Raman

[47] Search RRUFF Sample Data. *RRUFF* [online]. [cit. 2011-04-27]. Available: http://rruff.info/; Search RRUFF

[48] GOPAL, M., W.J.M CHAN, L.C DE JONGHE. Room temperature synthesis of crystalline metal oxides. *Journal of Materials Science*. Norwell: Kluwer Academic Publishers, 1997, vol. 32, no. 22, p.6001–6008. ISSN 0022-2461

[49] REYES-CORONADO, D, G RODRÍGUEZ-GATTORNO, M E ESPINOSA-PESQUEIRA, C CAB, R DE COSS, G OSKAM. Phase-pure TiO 2 nanoparticles: anatase, brookite and rutile. *Nanotechnology*. 2008-04-09, vol. 19, no. 14, p. 145605–145615. ISSN 0957-4484.

[50] FMF. *Minerals forum* [online]. 2006 [cit. 2011-04-27]. Available http://www.mineral-forum.com/message-board/viewtopic.php?t=429

[51] ZALLEN, R., M.P. MORET. The optical absorption edge of brookite TiO2. *Solid State Communications*. 2006, vol. 137, no. 3, p. 154–157. ISSN 00381098.

[52] NAGASE, Takako, Takeo EBINA, Takashi IWASAKI, Hiromichi HAYASHI, Yoshio ONODERA, Maya CHATTERJEE. Hydrothermal Synthesis of Brookite. *Chemistry Letters*. 1999, no. 9, p. 911–912. ISSN 0366-7022.

[53] POTTIER, Agnès, Corinne CHANÉAC, Elisabeth TRONC, Léo MAZEROLLES, Jean-Pierre JOLIVET. Synthesis of brookite TiO2 nanoparticles by thermolysis of TiCl4 in strongly acidic aqueous media. *Journal of Materials Chemistry*. 2001, vol. 11, no. 4, p. 1116–1121. ISSN 09599428.

[54] Available online at:
http://pakgma.com/Gallery/Courtesy%20by%20Herb%20Obodda%20%28info@obodda.com, cited 4. 3. 2011.

[55] MILLS, Andrew, Stephen LE HUNTE. An overview of semiconductor photocatalysis. *Journal of Photochemistry and Photobiology A: Chemistry*. 1997, vol. 108, no. 1, p. 1–35. ISSN 10106030.

[56] MILLS, Andrew, Phillip SAWUNYAMA. Photocatalytic degration of 4-chlorophenol mediated by TiO2: a comparative study of the activity of laboratory made and commercial TiO2 samples. *Journal of Photochemistry and Photobiology A: Chemistry*. 1994, vol. 84, no. 3, p. 305–309. ISSN 10106030.

[57] COSTA, Leonardo L., Alexandre G.S. PRADO. TiO2 nanotubes as recyclable catalyst for efficient photocatalytic degradation of indigo carmine dye. *J. Photochem. Photobiol. A,*. 2009, vol. 201, no. 1, p. 45–49. ISSN 1010-6030..

[58] GUPTA, A.K., Anjali PAL, C. SAHOO. Photocatalytic degradation of a mixture of Crystal Violet (Basic Violet 3) and Methyl Red dye in aqueous suspensions using Ag doped TiO2. *Dyes and Pigments*. 2006, vol. 69, no. 3, p. 224–232. ISSN 01437208.

[59] KAJITVICHYANUKUL, Puangrat, Jirapat ANANPATTARACHAI, Siriwan PONGPOM. Sol-gel preparation and properties study of TiO 2 thin film for photocatalytic reduction of chromium(VI) in

photocatalysis process. *Science and technology of advanced materials*. 2005, vol. 6, no. 3-4, p. 352–358. ISSN 1468-6996.

[60] BYRNE, J.A., B.R. EGGINS, N.M.D. BROWN, B. MCKINNEY, M. ROUSE. Immobilisation of TiO2 powder for the treatment of polluted water. *Applied Catalysis B: Environmental*. 1998, vol. 17, no. 1–2, p. 25–36. ISSN 09263373

[61] BUTTERFIELD, I. M., A. P. CHRISTENSEN, A. HAMNETT, K. E. SHAW, G. M. WALKER, S. A. WALKER, C. R. HOWARTH. Applied studies on immobilized titanium dioxide films as catalysts for the photoelectrochemical detoxification of water. *Journal of applied electrochemistry*. 1997, vol. 27, no. 4. p. 385–395. ISSN 0021-891x.

[62] CHEN, Z. J., G. L. ZHAO, H. LI, J. J. ZHANG, B. SONG, G. R. HAN. Preparation of nanocrystalline TiO2 by sol-gel-method at room temperature. *Journal of inorganic chemistry*. 2010, vol. 26, no. 5, p. 860–866. ISSN 1001-4861

[63] DIAZ-FONSECA, A. L., J. C. CHEANG-WONG. Synthesis and characterization of colloidal titania nanoparticles. *Materials Research Society Symposium Proceedings*. 2008, vol. 1034, p. 1074. ISSN 0272-9172.

[64] SCHUBERT, Ulrich. Chemical modification of titanium alkoxides for sol?gel processing. *Journal of Materials Chemistry*. 2005, vol. 15, mo. 35–36, p. 3701–3715. ISSN 0959-9428.

[65] ANDERSON, Marc A., Mary J. GIESELMANN, Qunyin XU. Titania and alumina ceramic membranes. *Journal of Membrane Science*. 1988, vol. 39, no. 3, p. 243–258. ISSN 03767388.

[66] BARBE, C. J., F. ARENDSE, P. COMTE, M. JIROUSEK, F. LENZMANN, V. SHKLOVER, M. GRATZEL. Nanocrystalline titanium oxide electrodes for photovoltaic applications. *Journal of the American Ceramic Society*. United States of America: Blackwell Publishing, Inc, 1997, vol. 80, no. 2, p. 3157–3171. ISSN 0002-7820.

[67] VORKAPIC, D., T. MATSOUKAS. Effect of temperature and alcohols in the preparation of titania nanoparticles from alkoxides. *Journal of the American Ceramic Society*. United States of America: Blackwell Publishing, Inc, 1998, vol. 81, no. 11, p. 2815–2820. ISSN 0002-7820.

[68] O'REGAN, Brian, Michael GRÄTZEL. A low-cost, high-efficiency solar cell based on dye-sensitized colloidal TiO2 films. *Nature*. 1991-10-24, vol. 353, no. 6346, p. 737–740. ISSN 0028-0836.

[69] CHATRY, M., M. HENRY, J. LIVAGE. Synthesis of non-aggregated nanometric crystalline zirconia particles. *Materials Research Bulletin*. 1994, vol. 29, no. 5, p. 517–522. ISSN 00255408

[70] SANCHEZ, C., J. LIVAGE, M. HENRY, F. BABONNEAU. Chemical modification of alkoxide precursors. *Journal of Non-Crystalline Solids*. 1988, vol. 100, no. 1–3, p. 65–76. ISSN 00223093.

[71] YANG, Juan, Sen MEI, J.M.F. FERREIRA. Hydrothermal synthesis of TiO2 nanopowders from tetraalkylammonium hydroxide peptized sols. *Materials Science and Engineering: C*. 2001, vol. 15, no. 1–2, p. 183–185. ISSN 09284931.

[72] CHAE, Seung Yong, Myun Kyu PARK, Sang Kyung LEE, Taek Young KIM, Sang Kyu KIM, Wan In LEE. Preparation of Size-Controlled TiO 2 Nanoparticles and Derivation of Optically Transparent Photocatalytic Films. *Chemistry of Materials*. 2003, vol. 15, no. 17, p. 3326–3331. ISSN 0897-4756.

[73] ZHANG, Qinghong, Lian GAO. Preparation of Oxide Nanocrystals with Tunable Morphologies by the Moderate Hydrothermal Method: Insights from Rutile TiO 2. *Langmuir*. 2003, vol. 19, no. 3, p. 967–971. ISSN 0743-7463.

[74] YANG, Songwang, Lian GAO. Fabrication and Characterization of Nanostructurally Flowerlike Aggregates of TiO2 via a Surfactant-free Solution Route: Effect of Various Reaction Media. *Chemistry Letters*. 2005, vol. 34, no. 7, p. 1044–1045. ISSN 0366-7022.

[75] YOSHIDA, Ryuhei, Yoshikazu SUZUKI, Susumu YOSHIKAWA. Syntheses of TiO2(B) nanowires and TiO2 anatase nanowires by hydrothermal and post-heat treatments. *Journal of Solid State Chemistry*. 2005, vol. 178, no. 7, p. 2179–2185. ISSN 00224596.

[76] ZHANG, Y.X., G.H. LI, Y.X. JIN, Y. ZHANG, J. ZHANG, L.D. ZHANG. Hydrothermal synthesis and photoluminescence of TiO2 nanowires. *Chemical Physics Letters*. 2002, vol. 365, no. 3–4, p. 300–304. ISSN 00092614.

[77] BAVYKIN, Dmitry V., Alexei A. LAPKIN, Pawel K. PLUCINSKI, Jens M. FRIEDRICH, Frank C. WALSH. Reversible Storage of Molecular Hydrogen by Sorption into Multilayered TiO 2 Nanotubes. *The Journal of Physical Chemistry B*. 2005, vol. 109, no. 41, p. 19422–19427. ISSN 1520-6106..

[78] DU, G. H., Q. CHEN, R. C. CHE, Z. Y. YUAN, L.-M. PENG. Preparation and structure analysis of titanium oxide nanotubes. *Applied Physics Letters*. 2001, vol. 79, no. 22, p. 3702–3704. ISSN 00036951.

[79] STRIDE, John A., Nam T. TUONG. Controlled Synthesis of Titanium Dioxide Nanostructures. *Solid State Phenomena*. 2010, vol. 162, p. 261–294. ISSN 1662-9779.

[80] PRESCOTT, Wesley V, Arnold I SCHWARTZ. *Nanorods, nanotubes, and nanomaterials research progress*. New York: Nova Science, c2008, p. 163–201. ISBN 978-1-60456-122-7.

[81] VIRIYA-EMPIKUL, N, N SANO, T CHARINPANITKUL, T KIKUCHI, W TANTHAPANICHAKOON. A step towards length control of titanate nanotubes using hydrothermal reaction with sonication pretreatment. *Nanotechnology*. 2008-01-23, vol. 19, no. 3, p. 035601–035606. ISSN 0957-4484.

[82] WONG, Chung Leng, Yong Nian TAN, Abdul Rahman MOHAMED. A review on the formation of titania nanotube photocatalysts by hydrothermal treatment. *Journal of Environmental Management*. 2011, vol. 92, no. 7, p. 1669–1680. ISSN 03014797.

[83] MA, Yutao, Yuan LIN, Xurui XIAO, Xiaowen ZHOU, Xueping LI. Sonication?hydrothermal combination technique for the synthesis of titanate nanotubes from commercially available precursors. *Materials Research Bulletin*. 2006, vol. 41, no. 2, p. 237–243. ISSN 00255408.

[84] SEO, Hyung-Kee, Gil-Sung KIM, S.G. ANSARI, Young-Soon KIM, Hyung-Shik SHIN, Kyu-Hwan SHIM, Eun-Kyung SUH. A study on the structure/phase transformation of titanate nanotubes synthesized at various hydrothermal temperatures. *Solar Energy Materials and Solar Cells*. 2008, vol. 92, no. 11, p. 1533–1539. ISSN 09270248.

[85] BYRAPPA, K a Masahiro YOSHIMURA. *Handbook of hydrothermal technology*: *a technology for crystal growth and materials processing*. Norwich, N.Y.: Noyes Publications, c2001, p. 691–753. ISBN 978-0-8155-1445-9.

[86] KIM, Chung-Sik, Byung Kee MOON, Jong-Ho PARK, Su TAE CHUNG, Se-Mo SON. Synthesis of nanocrystalline TiO2 in toluene by a solvothermal route. *Journal of crystal growth*. 2003, vol. 254, no. 3–4, p. 405–410. ISSN 0022-0248.

[87] KIM, Chung-Sik, Byung Kee MOON, Jong-Ho PARK, Byung-Chun CHOI, Hyo-Jin SEO. Solvothermal synthesis of nanocrystalline TiO2 in toluene with surfactant. *Journal of Crystal Growth*. 2003, vol. 257, no. 3–4, p. 309–315. ISSN 00220248.

[88] WEN, Baomei, Chunyan LIU, Yun LIU. Depositional Characteristics of Metal Coating on Single-Crystal TiO 2 Nanowires. *The Journal of Physical Chemistry B*. 2005, vol. 109, no. 25, p. 12372–12375. ISSN 1520-6106

[89] KAJIKAWA, Yuya. Roughness evolution during chemical vapor deposition. *Materials Chemistry and Physics*. 2008, vol. 112, no. 2, p. 311–318. ISSN 02540584.

[90] HELLER, Adam. Chemistry and Applications of Photocatalytic Oxidation of Thin Organic Films. *Accounts of Chemical Research*. 1995, vol. 28, no. 12, p. 503–508. ISSN 0001-4842.

[91] XU, Y.; YAN, X.T.: *Chemical vapour deposition*, Dordrecht, Springer, 2010, p. 1–341, ISSN 1619-0181.

[92] GLOCKER, David A, S SHAH, William D WESTWOOD. *Handbook of thin film process technology*. Philadelphia: Institute of Physics Pub., c1995, p. 313. ISBN 07503 03115.

[93] CHOY, K. Chemical vapour deposition of coatings. *Progress in Materials Science*. 2003, vol. 48, no. 2, p. 57–170. ISSN 00796425.

[94] WACHTELL, R. L. a R. P. SEELIG. *Diffusion coatings for metal articles* [patent]. U.S., US 1964-354440. (1966).

[95] PARK, Dong Gon, James M. BURLITCH. Nanoparticles of anatase by electrostatic spraying of an alkoxide solution. *Chemistry of Materials*. 1992, vol. 4, no. 3, p. 500–502. ISSN 0897-4756.

[96] OH, Chang Wook, Gun-Dae Lee SEONG, Soo PARK, Chang-Sik JU, Seong-Soo HONG. Synthesis of nanosized TiO2 particles via ultrasonic irradiation and their photocatalytic activity. *Reaction Kinetics and Catalysis Letters*. 2005, vol. 85, no. 2, p. 261–268. ISSN 0133-1736.

[97] GURAV, Abhijit, Toivo KODAS, Tammy PLUYM, Yun XIONG. Aerosol Processing of Materials. *Aerosol Science and Technology*. 1993, vol. 19, no. 4, p. 411–452. ISSN 0278-6826.

[98] I ISHIGAKI, T., S. M. OH, D. W. PARK. Titanium dioxide nano-particles through thermal plasma oxidation of titanium nitride powders. *Transactions of the Materials Research Society of Japan*. 2004, vol. 29, no. 8, p. 3415–3418. ISSN 1382-3469.

[99] NEDELJKOVIC, J.M., Z.V. SAPONJIC, Z. RAKOCEVI?, V. JOKANOVIC, D.P. USKOKOVIC. Ultrasonic spray pyrolysis of TiO2 nanoparticles. *Nanostructured materials*. 1997, vol. 9, no. 1–8, p. 125–128. ISSN 0965-9773.

[100] SCEPANOVIC, M., Z. DOHCEVIC-MITROVIC, I. HINIC, M. GRUJIC-BROJCIN, G. STANICIC, Z. V. POPOVIC. Photoluminescence of Laser-Synthesized Anatase Titanium Dioxide Nanopowders. *Materials Science Forum*. 2005, vol. 494, p. 265–270. ISSN 1662-9752

[101] CHEN, Xiaobo, Samuel S. MAO. Synthesis of Titanium Dioxide (TiO₂) Nanomaterials. *Journal of Nanoscience and Nanotechnology*. 2006-04-01, vol. 6, no. 4, p. 906–925. ISSN 15334880.

[102] SCHUBERT, Dirk W., Thomas DUNKEL. Spin coating from a molecular point of view: its concentration regimes, influence of molar mass and distribution. *Materials research innovations*. 2003, vol. 7, no. 5, p. 314–321. ISSN 1432-8917.

[103] DZIK, P., M. VESELY, J. CHOMOUCKA. Thin layers of photocatalytic TiO2 prepared by ink-jet printing of a sol-gel precursor. *Journal of advanced oxidation technologies*. 2010, vol. 13, no. 2, p. 172–183. ISSN 1203-8407.

[104] CERNA, Marcela, Michal VESELY, Petr DZIK. Physical and chemical properties of titanium dioxide printed layers. *Catalysis Today*. 2011, vol. 161, no. 1, p. 97–104. ISSN 09205861.

[105] *Dimatix material printer DMP-2800*, Available online at: http://www.dimatix.com/divisions/materials-deposition-division/printer_cartridge.asp, 2011-4-30.

[106] DZIK, P.; VESELY, M.: Uživatelské zkušenosti s materiálovou tiskárnou, *Seminár Polygrafia academica,* 2010, p. 107–114, ISBN 978-80-227-3340- 3.

[107] *The nature of light, cited 2012-06-08*
http://www.public.asu.edu/~laserweb/woodbury/classes/chm467/bioanalytical/spectroscopy/absflr.html,

[108] SWAPP, S.: Scanning electron microscopy, *Geochemical instrumentation and analysis*, available online at: http://serc.carleton.edu/research_education/geochemsheets/techniques/SEM.html, cited: 4. 3. 2011

[109] *Measurement thin film composition and thickness using SEM-EDS*, Oxford instruments, 2009, available online at: http://cmm.mrl.uiuc.edu/, cited 30.4.2011.

[110] BUBERT, J., H. JENETT. *Surface and thin film analysis*: *principles, instrumentation, applications*. Weinheim: Wiley-VCH, 2002, p. 277–283. ISBN 3-527-30458-4.

[111] FAHLMAN, Bradley D. *Materials chemistry*. Dordrecht: Springer, 2007, p. 357–433. ISBN 978-1-4020-6119-6.

[112] DUTROW, B. L.; Clark, C. M.: X-ray powder diffraction, *Geochemical Instrumentation and Analysis*, available online at: http://serc.carleton.edu/research_education/geochemsheets/techniques/XRD.html, cited. 1.2.2011.

[113] Introduction to X-ray diffraction, available online at:
http://www.asdlib.org/onlineArticles/ecourseware/Bullen_XRD/XRD, cited 1.2.2011.

[114] Transmission and scanning electron microscopy; available online at: http://inano.au.dk/research/competences-and-facilities/nanotools/transmission-and-scanning-electron-microscopy/, 30.3.2011.

[115] UCHEGBU, I. F., A. G. SCHATZLEIN. *Polymers in drug delivery*. Boca Raton: CRC/Taylor, 2006, p. 29–34. ISBN 0-8493-2533-1.

[116] GUN'KO, Vladimir M., Alla V. KLYUEVA, Yuri N. LEVCHUK, Roman LEBODA. Photon correlation spectroscopy investigations of proteins. *Advances in Colloid and Interface Science*. 2003, vol. 105, no. 1–3, p. 201–328. ISSN 00018686.

[117] SAFRAN, Samuel A. *Statistical Thermodynamics of Surfaces, Interfaces, and Membranes*. Massachusetts: Addison-Wesley Publishing Company, 1994, p. 101–132. ISBN 0-2016-2633-0.

[118] GOULD, Paula. Smart, clean surfaces. *Materials Today*. 2003, vol. 6, no. 11, p. 44–48. ISSN 13697021.

[119] WANG, Rong, Kazuhito HASHIMOTO, Akira FUJISHIMA, Makota CHIKUNI, Eiichi KOJIMA, Atsushi KITAMURA, Mitsuhide SHIMOHIGOSHI, Toshiya WATANABE. Light-induced amphiphilic surfaces. *Nature*. 1997, vol. 388, no. 6641, p. 431–432. ISSN 00280836.

[120] MAHMOODI, Niyaz Mohammad, Mokhtar ARAMI. Degradation and toxicity reduction of textile wastewater using immobilized titania nanophotocatalysis. *Journal of Photochemistry and Photobiology B: Biology*. 2009, vol. 94, no. 1, p. 20–24. ISSN 10111344.

[121] SAYILKAN, Funda, Sema ERDEMOGLU, Meltem ASILTÜRK, Murat AKARSU, Sadiye SENER, Hikmet SAYILKAN, Murat ERDEMOGLU, Ertugrul ARPAÇ. Photocatalytic performance of pure anatase nanocrystallite TiO2 synthesized under low temperature hydrothermal conditions. *Materials Research Bulletin*. 2006, vol. 41, no. 12, p. 2276–2285. ISSN 00255408.

[122] XU, Jingjing, Yanhui AO, Mindong CHEN, Degang FU. Low-temperature preparation of Boron-doped titania by hydrothermal method and its photocatalytic activity. *Journal of alloys and compounds*. 2009, vol. 484, no. 1–2, p. 73–79. ISSN 0925-8388.

[123] RICHARD, C., G. GRABNER. Mechanism of phototransformation of phenol and derivatives in aqueous solution. *Handbook of Environmental Chemistry*. 1999, vol. 2, p. 217–240, ISSN 1867-979X.

[124] SANO, Taizo, Eric PUZENAT, Chantal GUILLARD, Christaphe GEANTET, Sadao MATSUZAWA, Nobuaki NEGISHI. Improvement of Photocatalytic Degradation Activity of Visible-Light-Responsive TiO 2 by Aid of Ultraviolet-Light Pretreatment. *The Journal of Physical Chemistry C*. 2009, vol. 113, no. 14, p. 5535–5540. ISSN 1932-7447.

[125] DAVYDOV, L. Quantification of the Primary Processes in Aqueous Heterogeneous Photocatalysis Using Single-Stage Oxidation Reactions. *Journal of Catalysis*. 2000, vol. 191, no. 1, p. 105–115. ISSN 00219517.

[126] MUGGLI, D. Two Active Sites for Photocatalytic Oxidation of Formic Acid on TiO2: Effects of H2O and Temperature. *Journal of Catalysis*. 2002, vol. 209, no. 1, p. 105–113. ISSN 00219517.

[127] MROWETZ, Marta, Elena SELLI. Photocatalytic degradation of formic and benzoic acids and hydrogen peroxide evolution in TiO2 and ZnO water suspensions. *Journal of Photochemistry and Photobiology A: Chemistry*. 2006, vol. 180, no. 1–2, p. 15–22. ISSN 10106030.

[128] MILLS, Andrew a Jishun WANG. Photobleaching of methylene blue sensitised by TiO2: an ambiguous system. *Journal of Photochemistry and Photobiology A: Chemistry*. 1999, vol. 127, no. 1–3, p. 123–134. ISSN 10106030.

[129] PELIZZETTI, Ezio, Marco BORGARELLO, Claudio MINERO, Edmondo PRAMAURO, Enrico BORGARELLO, Nick SERPONE. Photocatalytic degradation of polychlorinated dioxins and polychlorinated biphenyls in aqueous suspensions of semiconductors irradiated with simulated solar light. *Chemosphere*. 1988, vol. 17, no. 3, p. 499–510. ISSN 00456535.

[130] SABIN, Frank, Thomas TÜRK, Arnd VOGLER. Photo-oxidation of organic compound in the presence of titanium dioxide: determination of the efficiency. *Journal of Photochemistry and Photobiology A: Chemistry*. 1992, vol. 63, no. 1, p. 99–106. ISSN 10106030.

[131] TANG, W. Z., Z. ZHANG, H. AN, M. O. QUINTANA, D. F. TORRES. TiO2/UV Photodegradation of Azo Dyes in Aqueous Solutions. *Environmental Technology*. 1997, vol. 18, no. 1, p. 1–12. ISSN 0959-3330.

[132] MATTHEWS, Ralph W. Purification of water with near-u.v. illuminated suspensions of titanium dioxide. *Water Research*. 1990, vol. 24, no. 5, p. 653–660. ISSN 00431354.

[133] CANDAL, Roberto J., Walter A. ZELTNER, Marc A. ANDERSON. Effects of pH and Applied Potential on Photocurrent and Oxidation Rate of Saline Solutions of Formic Acid in a Photoelectrocatalytic Reactor. *Environmental science*. 2000, vol. 34, no. 16, p. 3443–3451. ISSN 0013-936x.

[134] MROWETZ, Marta, Elena SELLI. Photocatalytic degradation of formic and benzoic acids and hydrogen peroxide evolution in TiO2 and ZnO water suspensions. *Journal of Photochemistry and Photobiology A: Chemistry*. 2006, vol. 180, no. 1–2, p. 15–22. ISSN 10106030.

[135] PAZ, Y., A. HELLER. Photo-oxidatively self-cleaning transparent titanium dioxide films on soda lime glass: The deleterious effect of sodium contamination and its prevention. *Journal of Materials Research*. 1997, vol. 12, no. 10, p. 2759–2766. ISSN 0884-2914.

[136] The home of the surface measurement. *Rubert & Co Ltd*. [online]. [cit. 2012-06-12]. http://www.rubert.co.uk/index.htm

[137] HAN, Yong, Donghui CHEN, Jifeng SUN, Yumei ZHANG, Kewei XU. UV-enhanced bioactivity and cell response of micro-arc oxidized titania coatings. *Acta Biomaterialia*. 2008, vol. 4, no. 5, p. 1518–1529. ISSN 17427061

[138] WATANABE, T, A NAKAJIMA, R WANG, M MINABE, S KOIZUMI, A FUJISHIMA, K HASHIMOTO. Photocatalytic activity and photoinduced hydrophilicity of titanium dioxide coated glass. *Thin Solid Films*. 1999, vol. 351, no. 1–2, p. 260–263. ISSN 00406090.

[139] ZUBKOV, Tykhon, Dirk STAHL, Tracy L. THOMPSON, Dimitar PANAYOTOV, Oliver DIWALD, John T. YATES. Ultraviolet Light-Induced Hydrophilicity Effect on TiO 2 (110)(1×1). Dominant Role of the Photooxidation of Adsorbed Hydrocarbons Causing Wetting by Water Droplets. *The Journal of Physical Chemistry B*. 2005, vol. 109, no. 32, p. 15454–15462. ISSN 1520-6106.

[140] YU, Jiaguo, Xiujian ZHAO, Qingnan ZHAO, Gao WANG. Preparation and characterization of super-hydrophilic porous TiO2 coating films. *Materials Chemistry and Physics*. 2001, vol. 68, no. 1–3, p. 253–259. ISSN 02540584.

[141] BREZOVA, V., M. CEPPAN, M. VESELY, L. LAPCIK. Photocatalytic oxidation of 2,6-dichloroindophenol in the titanium dioxide aqueous suspension. *Chemical papers*. 1991, vol. 45, no. 2, p. 233–249. ISSN 0366-6352.

[142] OLLIS, David F. Contaminant degradation in water. *Environmental Science*. 1985, vol. 19, no. 6, p. 480–484. ISSN 0013-936x

[143] DRBOHLAVOVÁ, J.: Preparation of photocatalytically active surfaces, Lyon, , 2008, p. 74, *Doctoral thesis, Université Claude Bernard Lyon 1, Brno University of Technology, Supervisors Dr. Chantal Guillard,* Doc. Ing. Mchal Veselý, CSc.

[144] YU, Jiaguo, Yaorong SU, Bei CHENG, Minghua ZHOU. Effects of pH on the microstructures and photocatalytic activity of mesoporous nanocrystalline titania powders prepared via hydrothermal method. *Journal of Molecular Catalysis A: Chemical*. 2006, vol. 258, no. 1–2, p. 104–112. ISSN 13811169.

[145] CHENG, Humin, Jiming MA, Zhenguo ZHAO a Limin QI. Hydrothermal Preparation of Uniform Nanosize Rutile and Anatase Particles. *Chemistry of Materials*. 1995, vol. 7, no. 4, p. 663–671. ISSN 0897-4756

[146] LIU, Jia, Yin ZHAO, Liyi SHI, Shuai YUAN, Jianhui FANG, Zhuyi WANG, Meihong ZHANG. Solvothermal Synthesis of Crystalline Phase and Shape Controlled Sn 4 -Doped TiO 2 Nanocrystals: Effects of Reaction Solvent. *ACS Applied Materials*. 2011-04-27, vol. 3, no. 4, p. 1261–1268. ISSN 1944-8244.

[147] CAI, D., D. BLAIR, F. J. DUFORT, M. R. GUMINA, Z. HUANG, G. HONG, D. WAGNER, D. CANAHAN, K. KEMPA, Z. F. REN, T. C. CHILES. Interaction between carbon nanotubes and mammalian cells: characterization by flow cytometry and application. *Nanotechnology*. 2008, vol. 19, no. 34, p. 1–10. ISSN 0957-4484.

[148] YIN, Hengbo, Yuji WADA, Takayuki KITAMURA, Shingo KAMBE, Sadao MURASAWA, Hirotaro MORI, Takao SAKATA, Shozo YANAGIDA. Hydrothermal synthesis of nanosized anatase and rutile TiO2 using amorphous phase TiO2. *Journal of Materials Chemistry*. 2001, vol. 11, no. 6, p. 1694–1703. ISSN 09599428.

[149] KIM, Dong Suk a Seung-Yeop KWAK. The hydrothermal synthesis of mesoporous TiO2 with high crystallinity, thermal stability, large surface area, and enhanced photocatalytic activity. *Applied Catalysis A: General*. 2007, vol.323, p. 110–118. ISSN 0926860x.

[150] DOERFFE, K.; ECKSCHLAGER, K.: Optimální postup chemické analýzy, SNTL, Leipzig, 1998, p. 22–23.

8 LIST OF ABBREVIATIONS

AFM	atomic force microscopy
BSE	back scattered electrons
CO_2	carbon dioxide
CTAB	cetrimonium bromide
CVD	Chemical vapour deposition
DCIP	2,6-dichloroindophenol
EBDS	diffracted back scattered electrons
eV	electron volt
FA	formic acid
FWHM	full width at half maximum
HCl	hydrochloric acid
H_2O	water
NaOH	sodium hydroxide
P25	commercial TiO_2 Degussa
PE	polyethylene
PEG	polyethylene glycol
PSC	photon correlation spectroscopy
PVD	physical vapour deposition
R_a	mean roughness
R_q	root mean square roughness
SEM	scanning electron microscopy
TEM	transmission electron microscopy
TiO_2	titanium dioxide
$TiOCl_2$	titanium oxochloride
TTIP	titanium (IV) isopropoxide
UV light	ultra violet light
XRD	x-ray diffraction